NOVA SCHOOL OF SCIENCE & TECHNOLOGY

MECHANICAL AND INDUSTRIAL ENGINEERING DEPARTMENT

JOANA AVISON AFONSO

Degree in Mechanical Engineering and Sciences

VALIDATION OF METODOLOGIES FOR THE CALIBRATION OF MICROFLOW RATE MEASURING INSTRUMENTS BY OPTICAL METHODS

MASTER'S IN MECHANICAL ENGINEERING

NOVA University Lisbon

march, 2022

NOVA SCHOOL OF SCIENCE & TECHNOLOGY

MECHANICAL AND INDUSTRIAL ENGINEERING DEPARTMENT

VALIDATION OF METODOLOGIES FOR THE CALIBRATION OF MICROFLOW RATE MEASURING INSTRUMENTS BY OPTICAL METHODS

JOANA AVISON AFONSO

Degree in Mechanical Engineering Sciences

Adviser: Rui Fernando dos Santos Pereira Martins, Associate Professor,
NOVA University Lisbon

Co-advisers: Elsa Maria Isqueiro Batista,
Portuguese Institute for Quality, Caparica
Andreia Furtado,
Portuguese Institute for Quality, Caparica

Jury:

President: António José Freire Mourão, Associate Professor,
NOVA University Lisbon

Examiners: Maria Isabel de Araújo Godinho, Head of the metrology department,
Portuguese Institute for Quality, Caparica
Helena Víctorovna Guitiss Navas, Assistant Professor,
NOVA University Lisbon

Member: Rui Fernando dos Santos Pereira Martins, Associate Professor,
NOVA University Lisbon

Master's in Mechanical Engineering

NOVA University Lisbon
march, 2022

Validação de Metodologias de Calibração de Instrumentos de Medição de Microcaudal por Métodos Óticos

Aos meus pais, pelo amor, apoio e sacrifícios
To my parents, for all their love, support and sacrifices

ACKNOWLEDGEMENTS

Firstly, I would like to thank the Portuguese Institute for Quality and the opportunity to develop this work, especially to Dr. Elsa Batista, responsible for the Volume and Flow Laboratory, and Dr. Andreia Furtado, responsible for the Properties of Liquids Laboratory, for their availability, dedication and motivation throughout this project.

Secondly, I want to thank Professor Rui Martins, coordinator of the Integrated Master in Mechanical Engineering of the Department of Mechanical and Industrial Engineering of the Faculty of Sciences and Technology, for his guidance, advice and contribution to the elaboration of this work and writing the dissertation.

Lastly, I give my deepest thanks to my friends and my family, my parents, my brothers and my boyfriend for all the support and encouragement they have given me along this journey. I also thank my grandparents, who always had faith in me and would have been very proud of this accomplishment.

"To measure is to know; if you can not measure it, you can not improve it."
(Lord Kelvin)

ABSTRACT

As the medical and pharmaceutical industries evolve, newer more complex devices are created and developed, aiming to aid society in its needs. Since patients in critical health situations depend on drug delivery devices, these devices must provide the right dose of the required medicine. To prevent inaccurate dosing, new traceable techniques for measuring volume, flow, pressure and response or delay time of existing drug delivery devices must be developed and improved.

The different flow measurement methods existing at the Volume and Flow Laboratory/IPQ are a step forward to achieving this goal of accurate measurements. The work carried out throughout this Master's Dissertation, supported by the MeddII - Metrology for Drug Delivery project, aims to optimize and validate methodologies for calibrating microflow rate measuring instruments by optical methods. The front tracking method measures the displacement of the meniscus of a liquid in a tube or capillary, over time, while the drop method measures the volume increase of a drop over time. These methods were tested at several flow rates, with different fluids and different instruments. To validate these methods, an internal comparison was performed, using the gravimetric method, which is the primary method. The error and uncertainty values obtained with the front tracking method were consistent with those of the gravimetric method, thus allowing the validation of the method. This method can be used to calibrate flow generating instruments, down to 1 μL/h with an uncertainty of 5.5% (k=2).

The properties of the used fluids, such as viscoelasticity, were studied at the Liquids Properties Laboratory/IPQ, as the knowledge of the physical properties of drugs, and their behaviour when mixed, is crucial to guarantee maximum accuracy in drug delivery. The obtained data revealed that the rheological properties of the tested drugs do not have a significant effect on the flow rate accuracy and uncertainty of the tested infusion system that operates in the microflow range.

Keywords: Calibration, microflow, gravimetry, optics

RESUMO

À medida que as indústrias médica e farmacêutica evoluem, novos equipamentos mais complexos são criados e desenvolvidos, com o objetivo de satisfazer as necessidades da sociedade. Como os pacientes que se encontram em situações críticas de saúde dependem de instrumentos doseadores de medicamentos, estes devem fornecer a dose correta do medicamento necessário. Para evitar uma dosagem imprecisa, novas técnicas rastreáveis para medir volume, caudal, pressão e resposta ou tempo de atraso destes dispositivos geradores de caudal devem ser desenvolvidas e melhoradas.

Os diferentes métodos de medição de caudal existentes no Laboratório de Volumes e Caudal/IPQ permitem atingir o objetivo de medições mais precisas. O trabalho desenvolvido ao longo desta Dissertação de Mestrado, apoiado pelo projeto MeddII - Metrology for Drug Delivery, visa melhorar e validar metodologias de calibração de instrumentos de medição de microcaudal por métodos óticos. O método *Front tracking* mede o deslocamento do menisco de um líquido escoado dentro de um tubo ou capilar, ao longo do tempo, enquanto o método da gota mede o aumento de volume de uma gota suspensa ao longo do tempo. Estes métodos foram testados com vários caudais, diferentes fluidos e diferentes instrumentos. Para validar estes métodos, foi realizada uma comparação interna, utilizando o método gravimétrico, que é o método primário. Os valores de erro e incerteza obtidos com o método *Front tracking* foram consistentes com os do método gravimétrico, permitindo assim a validação do método. Este método pode ser utilizado para calibrar instrumentos geradores de caudal, até 1 μL/h, com incerteza de 5,5% (k=2).

As propriedades dos fluídos utilizados, como a viscoelasticidade, foram estudadas no Laboratório de Propriedades do Líquidos/IPQ, sendo que o conhecimento das propriedades físicas de fármacos é fundamental para garantir a máxima precisão no seu doseamento. Os dados obtidos revelaram que as propriedades reológicas dos medicamentos testados não têm um efeito significativo na precisão e incerteza do caudal debitado pelo sistema de infusão que opera na gama de microcaudais.

Palavras-chave: Calibração, microcaudal, gravimetria, ótica

Index

LIST OF FIGURES

LIST OF TABLES

LIST OF ABBREVIATIONS AND ACRONYMS

BIPM	International Bureau of Weights and Measures (in French, *Bureau international des poids et mesures*)
CMC	Calibration and Measurement Capability
EMPIR	European Metrology Programme for Innovation and Research
EURAMET	European Association of National Metrology Institutes
FCT/UNL	Faculdade de Ciências e Tecnologia da Universidade Nova de Lisboa
GUM	Guide to the Expression of Uncertainty in Measurement
IPQ	Portuguese Institute for Quality (in Portuguese, Instituto Português da Qualidade)
LNM	National Metrology Laboratory (in Portuguese, *Laboratório Nacional de Metrologia)*
LPL	Liquids Properties Laboratory (in Portuguese, *Laboratório de Propriedades dos Líquidos*)
LVC	Volume and Flow Laboratory (in Portuguese, *Laboratório de Volume e Caudal)*
NL	Newtonian Liquid
NMI	National Metrology Institute
NNL	Non-Newtonian Liquid
OD	Oscillation-type density meter
OIML	International Organization of Legal Metrology (in French, *Organisation Internationale de Métrologie Légale)*
SI	International System of Units (in French, *Système International d'unitées*)
VIM	International Vocabulary of Metrology (in French, *Vocabulaire International de*

Métrologie)

LIST OF SYMBOLS AND SIGNS

Latin Characters (Small Letters)

f	frequency [Hz]
g	gravitation constant [m/s²]
h	gap dimension, layer thickness, fluid level [m]
k	coverage factor
lg	logarithm (to the basis 10)
ln	natural logarithm (to the basis e, Euler's number)
m	mass [kg]
p	pressure [0,1 Mpa =1 bar]
r	radius [m]
t	temperature [° C]
u	standard uncertainty
v	velocity [m/s]

Latin Characters (Capital Letters)

A	area [m²]
F	force [N]
G	shear modulus [Pa]
G^*	complex shear modulus [Pa]
G'	storage modulus [Pa]
G''	loss modulus [Pa]
Q	flow rate [mL/h]

T	(absolute) temperature [K]
U	expanded uncertainty
V	volume [m^3]

Greek Characters

γ	deformation or strain [%]
$\dot{\gamma}$	shear rate (strain rate; $d\gamma/dt$) [s^{-1}]
δ	phase shift angle, loss angle [º]
$tan\delta$	loss factor, damping factor [.]
η	(shear) viscosity [Pa s]
η^*	complex viscosity [Pa s]
η'	real part of the complex viscosity[Pa s]
η''	imaginary part of the complex viscosity [Pa s]
ν	kinematic viscosity [m^2/s]
ρ	density [kg/m^3]
τ	shear stress [Pa]
ω	angular frequency (oscillation) [s^{-1}]

1. INTRODUCTION

Infusion therapy, also known as IV therapy, is the commonly used technology in clinical health care because it allows a much more efficient treatment of chronic illnesses as it delivers medicine, antibiotics, and/or hydration directly into the bloodstream. Since critically ill patients often require continuous intravenous infusion of various drugs and medication, drug delivery devices, such as insulin pumps, peristaltic pumps, syringe pumps, and pain pumps, play a critical role in the safety of patients as medical errors associated with flow rate variability may occur [1, 2, 3].

In order to avoid severe health complications and fatalities, it is of most importance to guarantee that medical instruments deliver the correct dosage of medication at the correct rate. To ensure this, the instruments must be calibrated. Some drug delivery devices operate with ultra-low flow rates (<1 mL/h), and for flow rates lower than 0.01 mL/h the primary calibration method used by the National Metrology Institutes (NMI) for measuring microflow, the gravimetric method, is inaccurate due to the evaporation loss and setup characteristics [4, 5]. Therefore, new methods, such as optical methods, are being studied to improve the accuracy and precision of results.

One of the main objectives of the new EMPIR (European Metrology Programme for Innovation and Research) project MeDDII – Metrology for Drug Delivery, coordinated by the Portuguese Institute for Quality (IPQ) and financed by the EU (European Union), is the development of new calibration methodologies and expansion of the existing European metrological infrastructure. This three-year project, that begun in June 2019, aims to improve dosing accuracy and innovate traceable techniques for measuring volume, flow and pressure in existing drug delivery devices operating at very low flow rates [1, 5, 6].

Promising optical methods for measuring microflow, such as the front tracking method and the drop method, have been investigated and implemented at IPQ. Although various of these measurement methodologies have been demonstrated experimentally, more research and improvement need to take place and metrological validation of these methods still needs to be achieved.

This dissertation is the result of a partnership between the Faculty of Science and Technology, New University of Lisbon (FCT-UNL) and the Volume and Flow Laboratory (LVC) and the Liquids Properties Laboratory (LPL) of the Portuguese Institute for Quality, under the project MeDD II – Metrology for Drug Delivery, and its objective is the validation of methodologies for calibration of microflow rate measuring instruments by optical methods.

1.1. Objectives

Patients in critical health situations often depend on drug delivery devices, that must provide the right dose of the required medicine, and thus need to be calibrated with adequate methods for the flow rate range at which these medical devices operate. The primary calibration method, the gravimetric method, presents results with high uncertainties for within the microflow rate range.

The overall objective of this work is the improvement and validation of methodologies for calibrating microflow rate measuring instruments by optical methods and also to obtain further insight on the flow behaviour of commonly used drugs in medical applications.

A specific objective of this work is to increase the measuring range of IPQ-LVC down to 5 nL/min (0.3 μL/h) with a 2% (k=2) target uncertainty.

Another goal is to measure different flow rates, with different fluids, with different flow generators, using both optical methods, and comparing their measurement results to the results obtained by the primary method, which is the gravimetric method.

Finally, it is also an objective of this work to analyse the uncertainty component of each optical methods and to develop calibration procedures for existing infusion drug delivery equipment on the market.

1.2. Structure of the dissertation

This dissertation is organized in 8 chapters. In the first chapter an introduction to the subject is presented, as well as the objectives of the work. In the second chapter the Portuguese Institute for Quality and the framework of the Metrology for Drug Delivery II project are presented. In the third chapter concepts relevant to this work, such as metrology and rheology, are described in detail. Chapter 4 describes the materials and methods used during the development of this work. In chapter 5 an in-depth study about the sources of uncertainty of the front tracking method is presented, as well as the effort to reduce their influence. Chapter 6 describes the adjustments made to the image processing software of the drop method, in order to optimize the method, and provides an in-depth study about the

sources of uncertainty. Chapter 7 focuses on the methods and the instruments tested during this work and on the results and discussion about the obtained data. In the final chapter, chapter 8, conclusions about the work developed in this dissertation are taken and suggestions for future work are given.

2. FRAMEWORK

This chapter aims to give an overview on concepts of metrology and the national framework for quality matters in Portugal. This chapter also describes the project under which the work for this dissertation was developed, known as the new EMPIR (European Metrology Programme for Innovation and Research) project MeDDII – Metrology for Drug Delivery, which is coordinated by the Portuguese National Metrology Institute (NMI), the Portuguese Institute for Quality (IPQ), and has the overall objective to improve the accuracy in drug delivery for vulnerable patients.

2.1. Metrology

Metrology is the science of measurement. It is concerned with accuracy and traceability of measurements, development of measuring methods, analyses of results and determination of its uncertainties. In practical applications, Metrology is the enforcement, verification, and validation of predefined standards [7, 8].

Scientific or fundamental metrology deals with the organization, development and maintenance of international and national measurement standards with high metrological rigour. The top structures in this field are the primary laboratories. These often participate in BIPM (International Bureau of Weights and Measures) inter-laboratory comparisons and traceability of reference standards [8]. This form of metrology is of great importance as it is deeply involved with scientific research and development of new methodologies and technologies that can be applied to industries concerning government, healthcare, and commercial products [9].

Applied or industrial metrology's purpose is to ensure the proper functioning of measurement instruments used in a wide variety of industries, as well as in the production and metrological testing processes. Accredited and national laboratories, that have traceability of primary ones, carry out the calibration and quality control of measuring instruments [9].

Legal metrology concerns any application of metrology that is subjected to national laws or regulations and interferes in commercial transactions, health, public safety, environmental protection, and fiscal area. This branch of metrology is responsible for metrological control and requirements of measuring instruments and the development of metrological legislation to ensure the accuracy of measurements. Therefore, legal metrology seeks to protect the final consumer from the consequences of incorrect measurements and enable taxation and fair trade [7, 8, 9].

2.2. The Portuguese System for Quality (SPQ)

The Portuguese System for Quality (SPQ), established by the Decree-Law Nr. 165/83, amended by Decree-Law nr. 80/2014, on May 15th, is the national legal framework for quality matters in Portugal which integrates interrelated entities and organizations that follow internationally accepted principles, rules and procedures to boost quality and ensure the coordination of the three subsystems - standardization, qualification and metrology – and, therefore, promotes the development of the country and the quality of life of society. The SPQ is concerned with the certification of products and company quality systems, as well as the accreditation of entities in this field [10, 11, 12].

The Standardization subsystem encompasses the activities of elaboration of standards and other normative documents of national, European and international level [10, 12]. There are three types of standards, classified according to the scope of the responsible Standardization body: International Standards (ISO), European Standards (EN) and Portuguese Norms (NP) [11].

The Qualification subsystem comprises the accreditation, certification and other activities of competence recognition and conformity assessment. Within this subsystem there are the testing and calibration laboratories that meet the requirements of the standard NP EN ISO/IEC 17025, certification bodies which follow the general regulation of Accreditation DRC006 and the requirements of the NP EN 45011 (products), ISO EN NP 9001 (quality systems) ISO EN NP 14001 (environmental management systems) and ISO/17024 (for personnel), sector and vehicle inspection bodies that follow standard ISO/IEC 17020, and, at last, the GLP (Good Laboratory Practices) compliance with Ordinance nr 1070/90 and the requisites of Directive 88/320/EEC [11]

The Metrology subsystem guarantees the accuracy and precision of the measurements, ensuring their comparability and traceability, at national and international level, and the realisation, maintenance and development of the standards of the measurement units [10, 12].

The SPQ is governed by the following principles [10]:

1. Credibility and transparency - this operation of the SPQ is based on rules and methods known and accepted at national level or established by international consensus and is supervised by representative entities.
2. Horizontality - the SPQ may cover all sectors of activity of society as well as the respective society, as well as the respective economic agents and results in any sector.
3. Universality - the SPQ can cover all types of activity, its agents and results in any sector.
4. Gender mainstreaming - the operation of the SPQ aims to contribute to equality between women and men.
5. Coexistence - all sectorial systems or entities that demonstrate compliance with the established requirements and rules may join the SPQ.
6. Decentralization - SPQ is based on the autonomy of action of the entities that compose it and on the respect for the unity of doctrine and action of the System as a whole.
7. Free and voluntary membership - each entity decides on its membership of the SPQ.

2.3. The Portuguese Institute for Quality (IPQ)

The Portuguese Institute for Quality (IPQ), founded in 1986 through Decree-Law nr. 183/86 of July 12th, is a public institute with legal powers, which aims to protect the interests of the Portuguese State. According to Decree-Law nr. 71/2012 of March 21st, 2012, amended by Decree-Law nr. 80/2014, on May 15th, the IPQ pursues attributions of the Ministry of Economy and Employment (MEE) and has as its mission the management and coordination of the Portuguese Quality System (SPQ) and other regulatory qualification systems that are conferred by law, the promotion and coordination of activities aimed at accreditation of economic agents actions, the creation and availability of the necessary infrastructure to enable the practice of better processes and quality management methods, and also the development of the necessary activities for its functions as the National Metrology Institute (NMI) and National Standards Body (NSB) [11, 12, 13].

The IPQ is the entity responsible for the preparation of Portuguese standards, ensuring the coherence and updating of the national normative acquis, and for the adjustment of national legislation on products to European Union standards. As the National Metrology Institute, it is also responsible for ensuring the accuracy and precision of the measurements, guaranteeing their comparability and traceability, at national level, as well as at international level, and the achievement, maintenance and development of the standards of the units of measurement [12, 13]. Therefore, the IPQ is the national body responsible for normalisation, certification and metrology activities, integrating all fundamental elements for improving the quality of products, services and quality systems and the qualification of people, thus contributing to increased productivity, competitiveness and innovation in the public and private sectors. Although the IPQ is an institute integrated

in the State's internal administration, it has its own financial autonomy, administration and patrimony [12].

Figure 2.1 shows the internal structure of the IPQ.

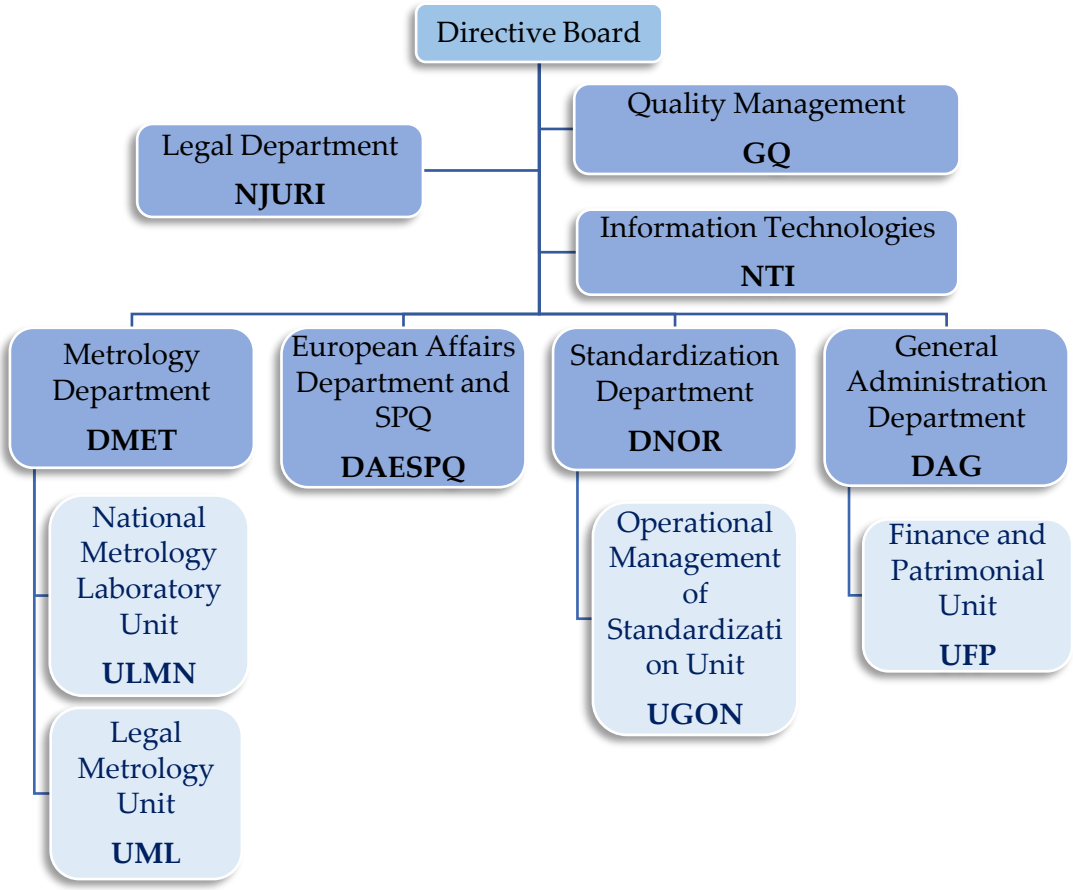

Figure 2.1 - Internal structure of the IPQ [12]

In reference to the Metrology Department (DMET), IPQ is the National Metrology Laboratory (LNM). The LNM ensures the accuracy and traceability of national measurements, through the measurement standards needed by the Portuguese industry and society and the contribution to the construction of a European metrological leadership [14]. This includes many laboratories such as the Liquids Properties Laboratory (LPL) and the Volume and Flow Laboratory (LVC), where the underlying work for this dissertation took place.

2.3.1. Volume and Flow Laboratory (LVC)

The Laboratory of Volume and Flow (LVC), which is divided into the Small Volume and Microflow Laboratory (Figure 2.2) and the Medium and Large Volume Laboratory (Figure 2.3), is the primary traceability laboratory in Portugal in the field of volume and flow

and micro flow. It provides services to the chemical and manufacturing industry, as well as to analytical and pharmaceutical laboratories and metrological verification bodies (water and fuel), in the following three distinct areas [15, 16]:

- Calibration of small volumes (Glassware and piston operated volumetric equipment);
- Calibration of medium and large volumes (Standard test measures and proving tanks);
- Liquid flow and microflow measurement (Liquid dosing instruments and flowmeters).

At the Laboratory of small volumes and microflow (Figure 2.2), the calibration of volumetric glassware such as pipettes, volumetric flasks, cylinders, pycnometers, burettes, syringes, peristaltic pumps, flow meters, fluid dosing instruments, perfusion syringes and instrument device analysers are performed [16]. In the large and medium laboratory (Figure 2.3) calibration of standard test measures and proving tanks are performed. Instrument calibration in this laboratory aims to quantify the difference between the nominal value and the true value, find systematic errors in analytical processes and correct them, when possible. It is with the help of high accuracy methods and standards that it is possible to ensure correct volume measurement [17].

Figure 2.2 - Small Volume and Microflow Laboratory [16]

Figure 2.3 - Medium and Large Volume Laboratory [16]

The traceability of the working standards used at the LVC is established to the national mass standards, temperature standards, time standards and density of the used liquid [17]. The LVC also has the Measurement and Calibration Capabilities (CMC) that are published in the database of the *Bureau International des Poids et Mesures* (BIPM), obtained through the participation with satisfactory results in international comparisons such as the European Association of National Metrology Institutes (EURAMET). Additionally, it coordinates and develops national comparisons between secondary laboratories in collaboration with the Portuguese Accreditation Institute (IPAC). In cooperation with universities, it develops several works of validation and improvement of calibration standard methods [16].

2.3.2. Liquid Properties Laboratory (LPL)

The Liquid Properties Laboratory (in Portuguese, *Laboratório de Propriedades de Líquidos)* is responsible for the development, and maintenance of national standards for density, viscosity, viscoelasticity and surface tension of liquids [18, 19].

The LPL carries out tests and studies within the scope of applied and scientific Metrology, calibrations, and certifications. It focuses on development, preparation and certification of liquid reference materials, and on the determination of the liquid properties, namely, density, surface tension, viscosity (dynamic and kinematic) and the rheological parameters of liquid samples and performs calibrations of the measuring instruments of these quantities, such as hydrometers and oscillation-type density meters, for density; viscometers (capillary, rotational and Stabinger), for viscosity; rheometers and rotational viscometers, for viscoelasticity; and tensiometers, for surface tension. This laboratory also

performs measurement audits of these measuring instruments and of the determination of liquids properties and develops new measurement methods, for said properties. The LPL not only participates and coordinates inter-laboratory comparisons, but also participates in national and international project development and research [18, 19].

The measurements traceability is obtained to national and international standards, and to certified reference materials. The accuracy of the measurements performed is proven through the participation in projects and in international comparisons, and it is demonstrated by the acceptance and inclusion of the CMC in the BIPM database [18].

2.4. MeDDII project - Metrology for Drug Delivery

Given that infusion therapy is commonly used in medicine, especially in critical health care situations, it is extremely important and vital that patients receive the right dose of the required substances at a given time. However, many infusion errors occur, with some resulting in severe health implications. This is especially the case in neonatology, where multiple pump infusion is typically combined with low flow rates. Therefore there is an urging need to prevent these adverse incidents [1, 19].

The new EMPIR (European Metrology Programme for Innovation and Research) project MeDDII – Metrology for Drug Delivery, coordinated by the IPQ, financed by the EU (European Union) has the overall aim to improve the accuracy in drug delivery for vulnerable patients. This three years joint research project started in June of 2019, involving 15 partners, including: 9 National and Designated Metrology Institutes (IPQ- Portugal, CETIAT – France, CMI – Chez Republic, DTI – Denmark, METAS – Switzerland, NEL – United Kingdom, NQIS – Greece, RISE – Sweden and KRISS – South Korea), 4 companies (DNV GL – The Netherlands, HSG-IMIT – Germany, INESC MN – Portugal, BHT – The Netherlands) and 2 University Hospitals (THL – Germany, UMCU – The Netherlands) [5, 6].

To prevent and reduce the number of adverse patient incidents related to poor and inaccurate dosing in infusion technology, the MeDDII project if focused not only on improving the dosing accuracy but also on developing new traceable techniques for measuring volume, flow, pressure and response or delay time of existing drug delivery devices (e.g. insulin pumps, syringe pumps, infusion device analysers and pain pumps), micro-chip pump devices and in-line sensors in relation to changes in flow rates, from 5 nL/min to 100 nL/min, using Newtonian liquids. For steady flow rates an uncertainty of 1 % or better is expected, whereas for fast changing flow rates, which are step changes between two flow rates within a second, an uncertainty of 2 % or better is expected. To achieve this, the existing metrological infrastructure will be expanded and new calibration methods and procedures for existing medical flow devices will be developed and validated. These

calibration procedures with traceability to a primary standard have a target uncertainty value of 2 % for a range of 5 nL/min up to 600 mL/min [1, 5, 6].

Existing flow facilities of the participating NMIs partners will be upgraded in order to enable the traceable in-line measurement of the dynamic viscosity of Newtonian liquids (Dopamine, dobutamine and saline solution), as a function of the flow rate and pressure drop, with a target uncertainty value of 2 %. Additionally, tests with non-Newtonian liquids will be performed in order to prove the concept. Transfer standards for the in-line measurement of dynamic viscosity and other physical properties of liquids (e.g., density) will be calibrated in order to be used for flow measurement and to determine the mixing behaviour of different liquids [1, 6].

A multi-infusion system setup will be designed and developed to investigate fluid flow rates, allowing the assessment of the performance of drug delivery devices, and fluid compositions in the outlet of the infusion line, thereby determining the concentration of each drug being administered. This multi-infusion system will contain check valves with several options for testing how liquids, with different viscosities mix and flow and how this affects drug concentration. The flow rates and pressures will be traceably calibrated in all infusion lines, as well as at the outlet of the syringe pump, to be able to analyse the effects of pressure-equalising devices and to detect occlusion phenomena and bad mixing configurations [1, 6].

Furthermore, a proof-of-concept on-chip microfluidic pump will be developed, in collaboration with the INESC (Institute for Systems and Computer Engineering) and used as a transfer standard in drug discovery and organ-on-a-chip applications for flow rates lower than 100 nL/min [6].

3.

BIBLIOGRAPHIC RESEARCH

This chapter aims to describe in detail concepts relevant to this dissertation, such as uncertainty of measurements and flow behaviour and to describe the flow measurement methods used throughout this work.

3.1. Error and uncertainty of measurement

When performing any measurements, there is always an error and uncertainty associated with the measured value, since this is not the true value of the quantity, but only an approximation. It would only be possible to obtain the true value in the case of a perfect measurement with absence of errors, which, in practice, is unachievable [21]. Therefore, when a measurement result of a physical quantity is reported, a quantitative indication of the quality of the result must be given, so that whoever receives this information can assess its reliability. Without such indication, it would not be possible to compare obtained results with reference values present in a specification, standard or certificate [22].

3.1.1. Error of measurement

The error of measurement is defined by Equation 3.1 as the difference between the measured value, M_V, and the true value, also known as reference value, R_V, of a quantity [21]:

$$\varepsilon = M_V - R_V \tag{3.1}$$

Errors generally depend on human accuracy, the instruments and experimental setup used or environmental conditions. According to the International Vocabulary of Metrology (VIM), errors can be classified as systematic or random [23].

Systematic errors remain constant or vary in a predictable way, affecting the measurement constantly in the same direction, either above or below the true value [21, 23]. These errors result from attributable factors, namely the measuring instruments, the

environmental conditions, and the experimental procedure. The only way to avoid systematic errors is to identify and eliminate the causes that originate them [24].

Random errors are those whose effect is unpredictable, that is, the results of successive repetitions are unpredictable, and are associated with the dispersion of the measurand around the true value. These errors cannot be excluded, since they are not controllable or predictable, but they can be compensated through data processing [21]. Random errors result from uncontrollable causes that are not always possible to identify due to their irregular, variable, and probabilistic nature. However, it is possible to minimize their effects by increasing the number of measurements, since the average progressively approaches the true value as the number of repetitions increases [24, 25].

A reference value for a systematic error corresponds to a measured value of a standard with negligible measurement uncertainty, while the reference value for a random error is the mean that would result from an infinite number of repeated measurements of the same measurand [23].

There are also errors that are neither random nor systematic. These are called gross errors and result from human negligence, generally due to poor use of instruments, lack of training or the metrologist's lack of attention to the experimental procedure [24].

It is recognized that even when all elements originating errors have been evaluated and the respective appropriate corrections have been applied, an uncertainty remains about how well the measurement result represents the true value of the quantity [22].

3.1.2. Uncertainty of measurement

The measurement uncertainty is the doubt regarding the accuracy of the obtained measurement result. For a given measurand, which is the quantity that is intended to be measured and a given measurement result, there is not just one value, but an infinite number of values dispersed around the mean value that are consistent with the observations and data collected. Uncertainty can therefore be seen as the range around the obtained mean value in which it is possible that the true value is located. In other words, the uncertainty of measurement is a non-negative parameter that characterizes the dispersion of values assigned to a measurand [22]. Thus, it is a property that must intrinsically accompany the entire measurement, whether in the act of carrying out a calibration, a test, or in the definition of a tolerance, so that there is a certain level of confidence in the interval where it is predicted that the measured value belongs to. The level of confidence associated with the measurement of the measurand is directly related to its uncertainty, i.e., the lower the uncertainty value, the greater the scientific credibility that the measured value has [23, 25].

In a global market era, it is imperative that the method for expressing and evaluating uncertainty is uniform throughout the world so that the accuracy of measurements made in

different countries, according to a standard or reference, can be easily compared. The Guide to the expression of uncertainty in measurement (GUM) establishes rules for the expression, assessment, and evaluation of measurement uncertainty to be used in measurement standardization, calibration, laboratory accreditation, and metrology services. This guide allows a uniform characterization of the quality of a measurement result using the following recommended steps [22]:

- Express, in mathematical terms, the dependence of the measured Y, in relation to the input quantities X_i;
- List all elements and sources of uncertainty;
- Assess the type of uncertainty (A or B);
- Calculate the standard uncertainty of each uncertainty component;
- Calculate the respective sensitivity coefficients;
- Assess the need to calculate covariances;
- Calculate the combined uncertainty;
- Calculate the expansion factor k;
- Determine the expanded uncertainty.

In a calibration (of instruments), as a rule, there is generally only one measurand or output quantity Y, which depends on a certain number of input quantities X_i $(i = 1,2, \dots, N)$ in accordance with Equation 3.2 [22]:

$$Y = f(X_1, X_2, \dots, X_N) \tag{3.2}$$

All input quantities, X_i, have a respective associated uncertainty value and can be grouped according to how their value and uncertainty were determined. The uncertainty value can be determined directly in the measurement, as in the case of evaluations of simple or repeated observations based on experience, or through corrections to instrument indications or corrections that depend on external conditions such as ambient temperature, relative humidity, pressure, etc. Input quantities can also come from sources that are external to the measurement, such as quantities associated with calibrated measurement standards, certified reference materials or reference data present in manuals. In some cases, the input quantities are themselves measurands and functions of other quantities, which can lead the function f to become too complex, sometimes making its analytical writing impossible. In these cases, the function f can only be determined experimentally, or sometimes, it will be a computer algorithm that will have to be evaluated numerically, at each measurement. The estimate of X_i is denoted by x_i [22, 26].

3.1.3. Measurement uncertainty evaluation

The uncertainty of measurement, associated with the estimates of the input quantities, generally encompasses various components, which are evaluated by two methods [24, 26].

In the type-A standard uncertainty evaluation method, components can be estimated from the statistical distribution of values obtained from a series of measurements and can be quantified by standard deviations. The standard uncertainty is the experimental mean standard deviation.

In the type-B standard uncertainty evaluation method, the components are estimated by methods other than the statistical analysis of a series of observations. The estimation of the standard uncertainty is obtained by standard deviations of probability density functions, based on prior information, whether from specialized publications, calculations, calibration certificates, certified reference materials or technical specifications of manufacturers, from previously proven experience, or just common sense [23, 24, 26].

3.1.3.1. Type-A standard uncertainty evaluation method

The type-A standard uncertainty evaluation method evaluates a measurement uncertainty component, through the statistical analysis of a series of measured values, acquired under defined measurement conditions [23].

The statistical analysis is performed using the experimental mean standard deviation of a set of observations, resulting from the calculation of the mean or the analysis of a mathematical regression [23]. This evaluation method can be used when a certain input quantity, X_i, is measured repeatedly, with several statistically independent observations ($n > 1$) and under the same measurement conditions, obtaining the estimated value of a quantity, $\bar{q}$, using the arithmetic mean of the observed values q_k $(k = 1,2, \dots, n)$, through Equation 3.3 [22]:

$$\bar{q} = \frac{1}{n}\sum_{k=1}^{n} q_k \tag{3.3}$$

The individual observations, q_k, differ in value due to random variations in the quantities of influence or other random effects. The square root of the experimental variance of the observations, $s^2(q)$, is the experimental standard deviation, $s(q)$, which is the statistical parameter that estimates the corresponding variance of the probability distribution, characterizing the variability of the observed values, q_k, that is, its dispersion in

relation to the average value of the input quantity, $\bar{q}$, according to Equation 3.4, with n being the number of observations [22]:

$$s(q) = \sqrt{\frac{1}{n-1}\sum_{k=1}^{n}(q_k - \bar{q})^2} \tag{3.4}$$

The estimate of the variance of the mean is given by the experimental variance of the mean, according to Equation 3.5:

$$s^2(\bar{q}) = \frac{s^2(q)}{n} \tag{3.5}$$

The standard uncertainty, $u(x_i)$, of the estimate of the input quantity, $\bar{q}$, is the experimental standard deviation of the mean, which is corresponds to the positive square root of the experimental variance of the mean, $s^2(\bar{q})$, according to Equation 3.6:

$$u(x_i) = s(\bar{q}) \tag{3.6}$$

3.1.3.2. Type-B standard uncertainty evaluation method

The standard uncertainty, $u(x_i)$, is estimated by scientific judgment based on experience and all available data about the possible variability of the input quantity, X_i. This set of information may include [22]:

- Data from previous measurements;
- Experience or general knowledge of the behaviour and properties of materials, of relevant instruments and measurement techniques;
- Manufacturer's specifications;
- Data from calibration and other certificates;
- Uncertainties attributed to reference data from manuals or other publications.

A type-B evaluation of standard uncertainty can be as reliable as a type-A assessment, especially when, in a measurement situation, the type-A assessment is based on a relatively small number of statistically independent observations [22].

This type of evaluation requires specific knowledge and experience for an adequate use of the available information, since it may be necessary to assume only the upper and lower limit values for the variation of the quantity and then consider that its value belongs to a normal, rectangular, or triangular probability distribution [24, 25].

Rectangular distributions are very common, but whenever there are reasons to assume that mean values are more likely, a triangular or even normal distribution can be chosen [25].

Normal Distribution

If the uncertainty value is obtained from a calibration certificate or manufacturer's specifications, a normal distribution is assumed and the standard uncertainty, $u(x_i)$, is obtained by dividing this given uncertainty value, u, by the expansion factor value, k, according to Equation 3.7 [22]:

$$u(x_i) = \frac{u}{k} \tag{3.7}$$

A normal probability distribution is illustrated in Figure 3.1:

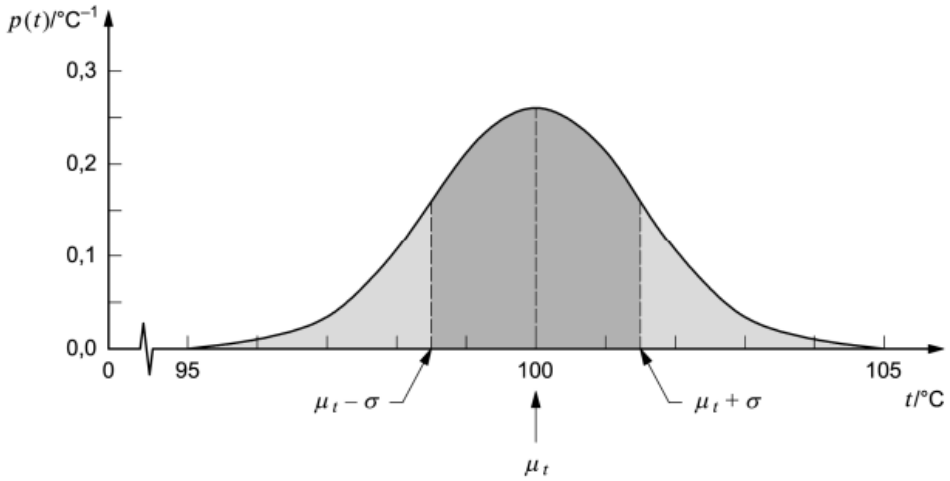

Figure 3.1 - Normal probability distribution [22]

Rectangular Distribution

A rectangular distribution (Figure 3.2) of possible values can be applied when there isn't enough knowledge about the values of the input quantity, X_i, and it is only possible to estimate the values of the lower and upper limits of variability of X_i, $a^-$and a^+, respectively. In other words, by knowing that the probability that the value of X_i lies within the interval $[a^-; a^+]$ is equal to one and, therefore, that the probability that X_i lies outside this range is zero, it is assumed that X_i is equally likely to be any value within the range, since there is no specific knowledge about the possible values of X_i. The expected value of X_i is, therefore, considered to be the midpoint in the interval (Equation 3.8) and the respective associated variance is given by Equation 3.9 [22]:

$$x_i = \frac{a^+ - a^-}{2} \tag{3.8}$$

$$u^2(x_i) = \frac{(a^+ - a^-)^2}{12} \tag{3.9}$$

If the difference between the lower and upper limit is equal to $2a$, the standard uncertainty is given by Equation 3.10 [22]:

$$u(x_i) = \frac{a}{\sqrt{3}} \tag{3.10}$$

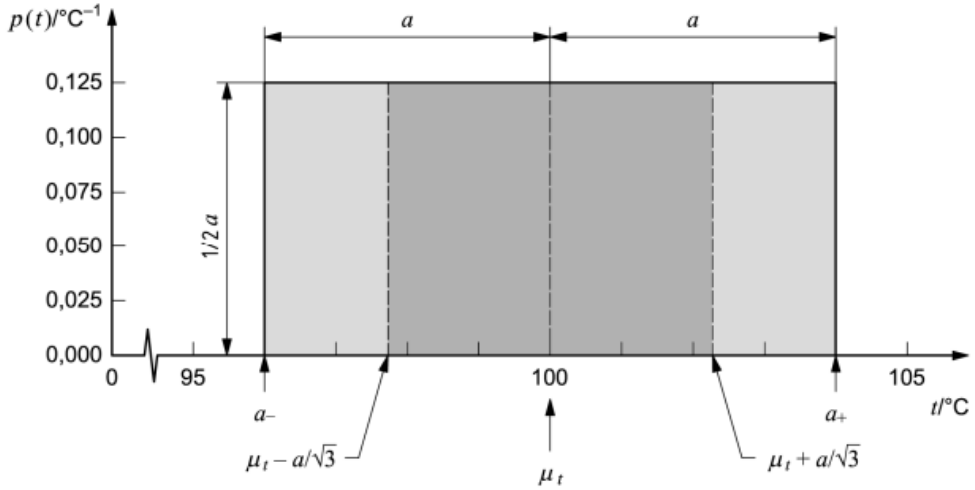

Figure 3.2 - Rectangular probability distribution [22]

Triangular Distribution

Whenever it is expected that the central values of the quantity have a higher probability of occurrence than the values of the limits, a triangular distribution (Figure 3.3) should be used. The standard uncertainty is given by Equation 3.11 [22]:

$$u(x_i) = \frac{a}{\sqrt{6}} \tag{3.11}$$

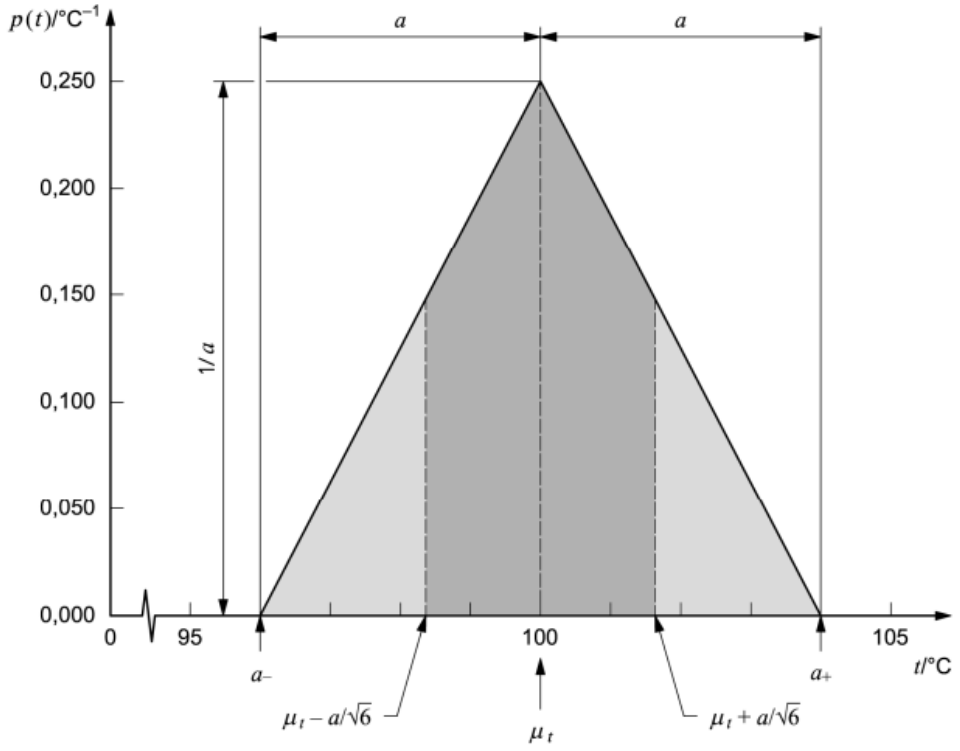

Figure 3.3 - Triangular probability distribution [22]

The standard uncertainty of a component that is composed of more than one variable is calculated according to Equation 3.12, [22].

$$u(x_i) = \sqrt{\sum_{i=1}^{n} \mathrm{u}^2} \tag{3.12}$$

3.1.4. Combined standard uncertainty

The standard uncertainty of the output quantity estimate, or measurement result, y, is obtained by combining the standard uncertainties of the input estimates $u(x_i)$. As such, it is termed the combined standard uncertainty and is denoted by $u_c(y)$. This uncertainty is determined according to the interdependence between the input quantities X_i $(i = 1,2, \dots, N)$, which can either be independent (or uncorrelated) or correlated. In the first case, the combined standard uncertainty, $u_c(y)$, given by Equation 3.13, is the positive square root of the combined variance, ${u_c}^2(y)$, obtained from all variance and covariance components [22]:

$${u_c}^2(y) = \sum_{i=1}^{N} \left(\frac{\partial f}{\partial x_i}\right)^2 u^2(x_i) \tag{3.13}$$

The partial derivatives $\partial f/\partial x_i$ given in Equation 3.13 are equal to $\partial f/\partial X_i$, evaluated for $X_i = x_i$. These partial derivatives of the model function f are known as the sensitivity coefficients, c_i, associated with the estimate of the input quantity x_i, according to Equation 3.14. A sensitivity coefficient describes how the output quantity estimate, y, is influenced by the variations of each value of the input quantities estimates, x_i $(i = 1,2, \dots, N)$. This coefficient is used to standardize units, so that the combined uncertainty, $u_c(y)$, has the same units of the measured quantity [22].

$$c_i = \frac{\partial f}{\partial x_i} \tag{3.14}$$

The component contribution to the combined standard uncertainty of the output estimate, y, generated by the standard uncertainty of input estimate, x_i, is given by Equation 3.15 [22]:

$$u_i(y) = c_i u(x_i) \tag{3.15}$$

When the input quantities are independent, that is, they do not correlate with each other, Equation 3.13 can be rewritten as Equation 3.16, giving the combined standard uncertainty of the estimate of the output quantity, y:

$$u_c(y) = \sqrt{\sum_{i=1}^{N} {u_i}^2(y)} \tag{3.16}$$

In the rare case that the input quantities are correlated with each other, the associated covariances must be taken into account and considered as an additional contribution to the uncertainty. According to the law of propagation of uncertainty, the combined variance, ${u_c}^2(y)$, associated with the measurement result is given by Equation 3.17, where x_i and x_j are the estimates of X_i and X_j and $u(x_i,\ x_j) = u(x_j,\ x_i)$ is the estimated covariance associated with x_i and x_j [22]:

$${u_c}^2(y) = \sum_{i=1}^{N} {u_i}^2(y) + 2\sum_{i=1}^{N-1}\sum_{j=i+1}^{N} \frac{\partial f}{\partial x_i}\frac{\partial f}{\partial x_j} u\left(x_i, x_j\right) \tag{3.17}$$

3.1.5. Expanded uncertainty

Although the combined standard uncertainty can be universally used to express the uncertainty of a measurement result, in some commercial, industrial, regulatory and health and safety applications, there is a need to provide an uncertainty measure that

defines a range around the measurement result that is expected to encompass a large fraction of distributions of values that could reasonably be attributed to the measurand. The expanded uncertainty, U, is the measure of uncertainty that satisfies this requirement and can be defined as the coverage probability or level of confidence of the interval about the measurement result. This uncertainty can be obtained by multiplying the combined standard uncertainty, $u_c(y)$, of the output quantity estimate by the coverage factor, k, according to Equation 3.18 [22, 25]:

$$U = ku_c(y) \tag{3.18}$$

Whenever the probability of distribution of a measurand is a normal distribution and the standard uncertainty associated with the estimation of the output quantity is sufficiently reliable, a coverage factor equal to 2 ($k = 2$) should be used. In this case, the indicated expanded uncertainty is equivalent to an expanded probability of approximately 95%. In other words, the expanded uncertainty is given with a 95% confidence interval [26].

It is also possible to determine the appropriate coverage factor based on the level of confidence required for the interval $[y - U; y + U]$, using the effective degrees of freedom, v_{eff}. Degrees of freedom is the number of independent values in the final calculation which are free to vary without violating constraints. When combining and evaluating multiple uncertainty components that are characterized by various probability distributions, the degrees of freedom may be undefined. Therefore, the effective degrees of freedom must be calculated to approximate de actual equivalent degrees of freedom. For such, it is necessary to consider the reliability of the standard uncertainty of the estimation of the output quantity. The determination of the effective degrees of freedom, v_{eff} is given by the *Welch-Satterthwaite* formula, according to Equation 3.19, where v_i represents the effective degrees of freedom for each standard uncertainty component $u_i(y)$ [22, 26].

$$v_{eff} = \frac{{u_c}^4(y)}{\sum_{i=1}^{N} \frac{{u_i}^4(y)}{v_i}} \tag{3.19}$$

For a given standard uncertainty of the input values obtained by a type-A evaluation, the number of effective degrees of freedom is given by $v_i = n - 1$. In the case of a type B evaluation, it becomes more complex to estimate the degrees of freedom. However, if limits a^- and a^+ are defined and chosen in a way that the probability of the quantity that is being analyzed laying outside these limits is extremely small, the degrees of freedom are assumed to be $v_i \to \infty$ [26].

It is possible to obtain the coverage factor, k, through Table 3.1. It is based on a t-student distribution for an expanded probability of 95.45%. If the value obtained by Equation 3.19 for v_{eff} is not an integer, one should opt for the antecedent integer [26].

Table 3.1 - Effective degrees of freedom according to the coverage factor [26]

v_{eff}	**1**	**2**	**3**	**4**	**5**	**6**	**7**	**8**	**10**	**20**	**50**	∞
k	13,97	4,53	3,31	2,87	2,65	2,52	2,43	2,37	2,28	2,13	2,05	2,00

Legend: v_{eff} – effective degrees of freedom; k – coverage factor

For type-A uncertainties, the degrees of freedom are equal to the number of samples minus one. For type B-uncertainties, considering a rectangular distribution, infinite degrees of freedom are considered, otherwise, it is assumed that they are equal to 50.

When the result is presented in a calibration certificate, it is only complete when it expresses the estimate of the measurand, y, and its associated expanded uncertainty, U, according to the Equation 3.20. The numerical values of the measurand estimate and its expanded uncertainty should not be given with an excessive number of digits, being that two significant digits usually suffice. However, to avoid round-off errors in subsequent calculations, in some cases it may be necessary to retain more than two digits [22, 26]:

$$Y = y \pm U \tag{3.20}$$

3.2. Flow calibration methods

The correct and reliable determination of volume and flow is important as many flow-dependent instruments are widely used in the health and pharmaceutical industries. In order to identify and reduce possible errors associated with measuring instruments, it is necessary to determine the volume and flow as accurately as possible. The use of appropriate methods is fundamental for correct calibration and essential to obtain the most accurate and reliable results [21].

3.2.1. Gravimetric Method

The gravimetric method determines the volume of a liquid, delivered or contained in a volumetric instrument to be calibrated, by weighing its mass. To determine the liquid's mass, the container is initially weighed empty, then weighed again at the end, when it is full of liquid. The value of the amount of liquid contained is calculated by the difference between the final mass and the initial mass of the container. This mass is then converted into

volume (Equation 3.21) according to NP EN ISO standard 4787 (2021), at a reference temperature of 20 °C [21, 23, 24].

$$V_0 = (I_L - I_E)\frac{1}{\rho_l - \rho_A}\left(1 - \frac{\rho_A}{\rho_B}\right)[1 - \gamma(T - T_0)] \tag{3.21}$$

Where:
V_0 - volume at reference temperature T_0, 20 °C, in mL
I_L - result of weighing with container filled with liquid, in g
I_E - result of weighing the container empty, in g
ρ_l - density of liquid to be calibrated, at calibration temperature t, in g/mL
ρ_A - air density, in g/mL (for temperatures close to 20 °C and at normal atmospheric pressure the average value of 0,0012 g/mL can be used)
ρ_B - reference density of balance masses (for masses according to OIML 33, normally used, this value is 8.0 g/mL)
γ - thermal expansion coefficient of the material of which the instrument to be calibrated is made, in $°C^{-1}$
T - temperature of the liquid used for calibration, in °C

To determine the flow rate (Equation 3.22), it is necessary to associate to the calculation, the measurement of the filling duration, i.e., the time between two mass measurements and the evaporation [23, 24].

$$Q = \frac{1}{t_f - t_i}\left[(I_L - I_E)\frac{1}{\rho_l - \rho_A}\left(1 - \frac{\rho_A}{\rho_B}\right)[1 - \gamma(T - T_0)]\right] + \delta V_{evap} \tag{3.22}$$

Where Q is flow rate (mL/s), t_f is the end time (s), t_i is the initial time (s) and δV_{evap} as evaporation (mL/s).

Additionally, to ensure the proper application of this method it is necessary to guarantee the most suitable environmental conditions in the test room during the measurements, i.e., the temperature of the room where the measurements are taken must be stable (20 ± 3) °C. Finally, attention must be paid to the cleanliness of the internal surface of the instruments that will be calibrated, as well as the weighing instruments since the existence of impurities or residues on them can affect the measuring results [16, 23].

Even though the gravimetric method can obtain high measurement accuracy and small associated uncertainty, it has some limitations. The main sources of error are fluid

evaporation, tube adsorption, mass measurement and repeatability. The uncertainty associated with the measuring standard increases as the flowrate decreases [25].

3.2.2. Optical Methods

Optical methods use a camera or sensor to capture several images of the fluid, of which volume and/or flow are to be measured. The image processing is performed by a software, which identifies the required properties, analysis the collected data and calculates the value corresponding to the measurement quantity. Two optical methods were used in this work, the front tracking method and the drop method.

3.2.2.1. Front tracking method

The Front Tracking method is an optical method, for microflow measurement, which has as its principle of measuring the displacement of the meniscus of a liquid in a tube or capillary, over time. The meniscus is the liquid-air interface in the tube, which is connected to the flow generator on one side and open to the atmosphere on the other. By knowing the cross-sectional area of the capillary or tube where the liquid moves, it is possible to calculate the volume and the flow rate, through Equation 3.23 [26]:

$$Q = \frac{\Delta_x}{\Delta_t}\pi r^2 \tag{3.23}$$

Where:
Q – flow rate, in mm^3/s;
Δx – liquid's displacement, in mm;
Δt – time interval, in s;
r – tube internal radius, in mm.

3.2.2.2. Drop method

The drop method is an optical method that measures the volume increase of a drop over time. Like other optical methods, a camera is used to capture images of the fluid, which in this case is in the form of a droplet. A software is then used to process the images, where the contours of the droplet are determined and the volume is calculated. With the variation in volume, in each image captured, and the time between the captures, it is possible to

calculate the flow rate. IPQ assumes that the shape of the drop is spherical and symmetrical around its axis. The calculation of the drop's volume, V, is done with Equation 3.24 [27, 28]:

$$V = \frac{4\pi}{3} R^3 \tag{3.24}$$

Where:

V – volume, in mm^3;

R – estimated drop radius, in mm.

3.3. Properties and flow behaviour of fluids

Rheology is the science of deformation and flow behaviour of matter under controlled testing conditions. It is an interdisciplinary field of material sciences, which describes the interrelation between force, deformation, and time, and derives from the Greek terms for flow (*rhi*) and science (*logos*) [29, 30, 31].

In medical and pharmaceutical applications, the knowledge of the physical properties of drugs and medicine, such as viscosity, is crucial to guarantee that right amount is being administered to the patient's bloodstream, when using drug delivery devices.

Flow can be described as the relative movement of adjacent particles of a fluid. There are two fundamental kinds of flow, these being shear flow and extensional flow. In shear flow, particles of the liquid flow over or past each other, while in extensional (or elongational, or stretching) flow, adjacent particles flow towards or away from each other (Figure 3.4) [31, 32].

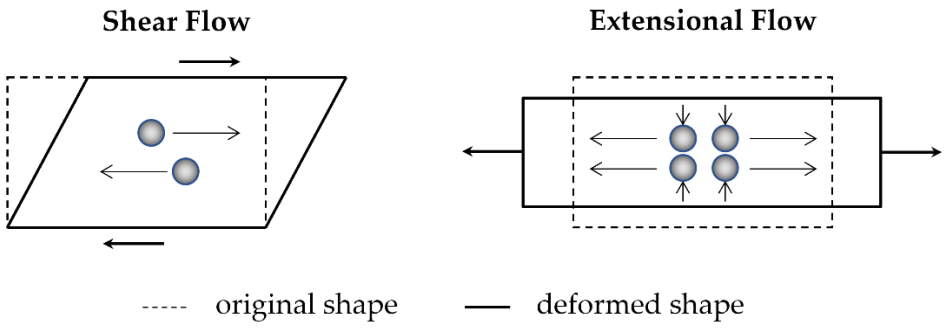

Figure 3.4 - Flow type

3.3.1. The two-plates model

The most common flow behaviour is shear flow. This kind of flow can be described by the two-plates model (Figure 3.5), in which the liquid can be imagined as hypothetical

layers sliding over one another, between two plates, with each layer moving faster than the one beneath it. The upper plate moves along at maximum velocity while the bottom plate is stationary. The movement of the upper plate subjects the fluid to a certain force, known as the shear force, F [32, 33].

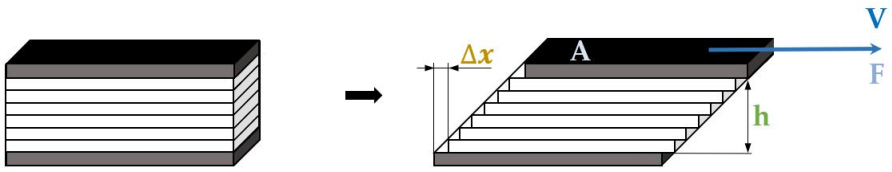

Figure 3.5 - Two-plates model

The shear force (that moves the upper plate), F, acting on the fluid per unit area (of the upper plate), A, is defined as the shear stress, τ, according to Equation 3.25.

$$\tau = \frac{F}{A} \left[\frac{N}{m^2} = Pa\right] \tag{3.25}$$

In response to the shear force, the upper layer moves a given distance from its state at rest, Δx, while the bottom layer remains stationary. Knowing the distance between the two plates, h, it is possible to define a displacement gradient known as the shear deformation or shear strain, γ, which is given by Equation 3.26. Shear deformation is dimensionless [32].

$$\gamma = \frac{\Delta x}{h} \left[\frac{m}{m}\right] \tag{3.26}$$

In the simplest form of shear flow, the relative movement of particles of a fluid increases the shear strain during the period of applied stress. Thus, it is possible to define a shear rate, $\dot{\gamma}$, also known as strain rate, which in the case of a liquid being sheared continuously between two plates is the gradient of the velocity in the direction at right angles to the flow, which is the rate of change of strain with time (Equation 3.27) [32, 33].

$$\dot{\gamma} = \frac{dV}{dh} = \frac{d\gamma}{dt} \left[\frac{m}{s.m} = \frac{1}{s}\right] \tag{3.27}$$

The coefficient of proportionality between the shear stress and shear rate is defined as the shear viscosity or dynamic viscosity, η, which is the quantitative measure of the friction between the moving particles of a fluid that is proportional to the velocity with which the particles are displaced (Equation 3.28). In other words, viscosity is the measure of a fluid's resistance to flow [31, 32].

$$\eta = \frac{\tau}{\dot{\gamma}} \left[Pa.s\right] \tag{3.28}$$

3.3.2. Viscosity

Viscosity can be referred to as either dynamic viscosity, absolute viscosity, simple viscosity, or, for day-to-day purposes, it is simply referred to as viscosity. The unit used to quantify viscosity is the pascal second; its symbol is $Pa.s$. For many liquids, it often convenient to use smaller, 'everyday' unit of the milli-pascal second, or $mPa.s$ rather than the pascal second. The viscosity that is measured using gravity is termed kinematic viscosity, ν, and is obtained by dividing the viscosity, η, by density of the fluid, ρ, according to Equation 3.29 [33, 34].

$$\nu = \frac{\eta}{\rho} \left[\frac{mm^2}{s}\right] \tag{3.29}$$

Currently, the internationally accepted standard values of the viscosity, η, of pure water at 20 °C and standard pressure are [33]:

$$\eta = 1.0017\ mPa.s$$

$$\nu = 1.0035 \frac{mm^2}{s}$$

These values can be used to calibrate viscometers or to standardise other liquids used for calibration.

Viscosity is not a constant. The most relevant influencing parameters include ambient conditions (temperature and pressure), inner structure of the fluid (chemical and physical composition), shear rate, time (shear time and relaxation time), miscellaneous (such as electric and magnetic field intensity), and pH value. Viscosity generally increases when pressure increases and/or temperature decreases. Out of all the influencing factors, temperature has the greatest effect on viscosity. Different materials show different temperature dependency, however, the higher the absolute value of viscosity, the higher the temperature dependency, i.e., the viscosity of higher-viscosity liquids, such as bitumen, decreases at a faster rate with the temperature than the lower-viscosity liquids, such as water [32, 33].

Having knowledge about the viscosity of a fluid, and how it may vary, is of high importance, since a particular viscosity is often needed to fulfil certain requirements. For manufacturers to be able to design and produce drug delivery devices, studies must be done on the fluids that these devices operate with, so that the viscosity range with which it is possible to work with becomes known [33].

3.3.3. Flow behaviour

When an external force acts on a material, the material will react to the imposed stress, exhibiting a certain deformation and flow behaviour. This behaviour depends mainly on the stressed material's inner structure, i.e., the architecture of its molecules, the amount of stress being applied, and the ambient conditions of the stressed material, most importantly the temperature. Thus, the essential elements of rheology are the material's inner structure, external force and ambient conditions [34].

Most materials are viscoelastic, made of a viscous portion and an elastic portion. While a liquid is a predominantly viscous material, a solid is a predominantly elastic material. The materials with the highest viscous portion are known as ideally viscous liquids, or Newtonian liquids.

3.3.3.1. Newtonian

The viscosity of Newtonian liquids is only a function of the temperature and pressure and not a function of outside stress (the applied shear rate) since the relation between shear rate, $\dot{\gamma}$, which is the gradient of the velocity in the direction at right angles to the flow, and shear stress, τ, which is the force that is produced when the fluid is sheared, does not change. I other words, the shear stress is linearly related to the shear rate [32, 34]. Therefore, at constant ambient conditions, i.e., at constant temperature and pressure, no matter how strongly they are sheared or stressed, ideally viscous liquids maintain their viscosity and always show the same flow behaviour, which does not include the display of any elastic properties or extensional anomalies [31, 34]. Water, mineral oil, bitumen, simple hydrocarbons, and dilute colloidal dispersions are examples of ideally viscous fluids [32].

3.3.3.2. Non-Newtonian

A non-Newtonian liquid's viscosity depends not only on the temperature and pressure, but also on the shear stress or shear rate imposed. Therefore, even if the ambient conditions are constant, the flow behaviour of these fluids constantly changes depending on time and external forces being applied. For most complex composition solutions, the viscosity usually decreases with the increase in shear rate or shear stress. Most fluids are non-Newtonian and can be classified as shear-thinning or shear-thickening fluids. For non-Newtonian shear thinning fluids, also known as pseudoplastic fluids, the viscosity, η, decreases with the increase in shear rate or shear stress, while for non-Newtonian shear thickening fluids, the viscosity increases with the shear increase [29, 34].

Shear-thinning or pseudoplastic flow is the most common type of non-Newtonian flow behaviour. At low enough shear rates, shear thinning fluids tend to show a constant viscosity value, known as the zero-shear viscosity plateau, or simply zero shear viscosity, η_0, which is given by Equation 3.30 [32, 34].

$$\eta_0 = \frac{\tau}{\dot{\gamma}_0} \tag{3.30}$$

Most suspensions and polymer structured materials are shear thinning.

3.3.4. Viscoelasticity

Most materials show rheological behaviour somewhere between that of liquid and solid, i.e., viscoelastic behaviour. This means that, whenever they are deformed, they store some of the deformation energy and lose the rest. To accurately describe a material's deformation and flow behaviour, the amount of energy the material stores and dissipates must be precisely determined. It is possible to combine springs and dashpots in such a way as to model or describe real viscoelastic behaviour [32, 34].

A material's elastic behaviour is based on its capacity to store energy. A spring is representative of a linear elastic solid that obeys Hooke's law. Hooke's law states that, for relatively small deformations of a solid, and as long as the elastic limit of the material is not exceeded, the applied deforming force, F, is proportional to the resultant deformation, S, according to Equation 3.31, where the proportional constant k is the spring constant and is a measure of the material's stiffness [29, 32, 34].

$$F = kS <=> k = \frac{F}{S} \tag{3.31}$$

When the applied force is removed, the spring returns to its initial shape. However, if the elastic limit is surpassed the spring will be permanently deformed.

These same principles can also be applied to simple shear (elastic) deformation, where Hooke's Law is expressed in terms of stress and strain. For relatively small stresses, stress is proportional to strain. Knowing the shear stress, τ, and the shear deformation, γ, via the two-plates model, it is possible to apply Hooke's law and define the constant of proportionality, which is the elastic modulus in shear, or shear modulus, G. The shear modulus, given by Equation 3.32, is the quantity for measuring a material's stiffness or resistance to deformation [32, 34].

$$G = \frac{\tau}{\gamma} \tag{3.32}$$

The flow behaviour of a purely elastic material shows no time dependence, meaning that when a stress is applied an immediate strain is observed and when the shear stress is removed the strain immediately disappears [32]. However, no shear modulus value is constant since it is influenced by several factors. The greatest influencer of a material's shear modulus is the temperature and, therefore, a shear modulus value can only be given for one reference temperature. A change in temperature means a change in shear modulus, and thus

a change in deformation and flow behaviour. The second vital factor is time. The shear modulus is a time-dependent value as a material's behaviour may change after being stressed for a certain amount of time [34].

A material with loose structure and unlinked molecules loses most of the energy as heat produced by internal friction, so it does not return to its original form, meaning that it shows viscous behaviour, also known as viscous shear heating. A material's viscous behaviour is based on the loss of energy [34]. Hooke's Law can be applied, via the two-plates model, to all viscoelastic materials and can be expressed in terms of stress and strain.

3.3.5. Experimental determination of fluid properties

Liquids are made to flow by imparting a velocity or by applying a force or displacement. It should be noted that all liquids are fluids but not all fluids are liquids. Fluids can either be gases or liquids. For a given velocity, the higher the viscosity, the greater the resulting force is, whereas for a given force, the higher the viscosity, the lower the velocity is. Higher viscosity liquids flow at a slower rate while low viscosity liquids flow at a faster rate [31].

Viscometry is the experimental technique used to measure the viscosity and flow properties of liquids by using gravity to generate flow in viscosity measuring instruments, such as flow cups and capillary viscometers. Inside these instruments, the liquid flows through a defined space within a given time, t, which is measured. Viscosity measured using gravity is called kinematic viscosity (mm^2/s). Although this method of measuring viscosity is reliable for Newtonian fluids, it is not for non-Newtonian liquids, since it is necessary to control the shear conditions to obtain precise measures, and it is not possible to control shear conditions of gravity [34].

Rheometry refers to the experimental technique used to determine the rheological properties of materials, using a rotational rheometer to generate force or displacement [31, 32]. Different viscosity values are measured in a continuous run, under changing conditions [34].

Viscometry is used only for Newtonian liquids, while Rheometry is used for all fluids and solids [34].

3.3.5.1. Rheometry

There are several rheological techniques for probing the viscoelastic behaviour of materials, including creep testing, stress relaxation and oscillatory testing. Oscillatory shear rheometry is the primary technique that is used to measure viscoelasticity on a rotational rheometer [32].

The rotational rheometer with coaxial or concentric cylinders, cone or plate and parallel plate geometries systems with a calculated flow field, gives absolute readings of the viscosity value [31]. The basic idea behind these setups is the Two-plates Model. All geometries consist of a measuring bob and a lower plate or cylindrical cup. The measuring bob is turned by the instrument's/rheometer's motor while the lower plate or cup stands still [34].

The most common rheological tests are rotational and oscillatory. In rotational tests, the measuring bob becomes a roundabout, and shears the sample by continued rotation. In oscillatory tests, the measuring bob becomes a pendulum, and shears the sample by oscillation [34]. Some parameters can be precisely controlled and precisely measured, such as the measuring system's deflection angle, φ, and the motor's torque, M, which is the amount of force the motor requires for the oscillation. These are the first and second set of raw data the rheometer gives [34].

3.3.5.1.1. Rotational tests

Rotational tests are performed to measure the flow behaviour of fluids by obtaining their flow curves and viscosity functions. When a liquid is rotated, it is possible to precisely observe how fast it rotates and how much force is applied to its rotation. In other words, its rotational speed, n, and its torque, M_d. There are two rotational test modes [29, 34].

In controlled shear rate (CR) tests, the rotational speed, n, or shear rate, $\dot{\gamma}$, is defined and controlled by the user and the shear stress, τ, is measured. Depending on the fluid's viscosity, while the measuring bob is rotating at the preset rotational speed it requires a certain torque, or a certain shear stress to shear the sample. With CR tests, certain process conditions can be simulated, like pipe flow [29, 34].

In controlled shear stress (CS) tests, the shear stress or torque is preset and controlled, and the shear rate or rotational speed of the measuring bob is measured. CS tests are used for measuring dispersions, gels and pastes. It is important that the shear rate conditions during the test come close or even replicate the real conditions to which the fluid will be submitted to, in order to have a clear measurement of how its viscosity will change under the defined conditions. If a CS test is performed, the rheometer starts at a shear rate or rotational speed of zero and is then gradually increased until the maximum is reached, over a defined period of time [29, 34].

3.3.5.1.2. Oscillation tests

Rheological oscillation tests are performed to measure the deformation and flow behaviour of materials. In these tests, a sinusoidal oscillation is applied by the rheometer. The controllable parameters of this wave are the maximum amplitude of the shear stress, τ_A,

in Pascal, which defines the motor's torque, the maximum amplitude of the deformation or strain, γ_A, given in percent, which is the deflection angle, the frequency, f, in hertz, or the angular frequency, ω, in radians per second, which defines the speed of the oscillation, as well as the temperature, T, in Kelvin [29, 34].

In oscillation tests, two modes can be used to study a sample. In the controlled shear stress (CS) mode, it is possible to control and preset the time-dependent shear stress, τ_A, that the rheometer produces. The sample is stressed according to the preset oscillating torque, causing it to deform spatially. This deformation, known as the angular displacement, γ_A is the quantity that is measured in CS tests. In the controlled shear strain or deformation (CD) mode, it is possible to control and preset the time-dependent shear strain, γ_A. The rheometer oscillates at the defined rotational speed, or angular displacement, at any given point of the measurement, and the motor's torque, or shear stress amount, τ_A, required to maintain the preset speed, or to reach the preset displacement is measured [29, 32, 34].

Whichever test mode that is chosen to work with, both the shear stress and shear deformation or strain values for the sample are obtained.

Oscillation tests include amplitude sweeps and frequency sweeps.

3.3.5.1.2.1. Amplitude sweeps

Amplitude sweep tests are performed at a constant temperature and a constant frequency, but with increasing amplitudes. During the amplitude sweep, the sample is increasingly sheared until it reaches its breaking point, where its structure begins to yield, i.e., break, and is permanently deformed. All fluids with viscoelastic behaviour have a linear viscoelastic range, LVR, which is the range where the sample's structure is not destroyed by the increasing shear. Within this non-destructive deformation range, the stress and strain are proportional, and the sample's storage modulus, G', and the loss modulus, G'', values remain constant. Thus, Hooke's Law applies and the material shows a constant stiffness. These values represent the elastic and viscous portions of the sample's viscoelastic behaviour, respectively. The value at the limit of the LVR is called yield point or yield stress, γ_y [29]. This corresponds to the point at which the sample becomes stress or strain dependent. On a flow curve that plots shear stress against shear rate, the yield point value is in the interception of the y-axis (the shear stress axis). Materials without a yield point immediately flow under any shear stress, so their flow curve begins at the origin (zero). These materials behave like fluids at rest [32, 34].

3.3.5.1.2.2. Frequency sweeps

Frequency sweep tests are performed at constant amplitude and constant temperature, but with variable frequencies, meaning that the speed of the oscillation is

changed during the test. This way, frequency sweeps give information regarding the dependence of the dynamic viscosity, η', with the angular frequency, ω. The preset constant amplitude must not exceed the limiting strain value. Therefore, frequency sweeps need to be performed within the sample's LVR, hence the need to perform an amplitude sweep first. Frequency sweeps are also used to investigate time-dependent behaviour of fluids by varying the frequency of the applied stress or strain. Since $\omega \approx 1/t$, by subjecting a sample to low frequencies, it is possible to simulate its long-term behaviour, approximating it to its behaviour at rest, which gives information about its long-term storage stability. If it shows a consistently dominant G' value, it will remain stable in storage due to the strength of its internal network forces. If it shows a consistently dominant G'' is will behave like a viscous liquid, which means it will probably separate and it too unstable for long-term storage. To simulate the short-term behaviour of a sample higher frequencies are used [29, 32].

4. MATERIALS AND METHODS

In this chapter, the instruments and equipment used at the Volume and Flow Laboratory (LVC) and the Liquid Properties Laboratory (LPL) for all the experiments and tests are presented.

4.1. LVC materials and methods

The materials used in the flow calibration methods during the development of this work are presented below, as well as the uncertainty results obtained by IPQ from measurements prior to this dissertation.

4.1.1. Environmental conditions

The ambient temperature and relative humidity are controlled, in order to keep the environmental conditions constant throughout the tests. The temperature working interval is [17; 23] °C and the relative humidity must be greater than 50%.

4.1.2. Calibration liquids

Tests were performed using type 1 water according to ISO 3696 [35], produced through a Millipore's Direct Q system. The density is determined by means of an equation determined experimentally by the Properties of Liquids Laboratory. Other calibration liquids, described in chapter 4.2, were used to calibrate the BBraun infusion pump.

4.1.3. Thermometer

The temperature of water and other fluids was measured by means of a thermometer from Luft model C100, with a resolution equal to 0.001 °C.

4.1.4. Thermometer hygrometer

The measurement of the relative humidity and air temperature was done with a Thermo hygrometer from Hygroclip model Multisens, which has a resolution and uncertainty equal to 0.1% and 0.1 °C.

4.1.5. Barometer

The atmospheric pressure was measured with a barometer from Druck model DPI142 model, with a resolution equal to 0.01 hPa.

4.1.6. Camera

The camera from Alvium model 1800U-1240 was used to capture the meniscus displacement. The camera was mounted on an aluminium support system that allowed for adjustment in two directions in the horizontal plane (x, y) and in the vertical plane (z), and rotation.

4.1.7. LED lamp

A LED lamp is pointed to the capillary tube to highlight the meniscus, in the front tracking method, and is pointed to the evaporation trap to highlight the droplet in the drop method.

4.1.8. Balance

To determine the liquid's mass a balance Mettler model AX26 was used. The balance is calibrated annually and has a 0.001 mg resolution and a 0 to 20.0 g measuring range.

4.1.9. Calibrating vessel

A 6 mL calibrating vessel with an evaporation control system (i.e., evaporation trap) was used.

4.1.10. Flow calibration methods

4.1.10.1. Gravimetric method

The gravimetric method is considered the "primary method" for microflow rate calibrations and is validated down to 2 μL/min in Europe. The IPQ is able to measure flow rates as low as 0.05 μL/min with an uncertainty of 6% (k=2), but its CMC only goes down to 120 μL/h [22, 36]. This method was used as the primary measurement reference throughout this dissertation.

4.1.10.2. Optical methods

4.1.10.2.1. Front tracking method

The results obtained with the experimental setup used at the IPQ, shown in Figure 4.1 are presented in Table 4.1.

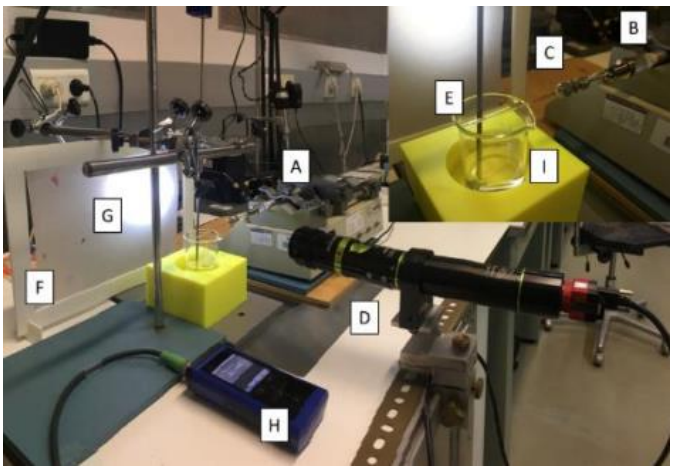

Figure 4.1 - Front tracking experimental setup at IPQ

Legend: (A) flow rate generator, (B) glass syringe, (C) stainless-steel tube, (D) camera, (E) glass capillary tube, (F) translucid paper, (G) LED lamp, (H) thermometer.

Table 4.1 – Results of flow rate measurements using the IPQ front tracking setup

Nominal flow rate / (μL/h)	Measured flow rate / (μL/h)	Relative Error / %	Relative Uncertainty / %
1	0.99	0.87	6.9
10	9.97	0.29	3.0
100	99.6	0.39	2.1
500	499.8	0.05	1.4
1000	997.1	0.30	1.5

4.1.10.2.2. Drop method

The results obtained with the experimental setup used at the IPQ, shown in Figure 4.2 are presented in Table 4.2.

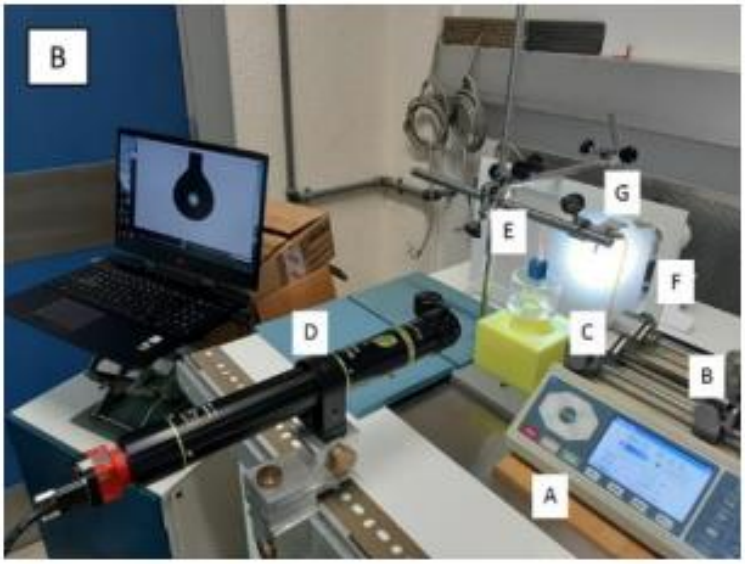

Figure 4.2 – Drop method experimental setup at IPQ

Legend: (A) flow rate generator, (B) glass syringe, (C) teflon tube, (D) camera, (E) evaporation trap, (F) translucid paper, (G) LED lamp.

Table 4.2 – Results of flow rate measurements using the IPQ drop method setup

Nominal flow rate / (µL/h)	Measured flow rate / (µL/h)	Relative Error / %	Relative Uncertainty / %
1	1.3	-20.4	87.2
10	10.1	-1.0	30.4
100	104.1	-4.0	9.8
500	519.1	-3.7	4.4
1000	1052.0	-4.9	3.2

The MeDDII project aims to develop and validate calibration procedures with traceability to a primary standard with a target uncertainty value of 2% for a range of 5 nL/min (0.3 µL/h) up to 600 mL/min ($3.6 \cdot 10^7$ µL/h) [6]. Table 4.1 shows that for flow rates lower than 10 µL/h the uncertainty values (> 3 %) are superior to the targeted value (2%). Table 4.2 shows that for all the flow rates the uncertainty values (> 3 %) are superior to the targeted value (2%).

4.2. LPL materials and methods

In clinical treatments most of the drug solutions used in multi-infusion systems are water-based solutions behaving like ideal viscous liquids and therefore behaving as Newtonian liquids when under flow. However, when the perfusion occurs within the μL/min range, some of the drugs with more complex composition, such as protein or particle-based, show viscoelastic flow behaviour, meaning that their viscosity depends on the flow rate imposed. This is the case of propofol, the drug used almost always to induce general anesthesia by using manually programmed infusion pumps or computer-controlled infusion pumps in a process called target controlled infusion (TCI). However, even though perfusion systems are widely used in therapeutics to infuse a multitude of drugs, few are the published studies about the influence of drugs physical properties, namely rheological, on the accuracy and uncertainty of the flow rate of these instruments. In addition, these infusion systems are only calibrated with water, which is a Newtonian liquid [37].

4.2.1. Materials

In the work developed at the LPL, Newtonian solutions similar to the ones used in medical applications were produced. Other than these liquids, non-Newtonian liquids were also submitted to rheological tests.

4.2.1.1. Non-Newtonian test fluids

Propofol (10 mg/mL, Noramed), dobutamine (12,5 mg/mL, Generis), dopamine (chloridrated) (40 mg/mL, Medinfar) and gelaspan (BBraun, 40 mg/mL) are commonly used drugs in multi-infusion systems for clinical applications. It is therefore important to characterize some of their most relevant physical properties, such as density and dynamic viscosity using conventional measurement methods able to produce results traceable to the SI units. For that, research on the fluid's mechanical behaviour within the flow rate interval of interest is necessary.

Propofol is used during general anesthesia for surgery or other medical procedures and to sedate patients under critical care that need a mechanical ventilator [38]. Propofol is not an aqueous solution but a protein-based solution that shows non-Newtonian behaviour for low flow rates. Propofol is insoluble in water, and it is formulated as a white oily intralipid-based emulsion. In addition to the active ingredient, propofol, the solution contains medium chain triglycerides, refined soybean oil, glycerol, egg lecithin, sodium oleothane, sodium hydroxide, and water for injections [39].

Dobutamine is a prescription medicine used to treat the symptoms of cardiac decompensation. In general, dobutamine solutions contain sodium bisulfite, hydrochloric acid, and/or sodium hydroxide [40].

Dopamine is a catecholamine, a family that also includes the neurotransmitters norepinephrine and epinephrine [41]. The presence of a benzene ring with this amine attachment makes it a substituted phenethylamine, a family that includes numerous psychoactive drugs. In general, dopamine solutions contain sodium metabisulfite, citric acid and sodium citrate buffer, hydrochloric acid, or sodium hydroxide [40].

Gelaspan is a colloidal substitute of plasma volume, with 4 % relative density solution of succinylated gelatine with an average molecular weight of 26 500 Da in a plasma–adapted, balanced isotonic electrolyte solution, used for the prophylaxis and treatment of hypovolemia and shock. The negative charges introduced into the molecule by succinylation cause an expansion of the molecule [42, 43].

4.2.1.2. Newtonian test fluids

Eight Newtonian liquids (Figure 4.3), with different compositions, were produced at the Laboratory of Properties of Liquids (LPL). The mass fractions, in cg/g, of sodium chloride, glucose and glycerol of these aqueous solutions are presented in Table 4.3. Tartaric acid (3 g/L) was added, as a preservative, to all solutions containing glucose, as per recommendation 124 from OIML [44]. In appendix C, information about how the composition of solutions A to H were obtained is presented.

Table 4.3 – Composition of solutions A-H

Solution	Description
A	Saline solution (0.9 cg/g)
B	Glucose solution (10 cg/g)
C	Glucose solution (20 cg/g)
D	Sodium chloride (0.22 cg/g) and glucose (2.75 cg/g) solution
E	Sodium chloride (0.22 cg/g) and glucose (5.55 cg/g) solution
F	Sodium chloride (0.45 cg/g) and glucose (5.54 cg/g) solution
G	Glycerol solution (52.04 cg/g)
H	Glycerol solution (58.8 cg/g)

Figure 4.3 - Bottled 500 mL of solutions A-H

4.2.2. Methods

The viscosity of the Newtonian samples was measured by capillary viscometers, while the viscosity and flow behaviour of the non-Newtonian samples were measured by a rotational rheometer. The density of all samples was measured by a oscillation-type density meter.

4.2.2.1. Viscometry

The kinematic viscosity of the Newtonian solutions A-H was measured with adequate glass capillary viscometers, in the temperature interval from 20 C to 30 °C.

To determine which capillary viscometer was the most appropriate to measure each sample, the nominal kinematic viscosity, ν, in $mm^2 \cdot s^{-1}$, was calculated according to Equation 3.29, where the nominal values of density, ρ, in $g \cdot cm^{-3}$, and dynamic viscosity, η, in mPa·s, where obtained using Annex D. The calculated nominal dynamic viscosity value of each sample is presented in Table 4.4, as well as the chosen capillary viscometer, which was chosen based on its constant K value.

Table 4.4 – Nominal dynamic viscosity of solutions A-H

Solution	$\nu_{20\,°C}$ / $(mm^2 \cdot s^{-1})$	Capillary viscometer	K / $(mm^2 \cdot s^{-2})$
A	1.013	VC02A	0.002804
B	1.282	VC03B	0.003212
C	1.763	VC05B	0.005023
D	1.008 – 1.125	VC03B	0.003212
E	1.008 – 1.282	VC03B	0.003212
F	1.013 – 1.282	VC03B	0.003212
G	5.909	VC08B	0.01006
H	8.697	VC12A	0.02977

For each sample the viscosity was obtained based on the measured time it took for the solution to cross the volume between the lines shown in Figure 4.4.

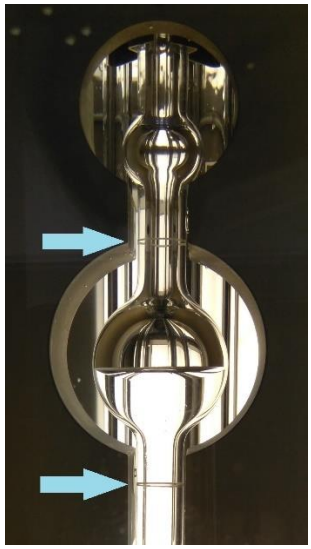

Figure 4.4 - Capillary viscometer

The kinematic viscosity measurement results of solutions A-H, performed with the different glass capillary viscometers, in the temperature interval from 20 C to 30 °C, are presented in Table 4.5.

Table 4.5 - Kinematic viscosity measurement results of solutions A-H performed with glass capillary viscosity meters in the temperature interval from 20 C to 30 °C

Solution	Kinematic viscosity				Viscosity-temperature coefficient	
	at 20 °C		at 30 °C			
	$\nu_{20\,°C}$ / ($mm^2 \cdot s^{-1}$)	$U_{\nu_{20\,°C}}$ / ($mm^2 \cdot s^{-1}$)	$\nu_{30\,°C}$ / ($mm^2 \cdot s^{-1}$)	$U_{\nu_{30\,°C}}$ / ($mm^2 \cdot s^{-1}$)	$\alpha_{\nu\ 20-30\,°C}$ / (K^{-1})	$U_{\alpha_{\nu\ 20-30\,°C}}$ / (K^{-1})
A	1.057	0.046	0.839	0.024	-0.02062	0.00090
B	1.336	0.059	1.048	0.031	-0.02156	0.00094
C	1.807	0.078	1.396	0.041	-0.02274	0.00098
D	1.102	0.051	0.884	0.026	-0.01978	0.00092
E	1.169	0.080	0.931	0.027	-0.02036	0.00140
F	1.185	0.052	0.936	0.027	-0.02101	0.00093
G	6.060	0.253	4.270	0.122	-0.02954	0.00123
H	17.95	0.760	6.100	0.175	-0.06602	0.00279

Notes: *U* expanded for *k* = 2,00; the viscosity-temperature coefficient was calculated for the temperature interval from 20 °C to 30 °C with equation: $\nu_t = \nu_{20}(1+\alpha\,(t-20))$

4.2.2.2. Rheometry

A rotational rheometer (Mars III, HAAKE ThermoScientific), shown in Figure 4.5 was used do carry out rotational and oscillation tests of the chosen non-Newtonian fluids.

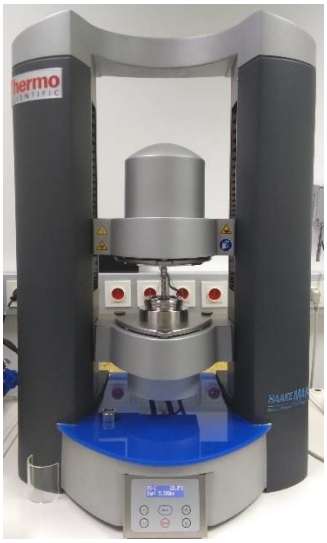

Figure 4.5 – Rotational rheometer Mars III HAAKE ThermoScientific

4.2.2.2.1. Rotational tests

With rotational tests the viscosity and flow curves of the different liquids were obtained. All samples were tested in controlled stress (CS) step mode, at 20 °C, in which the shear stress was controlled, and the shear rate was determined. The values from the viscosity curves of the propofol and dopamine samples were obtained using a double-gap concentric cylinder (CC27 Dg Ti) measuring geometry, in the shear stress interval from 0,0001 Pa to 0,5 Pa, while the dobutamine and gelaspan samples were tested in a concentric cylinder (CC25 DIN Ti) measuring geometry, in the shear stress interval from 0,0005 Pa to 0,2 Pa.

The flow rates values, Q_{rot}, in $m^3 \cdot s^{-1}$, were calculated according to Hagen-Poiseuille's equation (Equation 4.1), from the shear rates values, $\dot{\gamma}$, in s^{-1}, assuming a flow in a tube of radius, $\boldsymbol{r}$, in m.

$$Q_{rot} = \dot{\gamma} \frac{\pi r^3}{4} \tag{4.1}$$

4.2.2.2.1.1. Propofol

The propofol sample, exhibited a non-Newtonian shear thinning behaviour, in the low shear rate regime, between 0.11 s^{-1} and 2.11 s^{-1}, i.e., the viscosity decreases as shear rate increases, as illustrated in Figure 4.6. This flow behaviour may be caused due to propofol's lipidic emulsion kind of solution. At higher shear rates, within the interval from 6 s^{-1} to 258 s^{-1}, a constant viscosity plateau is observed, called the infinite shear viscosity plateau, η_∞. Therefore, the sample shows ideally viscous flow behaviour.

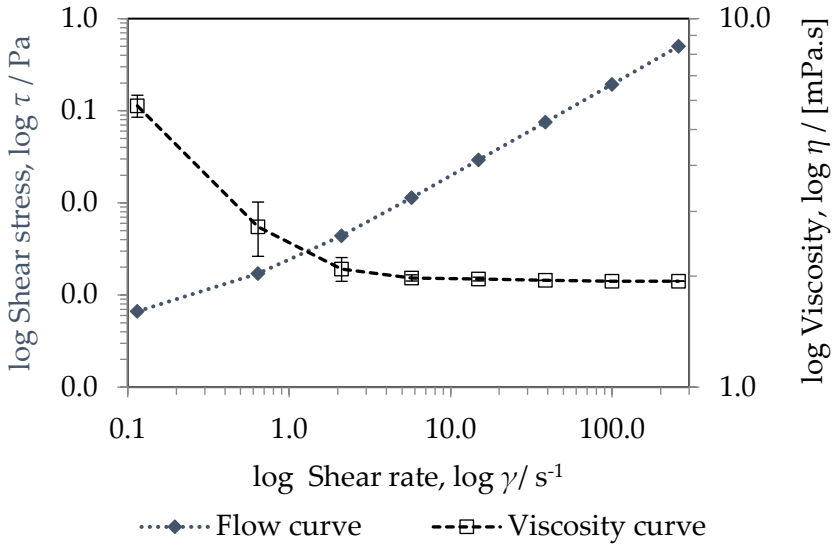

Figure 4.6 - Propofol flow and viscosity curves

4.2.2.2.1.2. Dobutamine

In the low shear rate regime (below 0.44 s^{-1}) the dobutamine sample shows a constant viscosity value, known as the zero-shear viscosity plateau, η_0 (Figure 4.7). Then, after passing the critical shear rate the sample enters the shear-thinning region where viscosity decreases as shear rate increases, exhibiting a non-Newtonian shear thinning behaviour. At higher shear rates, within the interval between 4.6 s^{-1} and 120 s^{-1}, the infinite shear viscosity plateau, η_∞, is reached, meaning that the viscosity of the sample remains constant, therefore showing ideally viscous flow behaviour.

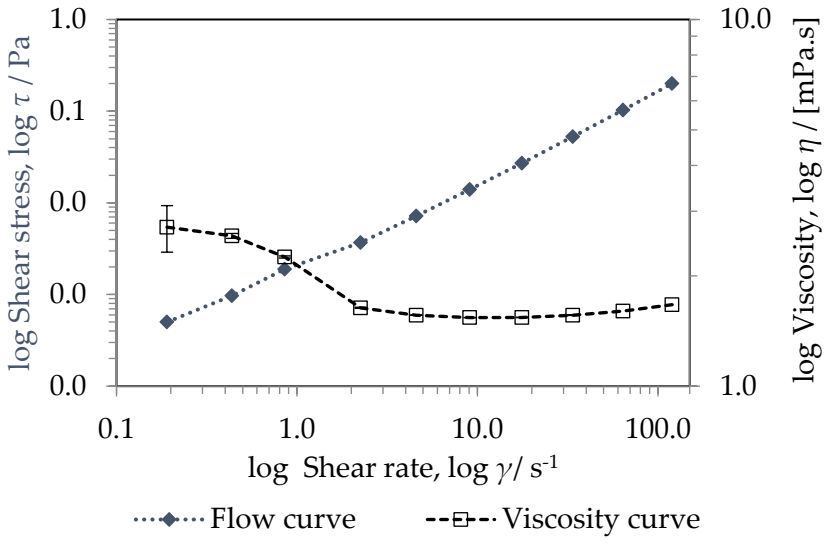

Figure 4.7 - Dobutamine flow and viscosity curves

4.2.2.2.1.3. Dopamine

In the shear rate regime between 1.67 s^{-1} and 12.91 s^{-1} the dopamine sample's viscosity (Figure 4.8) decreases with the increase of shear rate, exhibiting a non-Newtonian shear-thinning behaviour. The viscosity of the sample remains constant, within the shear rate interval from 12.91 s^{-1} to 356 s^{-1}, thus showing ideally viscous flow behaviour.

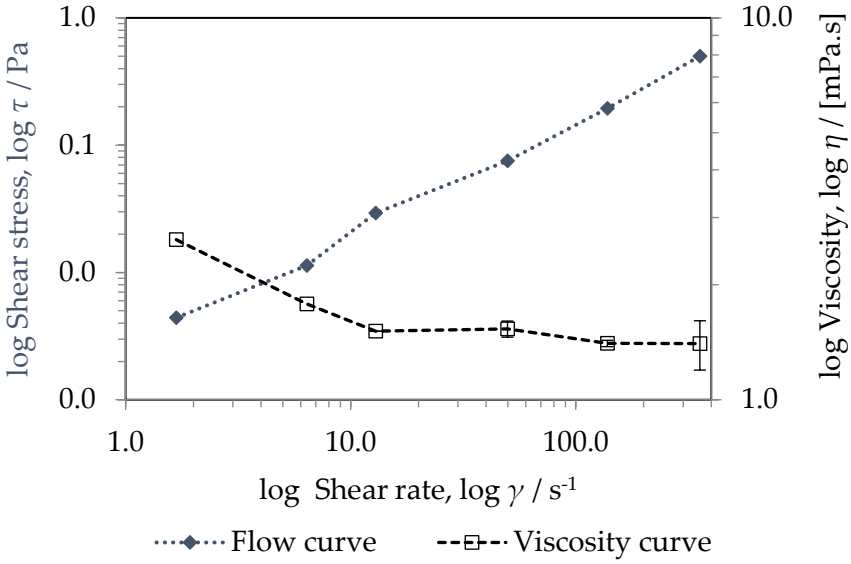

Figure 4.8 - Dopamine flow and viscosity curves

4.2.2.2.1.4. Gelaspan

The gelaspan viscosity decreases with the increase of shear rate, in the low shear rate regime, between 0.12 s^{-1} and 1.36 s^{-1}, exhibiting non-Newtonian shear thinning behaviour (Figure 4.9). This flow behaviour may be explained by gelaspan being a colloid, which is a high molecular weight substance. The change and position of a particle influences surrounding particles. Particles within a certain spatial range undergo elastic deformation in response to the imposed shear. During this process, a reference particle retains its original neighbours until the stress generated by shear is sufficient to cause local configurational rearrangement. Although colloidal forces dictate the form of the dispersion at low shear rate, when the shear rate is greater than the critical value, the viscosity begins to decrease.

The viscosity of the sample remains constant, within the shear rate interval from 3 s^{-1} to 74 s^{-1}, thus showing ideally viscous flow behaviour.

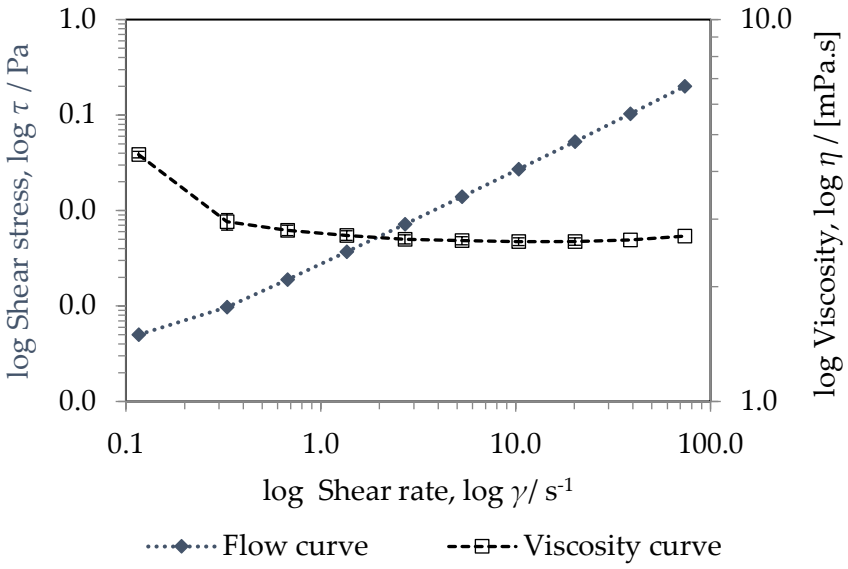

Figure 4.9 - Gelaspan flow and viscosity curves

4.2.2.2.1. Oscillation tests

Rheological oscillation tests were performed to measure the deformation and flow behaviour of the tested samples. All samples were tested at 20 °C in controlled deformation (CD) mode, i.e., with a pre-set deformation, γ, to obtain shear stress values.

For each sample, amplitude and frequency sweep tests were performed. The amplitude sweep tests were performed in the shear strain interval, γ, from 0,01 to 100 % (log ramp), at a constant angular frequency, ω, of 10 rad/s, to determine the linear viscoelastic range, LVR. The frequency sweeps results were obtained at a constant shear strain (amplitude), γ, of 1 % inside the LVR, for an angular frequency interval, ω, of 100 to 1 rad/s.

4.2.2.2.1.1. Amplitude sweep

Figures 4.10-4.13 show that, for each sample, the G' and G'' values remain constant within the shear strain interval, γ, from 0.1 to 100 % (log ramp). This means that this interval of strain is included in the LVR of all the samples, and that selecting a shear strain from this interval for the frequency sweep tests will not cause destruction of the fluid's structure. All the tested fluids show predominant and constant viscous behaviour, since there is no elastic portion ($G'=0$), meaning that the samples are liquid-like at rest.

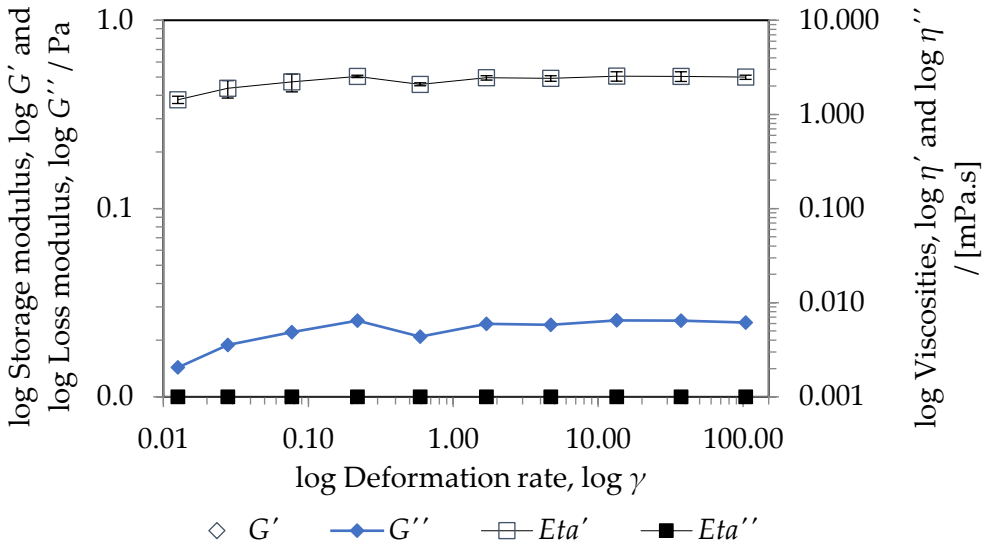

Figure 4.10 – Propofol amplitude sweep results

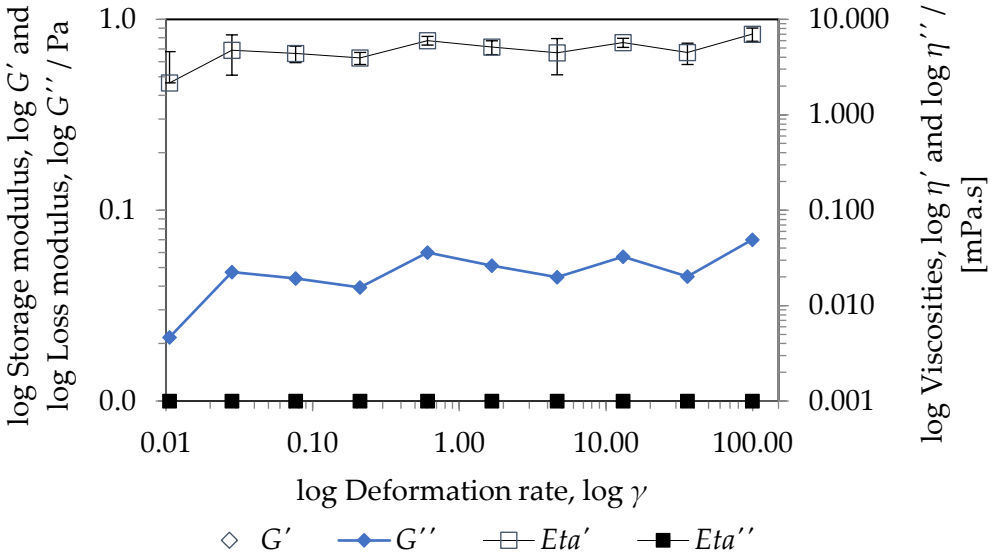

Figure 4.11 – Dobutamine amplitude sweep results

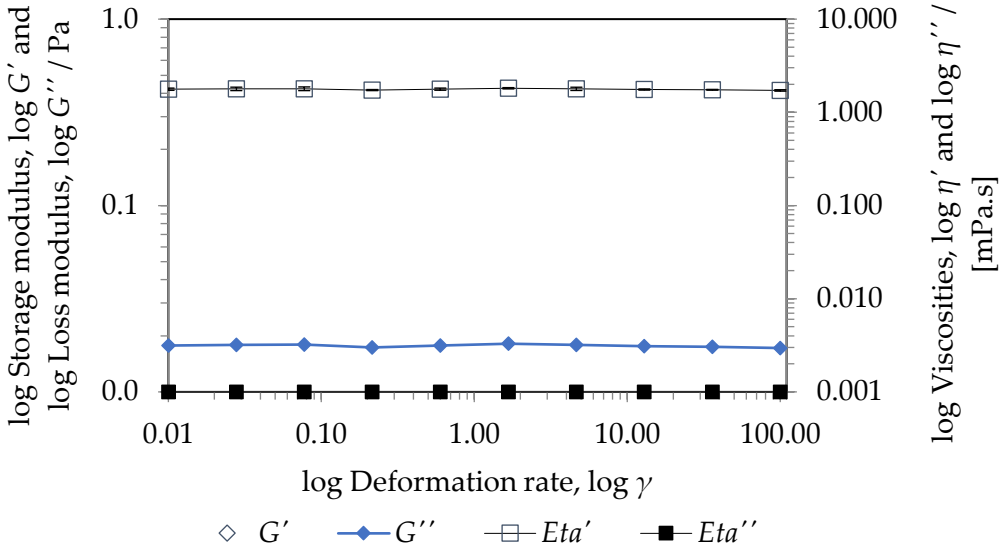

Figure 4.12 – Dopamine amplitude sweep results

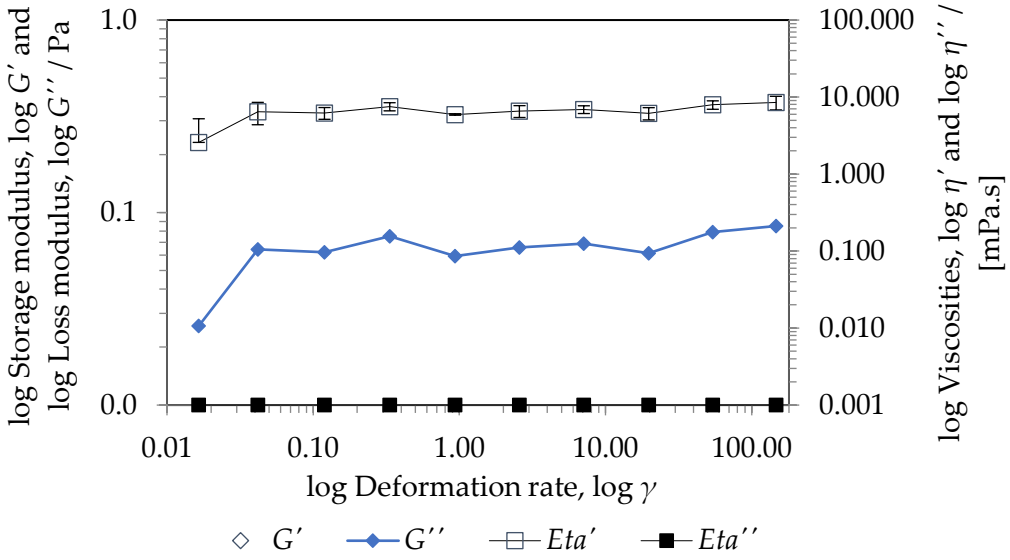

Figure 4.13 - Gelaspan amplitude sweep results

4.2.2.2.1.2. Frequency sweep

Based on the results of the amplitude sweep, a deformation, γ, of 1 % was selected to perform the frequency sweeps. Under these conditions, propofol sample exhibits viscoelastic liquid behaviour, behaving mainly viscous over the entire measuring range (Figure 4.14). The sample shows increasing viscous behaviour ($G' < G''$) with the increase in angular frequency, ω. For low angular frequencies (ω < 0,15 rad/s) the dynamic viscosity, η' decreases as the ω increases.

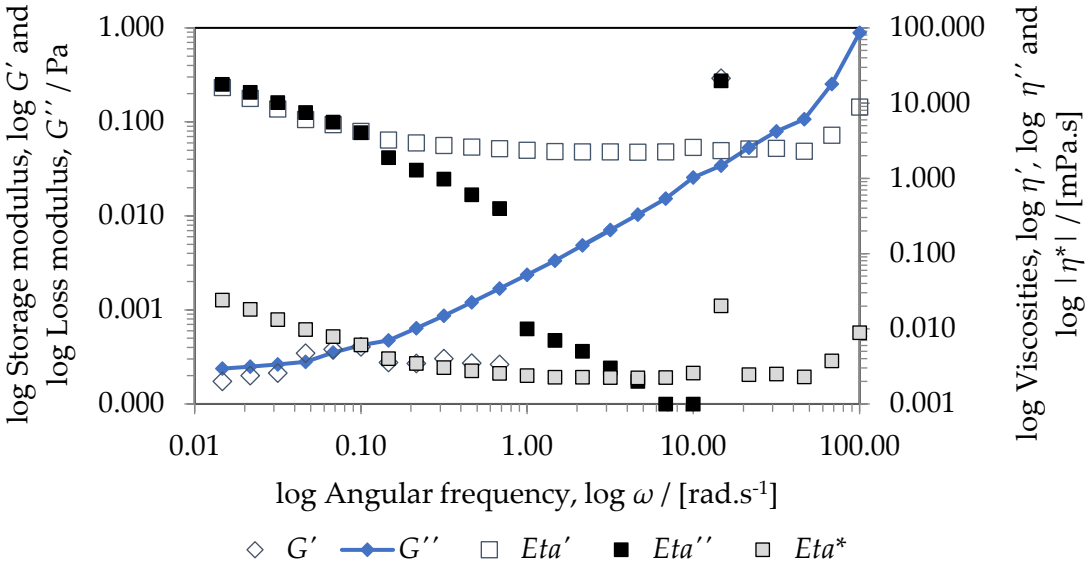

Figure 4.14 - Propofol frequency sweep results

Under the defined conditions, the dobutamine curve (Figure 4.15) shows that the loss modulus, G'', dominates at all frequencies. Therefore, dobutamine exhibits a predominant viscous behaviour, not only when sheared but also at rest. This predominant viscous behaviour at rest may suggest poor long-term storage stability, with particle sedimentation with time. The sample's viscous behaviour ($G' < G''$) increases with the increase in the angular frequency, ω. The dynamic viscosity, η', steadily decreases as the ω increases, reaching a plateau at 3.16 rad/s. It then begins to increase for angular frequencies higher than 10 rad/s. This increase can be explained by the appearance of inertial secondary flow patterns, known as Taylor vortices, that arise when high speed testing of low viscosity fluids is performed in concentric-cylinder geometry systems with a rotating bob and a fixed cup (such as the one used to test this sample - CC25 DIN Ti), in which, above a critical value of shear rate, the superposition of the laminar flow by the Taylor vortices increases the energy dissipation. This extra dissipation caused by the vortices can be misinterpreted as an increase of viscosity, since it causes an erroneous increase of the measured torque and the calculated viscosity of the sample. This phenomenon is difficult to avoid.

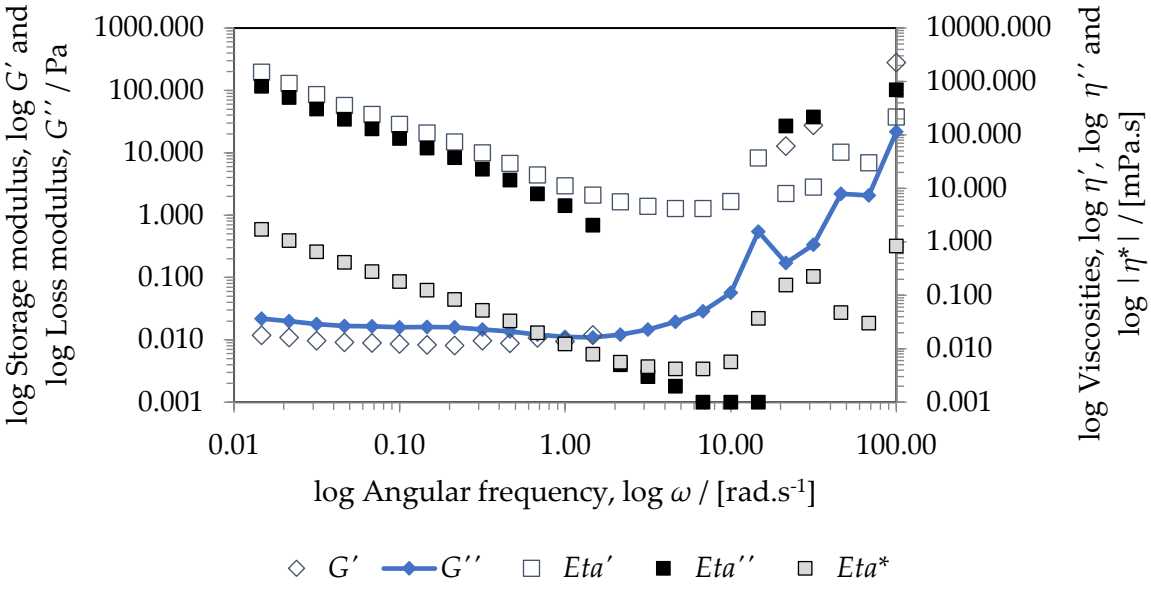

Figure 4.15 - Dobutamine frequency sweep results

Under the test conditions, the dopamine curve (Figure 4.16) shows that the storage modulus, G', dominates at lower frequencies ($G' > G''$). This means that dopamine exhibits a more predominant elastic behavior at rest and at angular frequencies up to 1.47 rad/s. From this point onwards, dopamine shows predominate viscous behaviour ($G' < G''$) that increases with the increase in angular frequency, ω. Since the predominant behaviour at rest is elastic, dopamine has a better long-term storage stability. Similarly, to the dobutamine sample, dopamine's dynamic viscosity, η', steadily decreases as the ω increases, reaching a plateau at 3.16 rad/s, and then increases for angular frequencies higher than 10 rad/s, which can also be explained by Taylor vortices.

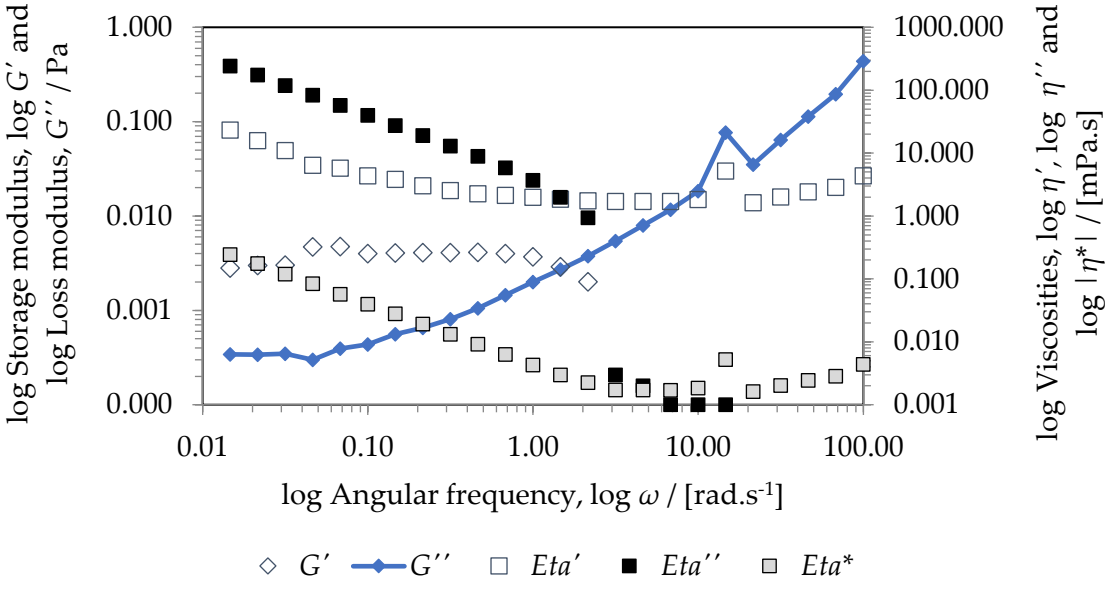

Figure 4.16 - Dopamine frequency sweep results

Under the test conditions, the gelaspan curve (Figure 4.17) shows that the loss modulus, G'', dominates at all frequencies. Therefore, gelaspan shows predominant viscous behaviour, not only when sheared but also at rest, which indicates a deficient long-term storage stability. Gelaspan shows increasing viscous behaviour (G'') with an increase in angular frequency, ω. For low angular frequencies (ω < 0.046 rad/s) the dynamic viscosity, η', decreases as the ω increases. It then remains constant until a frequency of 10 rad/s is reached. From then onwards, the viscosity increases, phenomenon which, as previously, can be explained by turbulent flow effects in the measuring geometry gap.

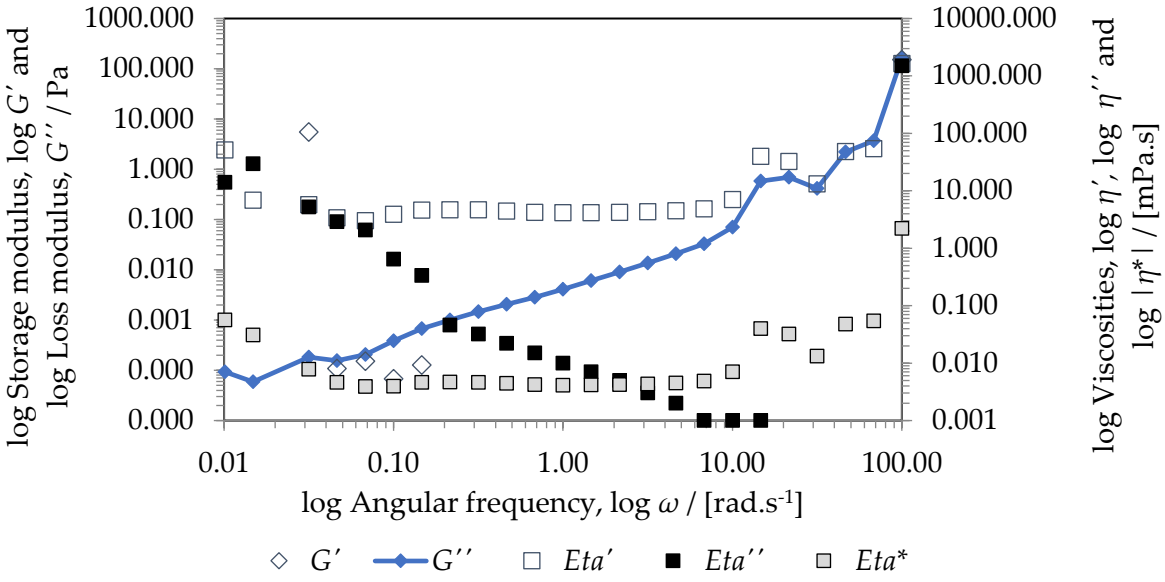

Figure 4.17 - Gelaspan frequency sweep results

4.2.2.3. Density determination

The density, ρ, of all the samples was measured with an oscillation-type density meter DMA 5000 (Anton Paar), shown in Figure 4.18, with a 10^{-3} kg·m^{-3} density resolution and a temperature resolution of 0,001 °C).

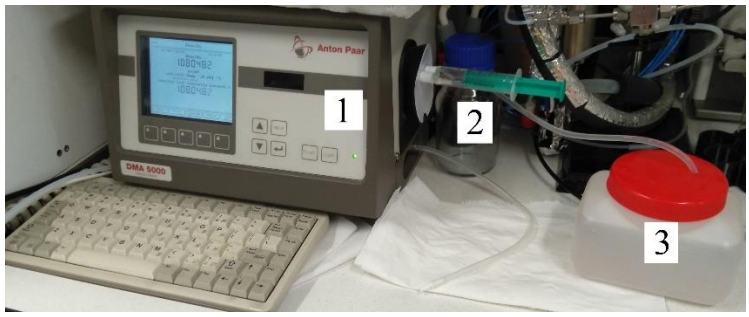

Figure 4.18 – Density measurement experimental setup. Label: (1) oscillation-type density meter DMA 5000 (Anton Paar), (2) BBraun syringe, (3) waste reservoir

The density of the non-Newtonian fluids, previously measured at IPQ, and which results are presented in Table 4.6, was measured in the temperature interval from 20 °C to 24 °C, while the Newtonian fluids' density was measured in the temperature interval from 20 °C to 30 °C. The density dependence on temperature $\rho(t)$ was fitted according to a 2nd degree polynomial equation.

Table 4.6 – IPQ density measurement results of the non-Newtonian fluids performed with an oscillation-type density meter (DMA 5000, Anton Paar) in the temperature interval from 20 C to 24 °C

Fluid	ρ, 20 °C / [g·cm^{-3}]	$U_{\rho,\ 20\,°C}$ / [g·cm^{-3}]	Coefficients of a 2nd degree polynomial $\rho(t) = at^2 + bt + c$			$U_{\rho,pol[20\text{-}24]\ °C}$
			a / [g·cm^{-3}·°C^{-2}]	b / [g·cm^{-3}·°C]	c / [g·cm^{-3}]	
Propofol	0.9965	$2.0\cdot10^{-5}$	$-4.9661\cdot10^{-6}$	$-8.6823\cdot10^{-5}$	1.0003	$2.0\cdot10^{-5}$
Dobutamine	1.0014	$7.0\cdot10^{-6}$	$-4.7306\cdot10^{-6}$	$-2.8330\cdot10^{-5}$	1.0039	$7.0\cdot10^{-6}$
Dopamine	1.0099	$8.0\cdot10^{-6}$	$-4.1399\cdot10^{-6}$	$-7.0511\cdot10^{-5}$	1.0130	$9.0\cdot10^{-6}$
Gelaspan	1.0174	$2.0\cdot10^{-5}$	$-4.3962\cdot10^{-6}$	$-6.8068\cdot10^{-5}$	1.0205	$2.0\cdot10^{-5}$

The density measurement results of solutions A-H performed with an oscillation-type density meter (DMA 5000, Anton Paar) in the temperature interval from 20 C to 30 °C are presented in Table 4.7.

Table 4.7 - Density measurement results of solutions A-H performed with an oscillation-type density meter (DMA 5000, Anton Paar) in the temperature interval from 20 C to 30 °C

Solution	ρ, 20 °C / [g·cm^{-3}]	$U_{\rho,\ 20\,°C}$ / [g·cm^{-3}]	ρ, 30 °C / [g·cm^{-3}]	Coefficients of a 2nd degree polynomial $\rho(t) = at^2 + bt + c$			$U_{\rho,pol[20-30]\ °C}$
				a / [g·cm^{-3}·°C^{-2}]	b / [g·cm^{-3}·°C]	c / [g·cm^{-3}]	
A	1.0046	$3.3\cdot10^{-5}$	1.0019	$-4.5824\cdot10^{-6}$	$-4.0771\cdot10^{-5}$	1.0073	$3.3\cdot10^{-5}$
B	1.0387	$3.3\cdot10^{-5}$	1.0357	$-4.0106\cdot10^{-6}$	$-1.0529\cdot10^{-4}$	1.0424	$3.3\cdot10^{-5}$
C	1.0805	$3.3\cdot10^{-5}$	1.0770	$-3.3993\cdot10^{-6}$	$-1.8313\cdot10^{-4}$	1.0855	$3.3\cdot10^{-5}$
D	1.0108	$3.3\cdot10^{-5}$	1.0081	$-4.5079\cdot10^{-6}$	$-4.8687\cdot10^{-5}$	1.0136	$3.3\cdot10^{-5}$
E	1.0207	$3.3\cdot10^{-5}$	1.0179	$-4.2373\cdot10^{-6}$	$-7.3898\cdot10^{-5}$	1.0239	$3.3\cdot10^{-5}$
F	1.0224	$3.3\cdot10^{-5}$	1.0195	$-4.2643\cdot10^{-6}$	$-7.5874\cdot10^{-5}$	1.0256	$3.3\cdot10^{-5}$
G	1.1323	$3.3\cdot10^{-5}$	1.1271	$-1.5271\cdot10^{-6}$	$-4.5131\cdot10^{-4}$	1.1420	$3.3\cdot10^{-5}$
H	1.1513	$4.2\cdot10^{-5}$	1.1457	$-1.4370\cdot10^{-6}$	$-4.8084\cdot10^{-4}$	1.1615	$4.2\cdot10^{-5}$

According to Equation 4.1, the nominal flow rate, Q_{rot}, of 1000 μL/h, corresponds to a shear rate, $\dot{\gamma}$, of 1,45 s^{-1}, considering a needle of inner radius, r, $6{,}25 \cdot 10^{-4}$ m. This shear rate value is within the non-Newtonian region for all samples, meaning that viscosity depends on the imposed shear rate, i.e., from the pre-set flow rate in the infusion system. So, any variation in the flow rate will lead to a consequent change of the sample's viscosity, and therefore its flow rate. However, the obtained results in chapter 7 revealed that the mechanical properties of the tested drugs do not have a significant effect on the flow rate accuracy and uncertainty of the tested infusion system that operates in the microflow range.

5. Front track method – an in-depth study about sources of uncertainty

This chapter aims to provide an in-depth study about the sources of uncertainty of the front track, or front tracking, method as well as the efforts to reduce their influence.

5.1. Working principle

The Front Tracking method has as its principle the measurement of the displacement, d, in mm, of the meniscus of a liquid in a tube or capillary, over time, Δt, in s. By knowing the cross-sectional area, πr^2, in mm^2, of the capillary where the liquid meniscus is visible, it is possible to calculate the flow rate, Q, in µL/h, according to Equation 5.1, where the coefficient of expansion of the capillary, γ, and the temperature of the calibration liquid, T, in °C, are considered.

$$Q = \frac{d}{\Delta t}\pi r^2[1 - \gamma(T - 20)] \cdot 3.6 \tag{5.1}$$

Being an optical measurement method, an image processing software is necessary to process the images captured by the camera and perform the measurement of the meniscus displacement. Using Python language, a software created and developed by Nova School of Science and Technology – Department of Mechanical and Industrial Engineering together with IPQ was designed specifically for this purpose (Figure 5.1) [45]. This software calibrates the scale, segments the image in order to be able to identify the liquid meniscus, determine its position over time and calculate the average flow rate in a given time interval. It then generates a text file with the with the determined distances, for later analysis. The program's input is a video, and the analysis is performed with a time interval between measurements defined by the user.

Figure 5.1 - Front tracking image software

5.2. Uncertainty components

The measurement's uncertainty of the front tracking method is estimated according to the Guide to the expression of Uncertainty in Measurement (GUM) [22]. Table 5.1 presents the uncertainty components associated with the determination of the measured flow rate by the front tracking method [45, 46].

Table 5.1 - Resume of the main uncertainty components of the front tracking method

Uncertainty component	Standard uncertainty	Uncertainty evaluation process	Uncertainty evaluation type	Uncertainty distribution
Displacement	$u_{\Delta x}$	Experimental	B	Normal
Time interval	$u_{\Delta t}$	Calibration certificate	B	Normal
Radius	u_r	Calibration certificate	B	Normal
Repeatability	u_{rep}	Mean standard deviation of the flow measurements	A	Normal
Stability	u_{stab}	Experimental	A	Normal
Lens focus	u_{focus}	Experimental	A	Normal
Material expansion	u_γ	Calibration certificate	B	Rectangular
Temperature	u_T	Calibration certificate	B	Rectangular

The sensitivity coefficient function (c_i), expressed by Equation 5.2, gives the relationship between the combined uncertainty $U_i(Q)$ and the uncertainty associated with each component.

$$U_i(Q) = c_i u(x_i) \tag{5.2}$$

Where:

$$c_i = \frac{\partial f(Q)}{\partial x_i} \tag{5.3}$$

The sensitivity coefficients of each variable are the following:

Displacement: $c_{i\,d} = \left(\frac{\partial Q}{\partial d}\right) = \frac{\pi r^2[1-\gamma(T-20)]}{\Delta t}$ (mm²/s) (5.4)

Time interval: $c_{i\,\Delta t} = \left(\frac{\partial Q}{\partial \Delta t}\right) = -\frac{d\cdot\pi r^2[1-\gamma(T-20)]}{\Delta t^2}$ (mm³/s²) (5.5)

Radius: $c_{i\,r} = \left(\frac{\partial Q}{\partial r}\right) = \frac{2d\cdot\pi r^2[1-\gamma(T-20)]}{\Delta t}$ (mm²/s) (5.6)

Repeatability: $c_{i\,rep} = \left(\frac{\partial Q}{\partial rep}\right) = 1$ (µL/s) (5.7)

Stability: $c_{i\,stab} = \left(\frac{\partial Q}{\partial stab}\right) = 1$ (µL/s) (5.8)

Lens focus: $c_{i\,focus} = \left(\frac{\partial Q}{\partial focus}\right) = 1$ (µL/s) (5.9)

Material expansion: $c_{i\,\gamma} = \left(\frac{\partial Q}{\partial \gamma}\right) = -\frac{d\cdot\pi r^2(T-20)}{\Delta t}$ mm³·°C/s (5.10)

Temperature: $c_{i\,T} = \left(\frac{\partial Q}{\partial T}\right) = -\frac{d\cdot\pi r^2\gamma}{\Delta t}$ mm³·°C^{-1}/s (5.11)

In this work several tests were performed in order to improve the uncertainty values of each component determined by M. Alvares [45]. The results are presented in the following sections.

5.2.1. Uncertainty associated with the meniscus displacement

The uncertainty associated with the determination of the meniscus displacement, $u_{\Delta x}$, is calculated according to Equation 5.12, where the contribution of half of the smallest division of the obtained scale is considered for the processing of the images is added to the contribution of the uncertainty of the calliper used to measure the outside diameter of the tube.

$$u_{\Delta x} = \sqrt{\left(\frac{scale/2}{\sqrt{3}}\right)^2 + \left(\frac{0.03}{2}\right)^2}\ (mm) \quad (5.12)$$

5.2.2. Uncertainty associated with the determinations of time intervals

The uncertainty associated with the determinations of time intervals between measurements is calculated according to Equation 5.13, considering two components:

- Chronometer uncertainty (u_{crono}), with the value of 0.0014 s.
- Uncertainty associated with time delay (u_{delay}), with the value of 0.01 s.

$$u_t = \sqrt{\left(\frac{u_{crono}}{2}\right)^2 + \left(\frac{u_{delay}}{\sqrt{3}}\right)^2} \ (s) \tag{5.13}$$

5.2.3. Uncertainty associated with the capillary internal radius

The uncertainty component associated with the capillary internal radius, u_r, was determined experimentally by gravimetry for different capillaries [46]. The obtained uncertainty values were 0.00294 mm, 0.00452 mm and 0.00251 mm for the capillaries with inner diameters of 1.61 mm, 1.15 mm and 0.5 mm, respectively.

5.2.4. Uncertainty associated with the repeatability

The uncertainty associated with the repeatability is calculated using the standard deviations of the mean value of the measured flow of a result set, $s(Q)$, according to Equation 5.14.

$$u_{rep} = \frac{s(Q)}{\sqrt{n}} \ (\mu L/s) \tag{5.14}$$

5.2.5. Uncertainty associated with the stability of the meniscus

The stability of the meniscus position over time is affected by vibrations of the flow generator, ambient conditions, and disturbances of the experimental setup (e.g., vibrations of the table).

At IPQ, the uncertainty component associated with the stability of the experimental setup, was obtained by measuring the meniscus displacement over time, with the flow generator switched on, but without generating flow. This experimental setup (setup A) used the flow generator Nexus 3000, a 1 mL A-class glass syringe, a glass capillary with an internal diameter of 1.15 mm, a stainless-steel tube, and the Alvium camera. The data acquisition was taken with intervals of 30 s, and a total duration of 5 h. The obtained uncertainty results for different durations are presented in Table 5.2.

Table 5.2 - Stability uncertainty for setup A

Total duration / s	Uncertainty / ($\frac{\mu L}{s}$)
1800	$2.0 \cdot 10^{-5}$
2700	$1.6 \cdot 10^{-5}$
3600	$1.4 \cdot 10^{-5}$

Through a non-linear regression, the obtained uncertainty results were approximated to an exponential curve (Figure 5.2). Thus, the equation shown in Figure 4.2 calculates the stability uncertainty value as a function of time [45].

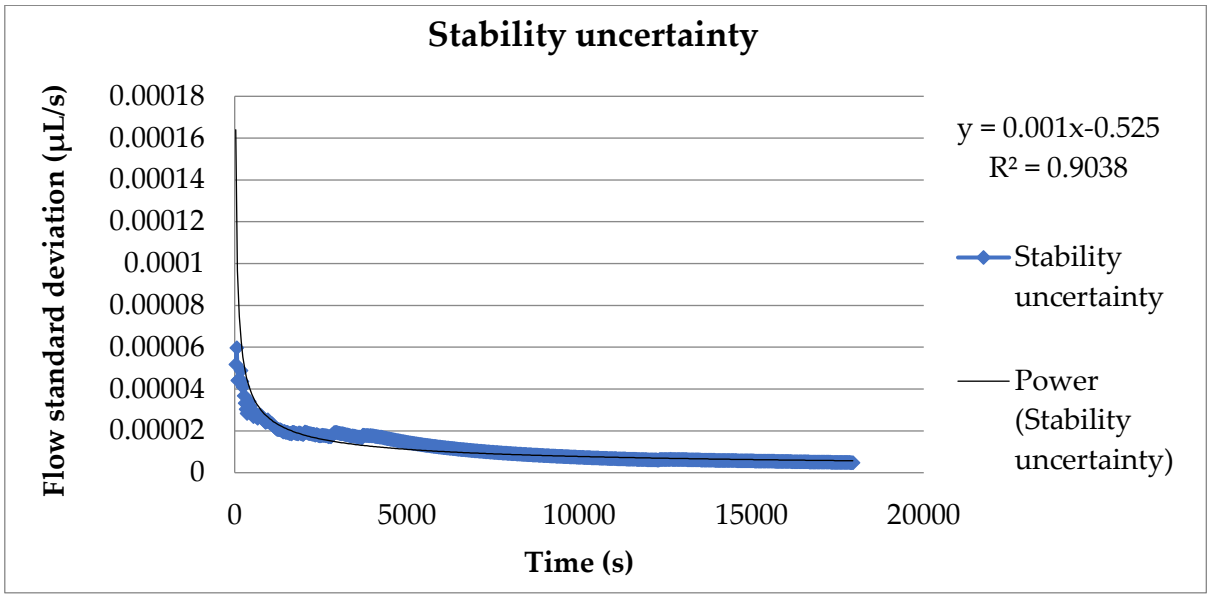

Figure 5.2 - Stability uncertainty (setup A)

To validate this stability uncertainty equation, measurements were taken using the same experimental setup (setup A), acquisition time of 30 s and total duration of 5 h. The obtained uncertainty results were also approximated to an exponential curve (Figure 5.3).

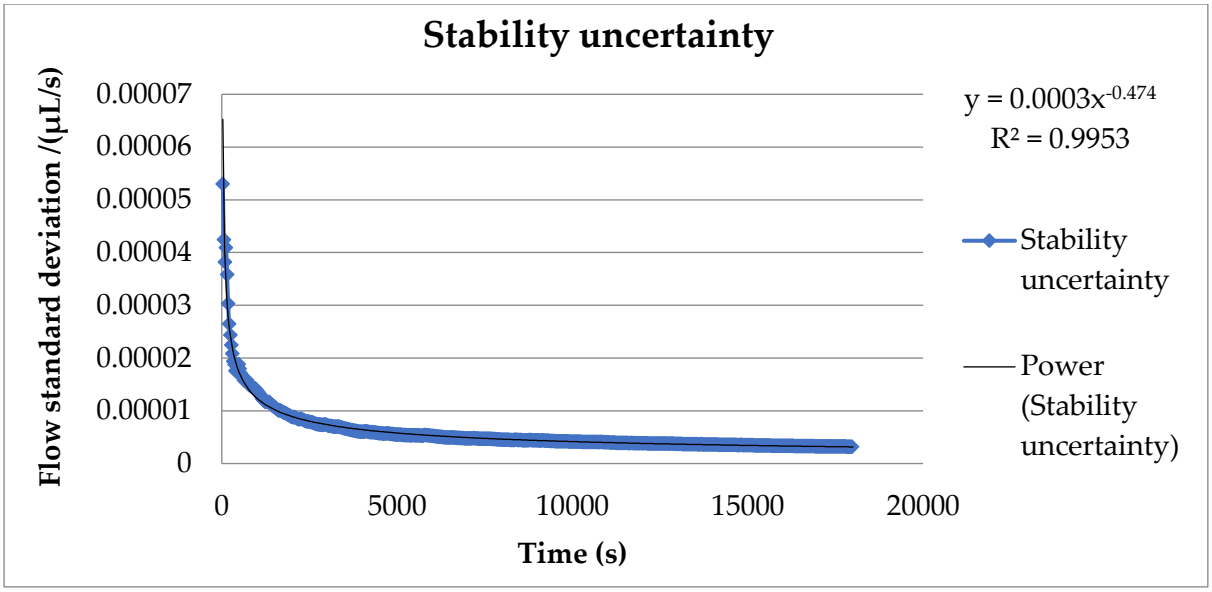

Figure 5.3 - Stability uncertainty validation (setup A)

The obtained uncertainty results for different durations are presented in Table 5.3. These uncertainty values are lower than the ones shown in Table 5.2. This difference could be due to lower disturbances of the experimental setup during the test.

Table 5.3 - Stability uncertainty for setup A validation

Total duration / s	Uncertainty / $(\frac{\mu L}{s})$
1800	$8.6 \cdot 10^{-6}$
2700	$7.1 \cdot 10^{-6}$
3600	$6.2 \cdot 10^{-6}$

To know if the acquisition time influenced the stability uncertainty, measurements were taken using experimental setup A and total duration of 5 h, but with acquisition times of 10 s and 60 s. The obtained uncertainty curves are shown in Figures 5.4 and 5.5, respectively.

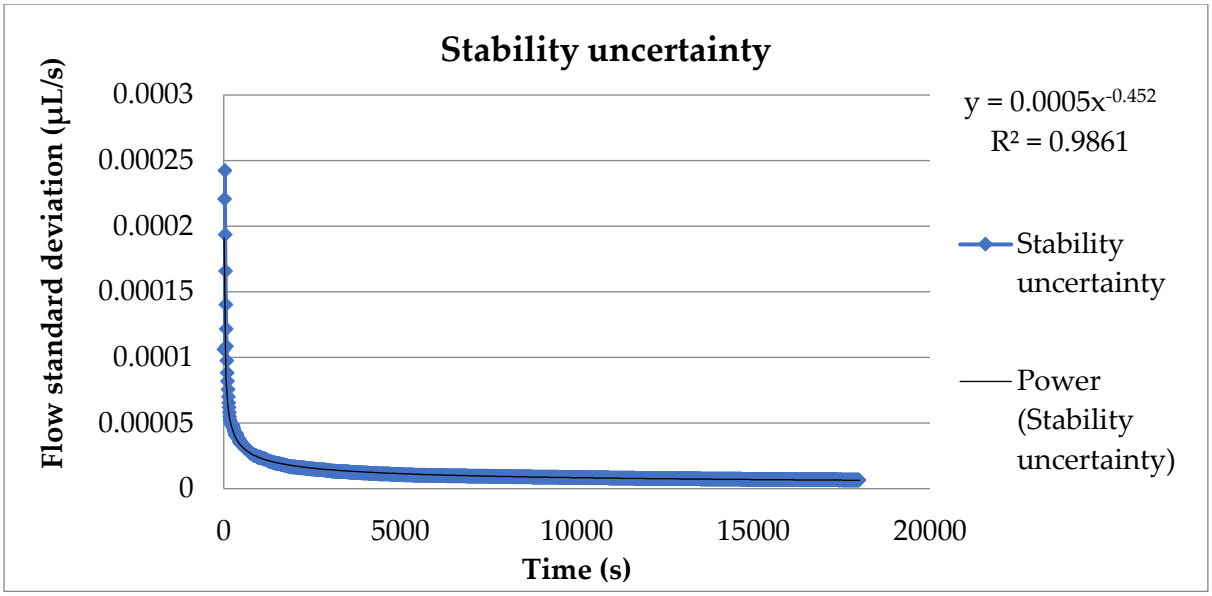

Figure 5.4 - Stability uncertainty - setup A - 10 s acquisition time

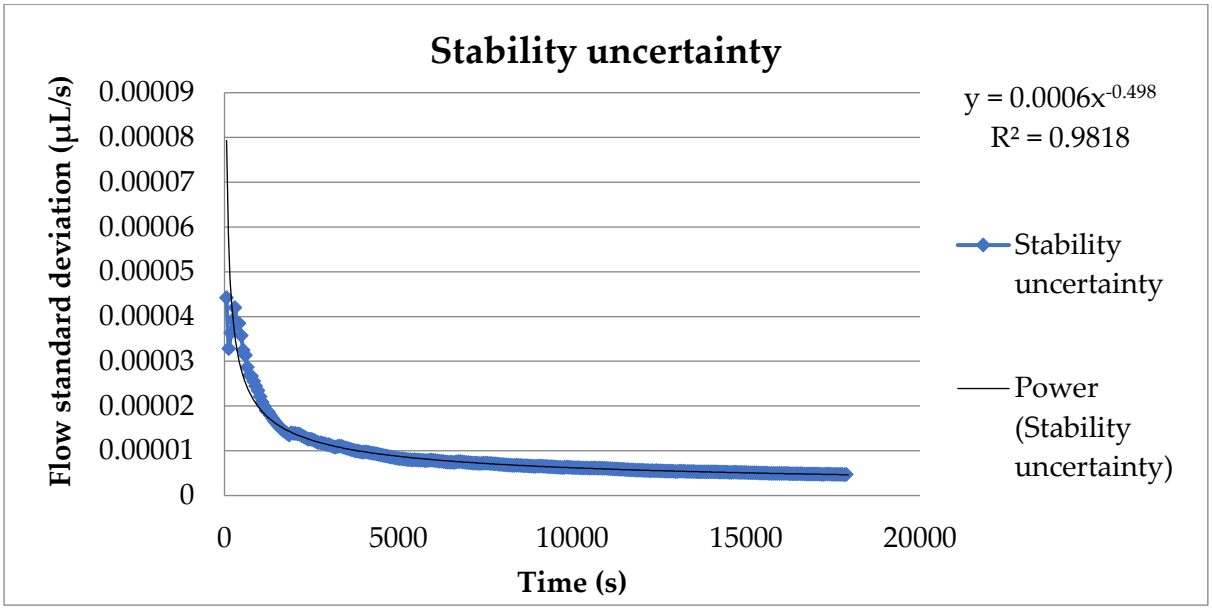

Figure 5.5 - Stability uncertainty - setup A - 60 s acquisition time

The obtained uncertainty results of the measurements taken with acquisition times of 10 s and 60 s, for different durations, are presented in Table 5.4. These uncertainty values are of the same magnitude, however, when compared to the results obtained with an acquisition time of 30 s, they are significantly higher.

Table 5.4 - Stability uncertainty - setup A - different acquisition times

Total duration / s	Uncertainty with 10 s / ($\frac{\mu L}{s}$)	Uncertainty with 60 s / ($\frac{\mu L}{s}$)
1800	$1.7 \cdot 10^{-5}$	$1.4 \cdot 10^{-5}$
2700	$1.4 \cdot 10^{-5}$	$1.2 \cdot 10^{-5}$
3600	$1.2 \cdot 10^{-5}$	$1.0 \cdot 10^{-5}$

The stability uncertainty only has a significant effect on measurements of flow rates lower than 10 µL/h, which are usually taken with acquisition times of 10 or 30 s, in order to reduce the uncertainty related to the repeatability.

Measurements were also taken using two similar experimental setups (setup B and setup C), with acquisition times of 30 s and total durations of 5 h. Setup B and setup C used two glass capillaries with internal diameters of 0.5 mm. One capillary had an internal coating (setup B) while the other didn't (setup C). The obtained uncertainty results for the capillaries with and without coating, which were also approximated to exponential curves, are shown in Figures 5.6 and 5.7, respectively.

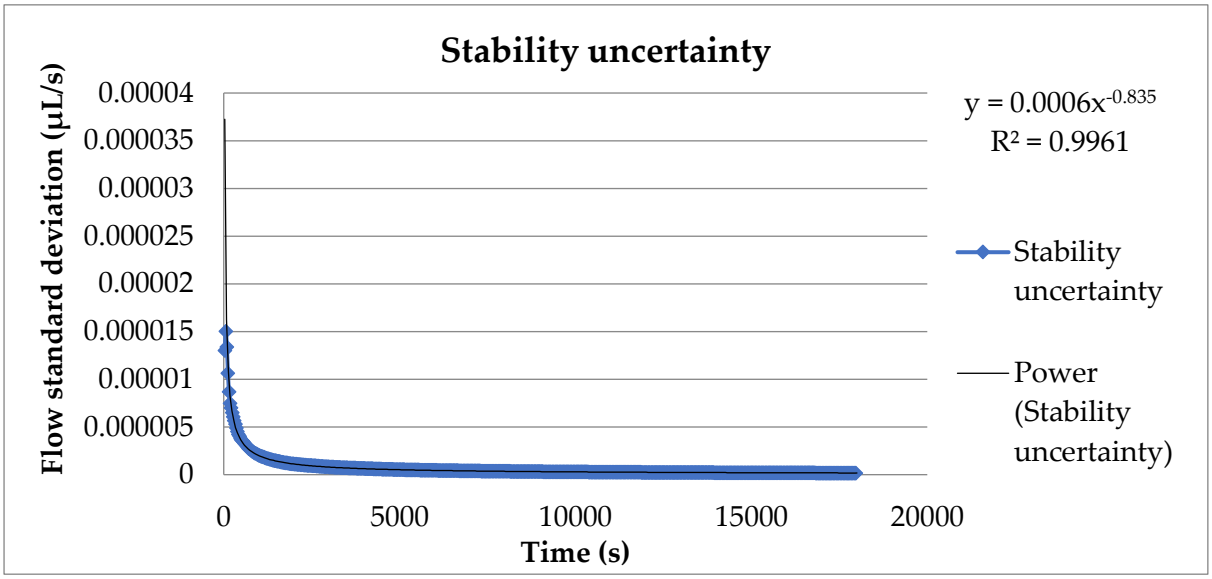

Figure 5.6 - Stability uncertainty - setup B - capillary with coating

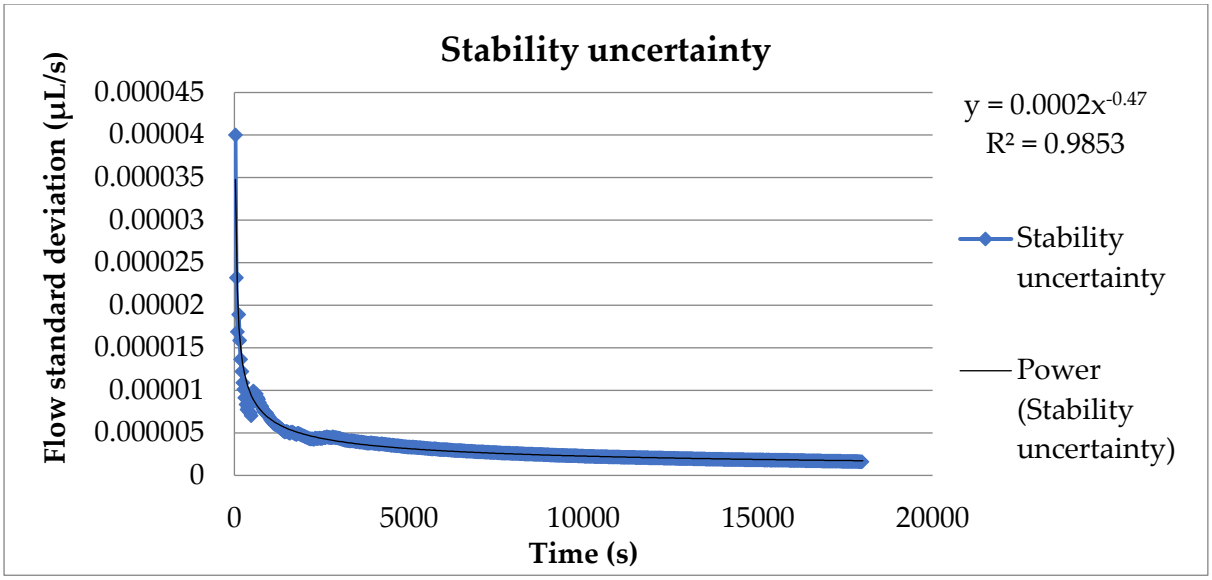

Figure 5.7 - Stability uncertainty - setup C - capillary without coating

The obtained uncertainty results of the measurements taken with the capillaries with and without coating, for different durations, are presented in Table 5.5. The uncertainty values of the capillary with coating are lower than the values of the capillary without coating. This difference may be due to fact that the internal coating diminishes the effect of fluctuating ambient conditions, mainly temperature, on the fluid inside the capillary.

Table 5.5 - Stability uncertainty comparison of setup B and C

Total duration / s	Uncertainty / ($\frac{\mu L}{s}$)	Uncertainty / ($\frac{\mu L}{s}$)
1800	$1.1 \cdot 10^{-6}$	$5.9 \cdot 10^{-6}$
2700	$8.2 \cdot 10^{-7}$	$4.9 \cdot 10^{-6}$
3600	$6.4 \cdot 10^{-7}$	$4.3 \cdot 10^{-6}$

To know if the camera magnification influenced the stability uncertainty, measurements were taken using experimental setup B, total duration of 30 minutes, acquisition time of 30 s, and magnifications of 1.5x and 2.5x. The obtained uncertainty curve of the 2.5x magnification results is presented in Figure 5.8. For the 1.5x magnification, the results shown in Figure 5.3 were used for comparison, considering only the first 30 minutes of measurements.

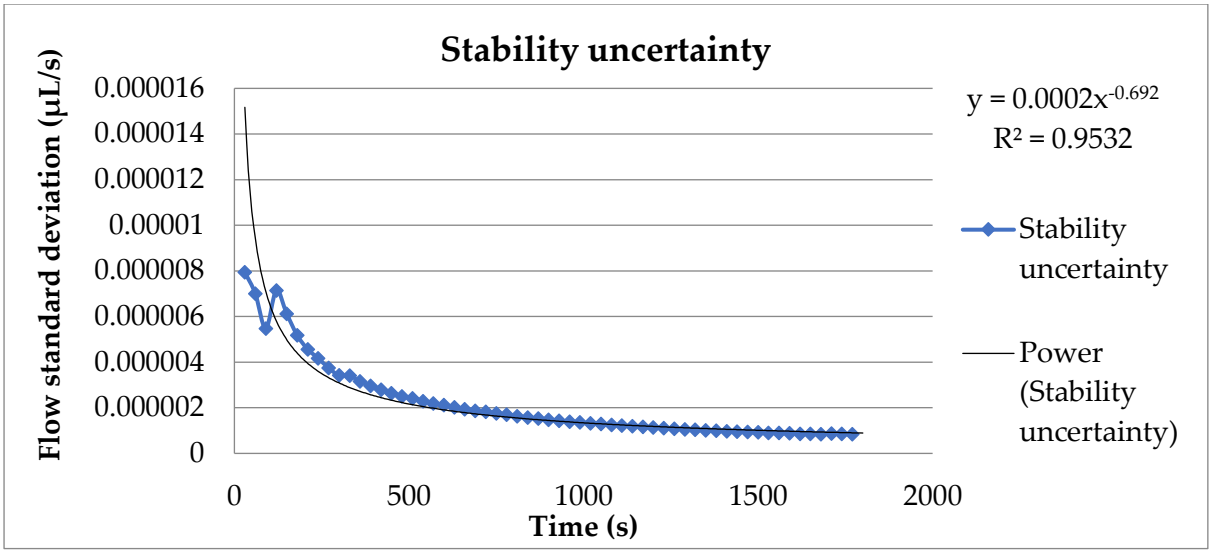

Figure 5.8 - Stability uncertainty - setup B - acquisition time 30s - magnification 2.5x

The obtained uncertainty results of the measurements taken with magnifications of 1.5x and 2.5x, for different durations, are presented in Table 5.6. These uncertainty values are of the same magnitude. Therefore, the camera magnification does not affect the stability uncertainty.

Table 5.6 - Stability uncertainty - magnification comparison

Total duration / s	Uncertainty / $(\frac{\mu L}{s})$	Uncertainty / $(\frac{\mu L}{s})$
1800	$1.1 \cdot 10^{-6}$	$1.1 \cdot 10^{-6}$
2700	$8.2 \cdot 10^{-7}$	$8.4 \cdot 10^{-7}$
3600	$6.4 \cdot 10^{-7}$	$6.9 \cdot 10^{-7}$

Additionally, measurements were taken with the experimental setup that used the BBraun infusion pump as the flow generator, a 10 mL polypropylene syringe, a polypropylene capillary with an internal diameter of 1.61 mm, a teflon tube, and the Alvium camera (setup D). The data acquisition was taken with intervals of 30 s, and a total duration of 5 h. The obtained uncertainty curve of the results of the measurements taken with setup D is presented in Figure 5.9.

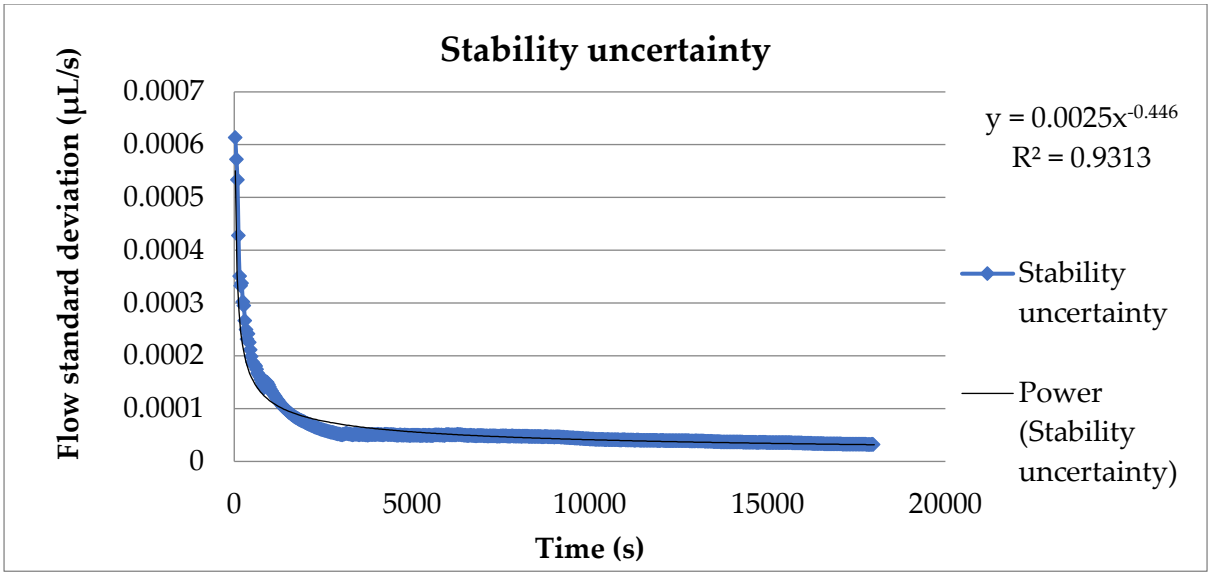

Figure 5.9 - Stability uncertainty for setup D

The obtained uncertainty results for different durations using are presented in Table 5.7.

Table 5.7 - Stability uncertainty – setup D

Total duration / s	Uncertainty / ($\frac{\mu L}{s}$)
1800	$9.2 \cdot 10^{-5}$
2700	$7.6 \cdot 10^{-5}$
3600	$6.7 \cdot 10^{-5}$

5.2.6. Uncertainty associated with the lens focus

The uncertainty component associated with the level of focus of the camera lens chosen by the operator, u_{focus}, was determined experimentally, with measurements taken with the camera placed in different positions on its y axis. The camera was moved forwards and backwards, using very small displacements, into positions in which the focus of the image was considered, by the operator, to be equally optimal. The obtained uncertainty value was equal to $1.3 \cdot 10^{-7}$ µL/s.

5.2.7. Uncertainty associated with the material expansion

The uncertainty associated with the expansion of the capillary material, u_{γ}, corresponds to 0.5% of the material's volumetric expansion coefficient, according to Equation 5.15:

$$u_\gamma = \frac{0.005\gamma}{\sqrt{3}}\ (/°C) \tag{5.15}$$

5.2.8. Uncertainty associated with the temperature

The uncertainty component associated with the temperature determination of the calibration fluid, u_T, is calculated according to Equation 5.16, where the thermometer uncertainty is equal to 0.01 °C.

$$u_T = \frac{0.01}{2}\ (°C) \tag{5.16}$$

5.2.9. Combined uncertainty

The combined uncertainty associated with the flow determination $u(Q)$, is calculated according to Equation 5.17:

$$u(Q) = \sqrt{\begin{matrix}(u_{\Delta x} \times c_{i\ \Delta x})^2 + (u_{\Delta t} \times c_{i\ \Delta t})^2 + (u_r \times c_{i\ r})^2 + u_{rep} + u_{stab} + u_{focus} + \\ +(u_T \times c_{i\ T})^2\end{matrix}}\ (\mu L/s) \tag{5.17}$$

5.2.10. Expanded uncertainty

The expanded uncertainty is expressed by the combined uncertainty multiplied by the expansion factor according to Equation 5.18 [22], where the expansion factor k is calculated from the inverse distribution of the t-Student distribution to an expanded probability of 95.45%.

$$U = ku(Q) \tag{5.18}$$

5.3. Experimental setup and procedure

In chapter 7, a few experimental setups for the calibration of drug delivery devices are shown for the front tracking method, which are similar between each other, being that the only changes are of the flow generator, the capillaries, and connection lines that are used. In general, as show in Figure 5.10, the experimental setup is composed of the flow generator (A), in which a syringe is installed (B) and is connected to a tube (C) which itself is connected to a capillary tube (E). The high-resolution camera Alvium 1800U-1240 (D) is placed in front of the capillary tube, aligned with the translucent paper (F) that is used to diffuse the light coming from the LED lamp (G).

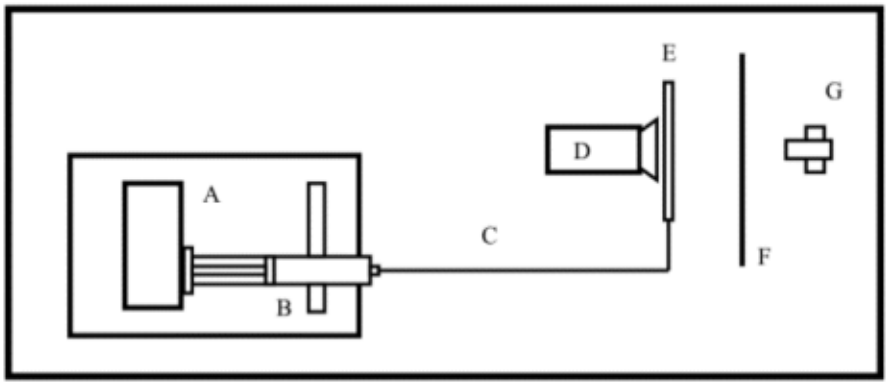

Figure 5.10 - Generalized front tracking method experimental setup [45]

The experimental procedure for the calibrations performed with the front tracking method in chapter 6 is the following:

1. Check environmental conditions (temperature, relative humidity and pressure) and record on the excel spreadsheet;
2. Measure the temperature of the syringe's feed liquid and record it on the spreadsheet;
3. Fill the syringe with water manually and connect it to the steel tube. Ensure there are no air bubbles inside the syringe;
4. Mount the syringe onto the flow generator and select syringe from the machine menu;
5. Connect the tube to the capillary tube;
6. Position the camera close to the capillary tube, ensuring that its field of view includes the liquid's meniscus;
7. Start image processing software for the Front Tracking method (wait for the program window to appear);
8. Start video mode to view the image captured by the camera and perform adjustments (position/focus);
9. Select the time interval between measurements and choose the inner and outer diameter of the capillary;
10. Set scale by manually selecting the outer diameter of the capillary tube;
11. Set Threshold value;
12. Start image capture and measurement;
13. At the end of the measurement, save the results;
14. Fill in the spreadsheet with the collected data.

6. DROP METHOD – an in-depth study about sources of uncertainty

This chapter aims to describe the adjustments made to the image processing software of the drop method, in order to improve this method, and to provide an in-depth study about the sources of uncertainty.

6.1. Working principle

The drop method has as its working principle the measurement of the increase in volume of a drop over a given time, through the capture of images. Knowing the internal diameter of the capillary/needle used and the difference in volume and time between captured images, it is possible to determine the flow rate, considering that the drop is symmetrical in relation to its axis of revolution. The instantaneous flow is calculated through the difference between volumes, V, in mL, in a period of time, Δt, given in s. The average flow, Q_m, given in mL/h, is determined by averaging the instantaneous flows calculated for the duration of the test, given by Equation 6.1:

$$Q_m = \frac{V}{\Delta t} \tag{6.1}$$

Using a Python programming language, a customized software was designed specifically for this purpose by Nova School of Science and Technology – Department of Mechanical and Industrial Engineering and IPQ. More specifically, this method uses two different softwares. The first software was developed in order for the camera to take several photographs, as many as defined by the user, with a set time interval between each capture, also defined by the user (Figure 6.1).

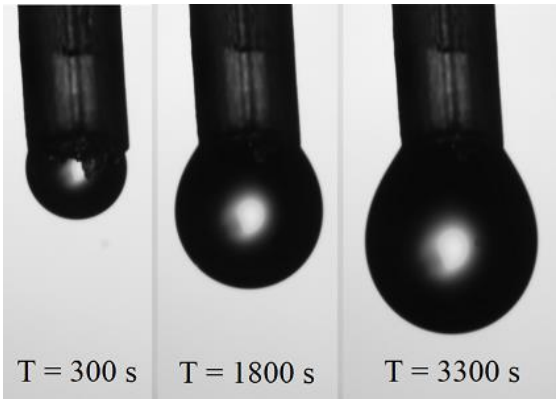

Figure 6.1 - Image capture software

The second software was developed for processing the captured images [45]. Firstly, the OpenCV library is imported. Then, the scale is calibrated, the images are segmented, and the contours are defined for each captured image (Figure 6.2). Finally, the volume of the droplet in each image is calculated and a text file with the determined volumes is generated. Knowing the increase in volume and the time between each image it is possible to calculate the flow rate.

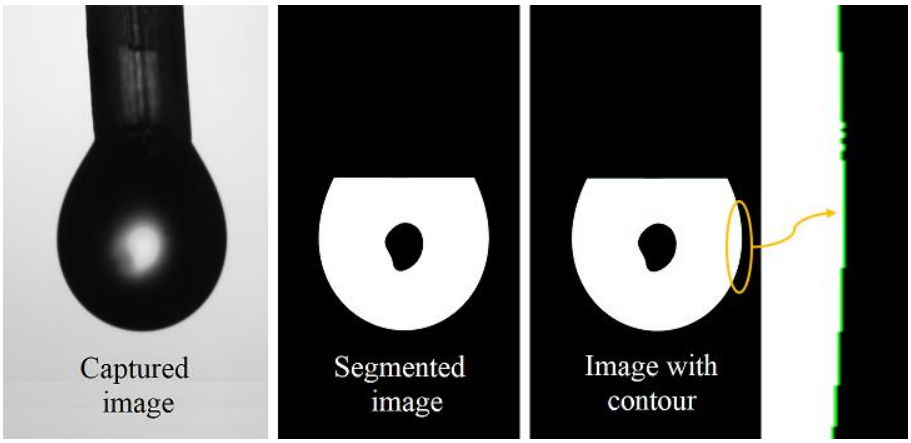

Figure 6.2 - Image processing software

At the start of each measurement, the scale is calibrated based on the known external diameter of the capillary tube that is being used. A section of the tube is selected manually, as shown in Figure 6.3, and the processing software segments the image, illustrated in Figure 6.4, and obtains the number of pixels between the edges, giving the diameter of the tube in pixels. The scale is determined by dividing the diameter in pixels by the known diameter in mm.

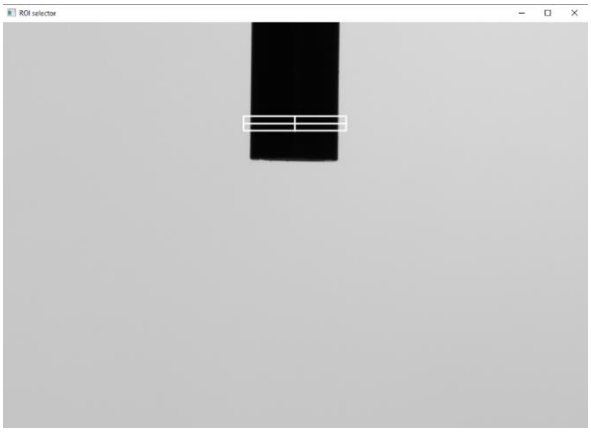

Figure 6.3 - Selection of section of the tube

Figure 6.4 - Segmented tube section

6.2. Improvement of the image processing software

Disturbances of the lighting conditions during measurements cause disturbances in the identification of the contours of the drops, as shown in Figure 6.5, which leads to incorrect calculations of volume. When this happens on one or two photographs, it is simple to delete these outliers. However, when multiple photographs are affected, the test must be done again. This can be very inefficient when time constraints are at play and measurements take long periods of time, since it is only possible to know the contours are not being correctly identified after the measurement is finished.

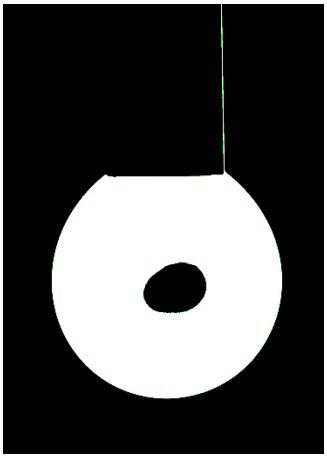

Figure 6.5 - Incorrect contour determination

To avoid this issue, an additional step was added to the processing program, where one can select the area of interest to study the contours, by drawing a black rectangle over the area below the tube, as show in Figure 6.6.

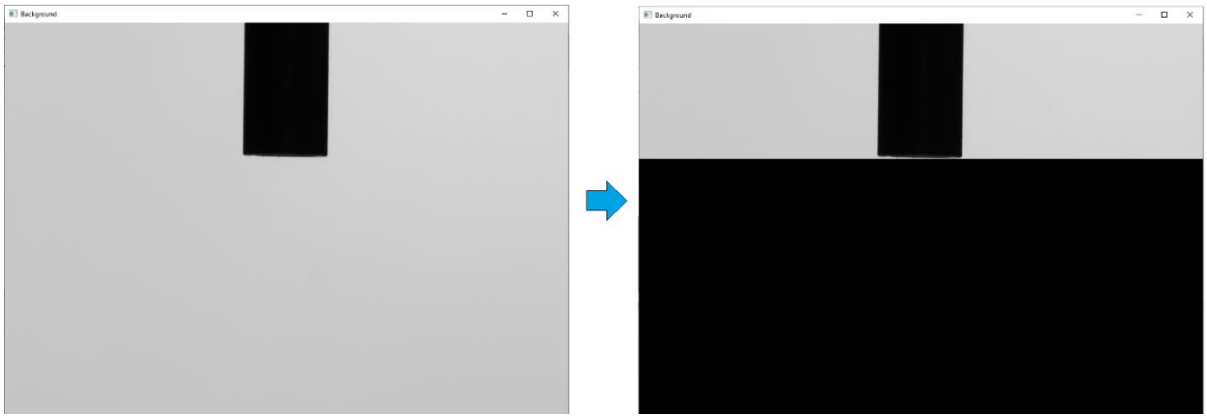

Figure 6.6 – Selection of area of interest

With this step it is possible to ensure that the lighting hitting the tube will not cause interferences in the contour and volume determinations, as show in Figure 6.7, and thus will reduce the uncertainty associated with the repeatability.

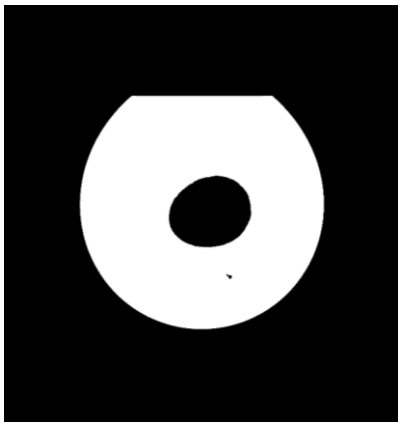

Figure 6.7 - Contour determination with optimized program

6.3. Uncertainty components

The measurement's uncertainty of the drop method is estimated according to the Guide to the expression of Uncertainty in Measurement (GUM) [22]. Table 6.1 presents the uncertainty components associated with the determination of the liquid flow by the drop method. The main standard uncertainties are the volume determination, V, time, t evaporation, δQ_{evap}, and standard deviation of the measurements or repeatability, δQ_{rep} [45, 46]. The equation used to calculate the flow is Equation 6.1.

Table 6.1 - Resume of the main uncertainty components of the drop method

Uncertainty component	Standard uncertainty	Uncertainty evaluation process	Uncertainty evaluation type	Uncertainty distribution
Volume	$u(V)$	Experimental	B	Normal
Time	$u(t)$	Calibration certificate	B	Normal
Evaporation	$u(\delta Q_{evap})$	Experimental	A	Normal
Repeatability	$u(\delta Q_{rep})$	Mean standard deviation of the flow measurements	A	Normal

The sensitivity coefficient function (c_i), expressed by Equation 6.2, gives the relationship between the combined uncertainty $U_i(Q)$ and the uncertainty associated with each component.

$$U_i(Q) = c_i u(x_i) \tag{6.2}$$

Where:

$$c_i = \frac{\partial f(Q)}{\partial x_i} \tag{6.3}$$

The sensitivity coefficient of each variable is the following:

Volume: $c_{i\,V} = \left(\frac{\partial Q}{\partial V}\right) = \frac{1}{t}$ (1/s) (6.4)

Time: $c_{i\,\Delta t} = \left(\frac{\partial Q}{\partial t}\right) = -\frac{V}{t^2}$ (μL/s²) (6.5)

Evaporation: $c_{i\,evap} = \left(\frac{\partial Q}{\partial evap}\right) = 1$ (μL/s) (6.6)

Repeatability: $c_{i\,rep} = \left(\frac{\partial Q}{\partial rep}\right) = 1$ (μL/s) (6.7)

In this work several tests were performed in order to improve the uncertainty values of each component determined by M. Alvares [45], the results are presented in the following sections.

6.3.1. Uncertainty associated with the volume determination

The uncertainty associated with the determination of the volume of the drop, u_V, is calculated considering three components:

- Uncertainty associated with the scale determination (u_{scale}).
- Uncertainty associated with the lens focus (u_{focus}).
- Uncertainty associated with the contour determination ($u_{contour}$).

The uncertainty associated with the volume determination is calculated according to Equation 6.8:

$$u_V = \sqrt{\left(\frac{u_{scale}}{2}\right)^2 + \left(\frac{u_{focus}}{2}\right)^2 + \left(\frac{u_{contour}}{2}\right)^2} \ (mm^3) \tag{6.8}$$

6.3.1.1. Uncertainty associated with the scale determination

The uncertainty component associated with the scale determination, u_{scale}, was determined experimentally, by selecting different scales, as many as the Python software could recognise for the analysed measurement and measuring the volume increase between two consecutive drops. The obtained value was equal to 0.0001129 mm^3. Since it was an experimentally obtained value, a normal distribution was considered. Details of the measured volume increases can be seen in Appendix A.1.

6.3.1.2. Uncertainty associated with the lens focus

The uncertainty component associated with the level of focus of the camera lens chosen by the operator, u_{focus}, was previously estimated at IPQ, based on experimental knowledge, to be equal to 0.01% of the volume of the drop. Since it was an estimated value, a rectangular distribution was considered.

To determine its value experimentally, one single droplet was photographed, with the flow generator turned off, with the camera placed in different positions on its y axis. The camera was moved forwards and backwards, using very small displacements, into positions in which the focus of the image was considered, by the operator, to be equally optimal. The uncertainty associated with the level of focus of the camera lens chosen by the operator was determined by calculating the standard deviation of the measured volume values obtained for the different positionings, selecting the same scale when processing each photograph, and dividing it by the square root of the number of observations, which were fifteen. Since the droplet was hanging for the duration of the measurements, evaporation was inevitable, and so was accounted for in each measured volume. Details of the measured volumes and

their evaporation compensation can be seen in Appendix A.2, as well as the determined uncertainty value of 0.001026 mm^3.

6.3.1.3. Uncertainty associated with the contour determination

The uncertainty component associated with the determination of the contour of the droplet, $u_{contour}$, was previously determined at IPQ and was equal to 0.005% of the volume of the drop. This uncertainty component was obtained using a CAD model of the drop method designed in SolidWorks, shown in Figure 6.8, which was composed of a tube, with a known diameter of 0.91188 mm, and a sphere with a known volume.

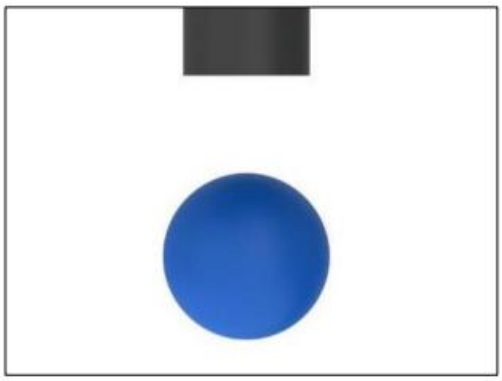

Figure 6.8 - Drop method model in SolidWorks

Different threshold values were tested using the processing software and it was determined that a threshold value of 43 returned results with the lowest average relative error, as can be confirmed in Table 6.2.

Table 6.2 – Threshold choice in the drop method CAD model

Threshold	Average relative error / %
55	-0.350
50	-0.210
45	-0.060
44	-0.030
43	0.005
42	0.030
20	0.830

Before determining this uncertainty component value experimentally, the same threshold values presented in Table 6.2 were applied to a measurement of a flow rate of 100 μL/h, in which the nominal value of the volume was of 7.9234 mm^3, in order to confirm if

the threshold value of 43 would return the results with the lowest relative error using the experimental setup, as it did with the CAD model setup. In Table 6.3 it is possible to confirm that the threshold of 43 is the value that should be used in the image processing software.

Table 6.3 – Threshold choice in the drop method experimental setup

Threshold	Measured volume / mm³	Average relative error / %
55	7.9018	0.273
50	7.9078	0.197
45	7.9229	0.006
44	7.9228	0.008
43	7.9235	-0.001
42	7.9237	-0.004
20	7.9988	-0.943

The threshold that is applied to a monochromatic image is the value for which all pixels with an intensity lower or greater than said value are replaced by a white or a black pixel, respectively. Thus, for a same threshold value, different lighting conditions will lead to different obtained binary images and, therefore, determined contours.

To determine the uncertainty component associated with the determination of the contour of the droplet, $u_{contour}$, experimentally, using a threshold value of 43 and selecting the same scale for each test, two consecutive photographs from a measurement were edited on Windows Photo Editor to have different brightness's (from -100 to 100), making the images darker and lighter than the original, in order to simulate different lighting conditions, as illustrated in Figure 6.9.

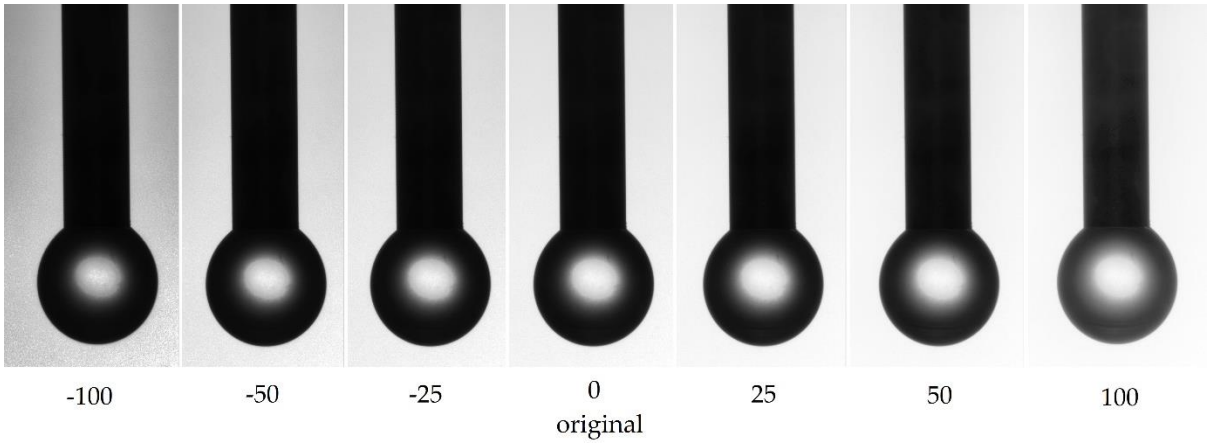

Figure 6.9 - Threshold lighting conditions

The uncertainty associated with the contour determination was determined by calculating the standard deviation of the measured volume increases for the different

lighting conditions, selecting the same scale when processing each photograph, and dividing it by the square root of the number of observations, which were forty-two. Details of the measured volume increases can be seen in Appendix A.3, as well as the determined uncertainty value of 0.0003106 mm^3.

6.3.2. Uncertainty associated with the determinations of time intervals between drops

The uncertainty associated with the determinations of time intervals between droplets photographs is calculated according to Equation 6.9, considering two components:

- Chronometer uncertainty (u_{crono}), with the value of 0.0014 s.
- Uncertainty associated with time delay (u_{delay}), with the value of 0.01 s.

$$u_t = \sqrt{\left(\frac{u_{crono}}{2}\right)^2 + \left(\frac{u_{delay}}{\sqrt{3}}\right)^2} \ (s) \tag{6.9}$$

6.3.3. Uncertainty associated with the evaporation

The uncertainty associated with the evaporation is calculated using the standard deviation of the average value of the measured evaporation flow, Q_{evap}, in each test according to Equation 6.10:

$$u_{evap} = \frac{s(Q_{evap})}{\sqrt{n}} \ (\mu L/s) \tag{6.10}$$

6.3.4. Uncertainty associated with the repeatability

The uncertainty associated with the repeatability is calculated using the standard deviations of the average value of the measured flow of a result set, $s(Q)$, according to Equation 6.11:

$$u_{rep} = \frac{s(Q)}{\sqrt{n}} \ (\mu L/s) \tag{6.11}$$

6.3.5. Combined uncertainty

The combined uncertainty associated with the flow determination $u(Q)$, is calculated according to Equation 6.12:

$$u(Q) = \sqrt{(u_v \times c_{i\ V})^2 + (u_t \times c_{i\ \Delta t})^2 + u_{evap} + u_{rep}} \ (\mu L/s) \tag{6.12}$$

6.3.6. Expanded uncertainty

The expanded uncertainty is expressed by the combined uncertainty multiplied by the expansion factor according to Equation 6.13 [22], where the expansion factor k is calculated from the inverse distribution of the t-Student distribution to an expanded probability of 95.45%.

$$U = ku(Q) \tag{6.13}$$

6.4. Experimental setup and procedure

In the next chapter a few experimental setups for the calibration of drug delivery devices are shown for the drop method, which are similar between each other, being that the only changes are of the flow generator and connection line that are used. In general, as show in Figure 6.10, the experimental setup is composed of the flow generator (A), in which a syringe is installed (B) and is connected to a capillary tube (C) that ends inside the *evaporation trap* (E). As the name suggests, this trap is used to avoid the evaporation of the calibration fluid during the measurement. The high-resolution camera Alvium 1800U-1240 (D) is placed in front of the evaporation trap, aligned with the translucent paper (F) that is used to diffuse the light coming from the LED lamp (G).

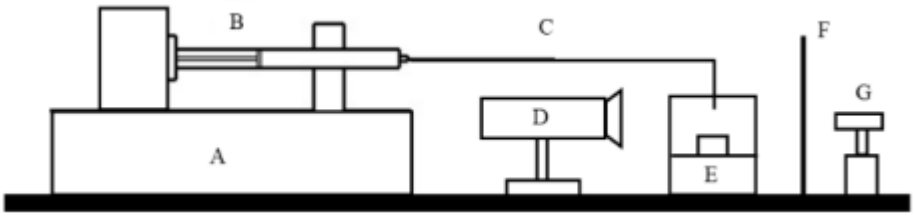

Figure 6.10 – Generalized drop method experimental setup [45]

The experimental procedure for the calibrations performed with the drop method in chapter 6 is the following:

1. Check that the evaporation trap is clean (with no stains or dust on its surface) in the area that is included in the camera's field of view. If not, clean with water and dry with paper to avoid limescale stains or impurities;
2. Check whether the evaporation trap contains water. If not, add water with the aid of a Pasteur pipette, to avoid splashes on the wall that affect the captured images;
3. Put water in a beaker, measure the temperature and record it in the spreadsheet "Template Drop Method (Alvium)";
4. Fill the syringe manually, ensuring that there are no air bubbles inside. Transfer part of the remaining water to a 10 mL beaker, or similar container, and place it inside the evaporation trap;

5. Check the environmental conditions (temperature, relative humidity and pressure) and record them in the spreadsheet;
6. Connect the tube to the syringe;
    a. For the insulin pump calibration, connect the polypropylene capillary to the syringe.
    b. For the Nexus 3000 syringe pump calibration, connect the stainless-steel tube to the glass syringe;
    c. For the BBraun infusion pump calibration, connect the teflon tube to the polypropylene syringe and connect the capillary tube to the Teflon tube, as shown in Figure 6.11:

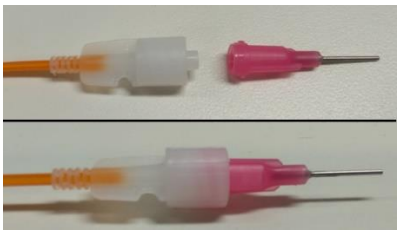

Figure 6.11 - Capillary tube and teflon tube connection

7. Place the end of the tube attached to the syringe inside the evaporation trap and place the syringe in the flow generator. The evaporation trap must be placed inside its support and between the light diffuser (translucent paper) and the camera.
    a. For the nexus 3000 calibration, select the syringe in the machine menu.
    b. For the BBraun infusion pump calibration, install the syringe inside the equipment as per instructions of the manufacturer. Select the syringe in the machine menu.
8. Select the pump infusion mode in order to load the tube and eliminate air bubbles contained inside the syringe and tubing;
9. Create a work directory, where the photographs will be stored;
10. Turn on LED light;
11. Open and start the image capture program “Capture_Gota (Alvium)” (see Appendix B.1 – points 1, 2, 3, 4 and 5);
12. Start image mode (see Appendix B.1 – point 6). With the image mode started, it is possible to make the necessary adjustments to the experimental setup, position, magnification and focus of the camera. Position the camera close to the evaporation trap, ensuring that its field of view includes the end of the capillary tube and the entire droplet. The positioning of the camera, or setup, must be such that the end of the capillary tube is in the center of the camera's field of view. To focus the image, rotate the focus ring. It is also possible to check for air bubbles in the tubing, as illustrated in Figure 6.12, by selecting the pump's perfusion mode in order to load the tube;

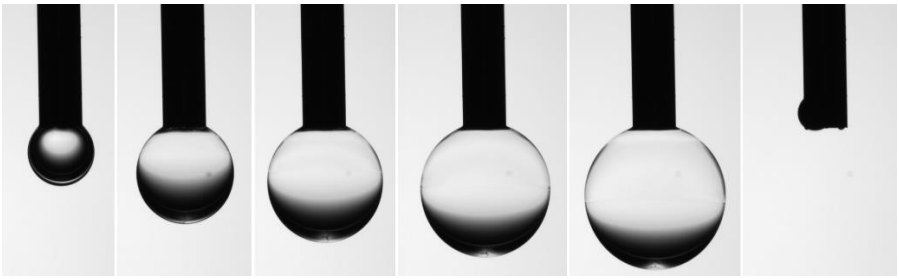

Figure 6.12 - Air bubble trapped inside capillary tube

13. If there is a drop hanging at the end of the tube, use paper to absorb it, in order to make step 15 possible;
14. Ensure that all parts (camera, LED light, tube, evaporation trap) are properly positioned and fixed, so that there are no changes in position during the test;
15. Capture the image of the tube without the hanging Droplet (see Appendix B.1 – point 7). This image is saved by the program under the name "Background", and is used for image segmentation during image processing;
16. Choose the test flow to be delivered and select the pump infusion mode;
17. Initiate the flow:
    a. Click the "ACT" button of the insulin pump and allow the test flow to stabilize for 30 min. After that time, start image acquisition (see Appendix B.1 – point 8);
    b. Click the "Start" button on the Nexus 3000 syringe and allow the test flow to stabilize for 10 min. After that time, start image acquisition (see Appendix B.1 – point 8);
    c. Click the "START/STOP" button on the BBraun infusion pump and allow the test flow to stabilize for the duration indicated in Table 6.4. After that time, start image acquisition (see Appendix B.1 – point 8);

Table 6.4 – Threshold choice in the drop method experimental setup

Flow rate / (µL/h)	Stabilization time	Acquisition time / s
10	12 h	300
100	45 - 60 min	30
1000	15 min	10

18. After capturing images, close the program.
19. Measure the temperature of the water contained in the 10 mL beaker. Calculate the average with the water temperature recorded at the beginning of the test and record in the spreadsheet;

20. Open the image processing program “Hanging droplet image processing (Alvium)” (see Appendix B.2 – point 1). Check if the tube diameter value indicated in the code is correct. If not, write the correct value and save the program (see Appendix B.2 – point 2);
21. Select the work directory (directory where the photos of the test are found) and create a folder “Contours”, where the contours of the drop will be stored for later analysis (see Appendix B.2 – points 3 and 4);
22. Select the rectangle of the area (of the drop) to be analyzed and click on the “s” key to record (see Appendix B.2 – point 5);
23. Select the number of photographs to be analyzed (see Appendix B.2 – point 6);
24. Select rectangle to calculate the scale (see Appendix B.2 – point 7);
25. the image processing program (see Appendix B.2 – point 8);
26. the spreadsheet and copy results from the “Volumes” file generated by the processing program and from the “Time” file generated by the image capture program, and place a time interval between photos;

7. CALIBRATION OF DRUG DELIVERY DEVICES

This chapter aims to describe the measurements performed using the optical and gravimetric methods, and to present and discuss the results of the calibrations of the three instruments tested during this work, which were an insulin pump, the Nexus 3000 syringe pump and the BBraun infusion pump.

7.1. Insulin pump

Insulin pumps use stepper motors that operate for a short moment at a time. Young diabetic children require small amounts of insulin to regulate their blood sugar. At very slow rates of continuous insulin infusion, often in the order of 1.0 μL/h. It is then important to calibrate insulin pumps at low flow rates to assure that the right amount of insulin is being administered and that no malfunctions occur, like occlusion problems [47]

The tested insulin pump is a flow generator with a removable reservoir that is attached to a capillary tube (Figure 7.1). This device was calibrated at flow rates of 0.25 μL/h, 1 μL/h, 3 μL/h, 6 μL/h, and 10 μL/h by the optical methods and at a flow rate of 10 μL/h by the gravimetric method.

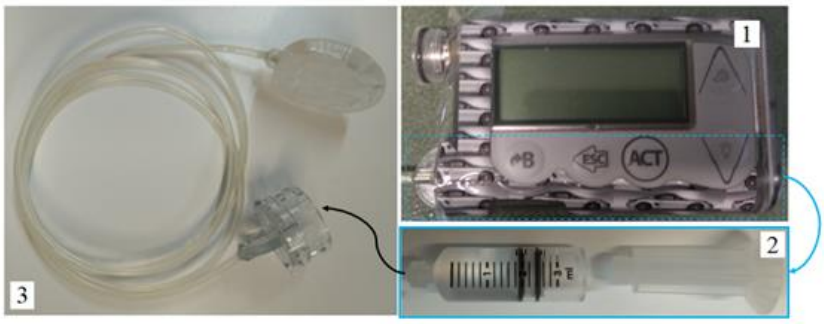

Figure 7.1 - Insulin pump system, where (1) is the insulin pump, (2) is the reservoir and (3) is the polypropylene capillary tube

7.1.1. Front tracking method

As shown in Figure 7.2, the insulin pump (1) was connected to a polypropylene capillary tube (2), which itself was connected to an glass capillary tube (3); a LED lamp (4) was turned on and pointed towards the glass capillary tube; a translucid paper (5) was placed in between the glass capillary tube and the lamp, in order to diffuse de light; the thermometer (6) measured the temperature of the water contained in a beaker placed near the glass capillary tube, since it is not possible to measure the temperature inside the tube; the camera (7) was positioned so that at the right edge of its field of view the meniscus of the liquid appeared. The camera software (8) was used to aid visualisation of the necessary adjustments.

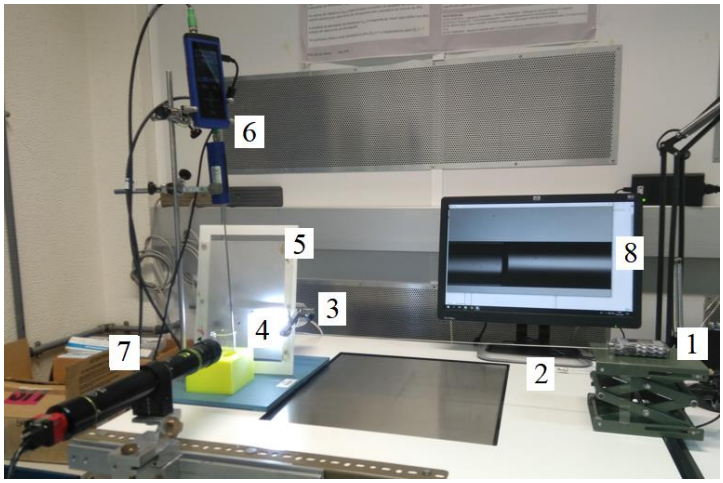

Figure 7.2 – Front tracking method experimental setup for insulin pump calibration

Measurements were performed using different glass capillary tubes (Figure 7.3), one with an internal diameter of 1.15 mm and two others with internal diameters of 0.5 mm. The difference between the 0.5 mm diameter capillaries was an internal coating.

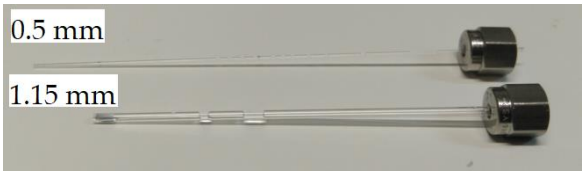

Figure 7.3 - Glass capillary tubes

The measurements performed with the 1.15 mm diameter capillary had an initial wait time of 10 minutes, meaning that the insulin pump was operating at the set flow rate for 10 minutes before each test began. The set acquisition time (time between measurements) was of 10 s and the total duration of each test was of one hour. The results of these measurements are presented in Table 7.1. The results show that within the range of the measured flow rates, the uncertainties do not vary greatly. The highest uncertainty

contribution for all measurements was the repeatability, in other words, the flow variability of the insulin pump. This flow variability can be easily observed in Figure 7.4, where the insulin pump shows a pulse-like behaviour in the flow delivery. In Table 7.2, the uncertainty components of the measurement of the flow rate of 3 µL/h are presented. The uncertainty calculation was determined according to the GUM [22] considering Equation 5.1. Even though this flow rate test has the lowest uncertainty value, the biggest contributor is still the repeatability.

Table 7.1 - Front track method results with 1.15 mm internal diameter capillary

Nominal flow rate /(µL/h)	Measured flow rate /(µL/h)	Relative Error / %	Relative Uncertainty / %
0.25	0.46	84	13
1	1.00	0.00	17
3	3.00	0.00	12
6	6.03	0.50	29
10	10.03	0.30	14

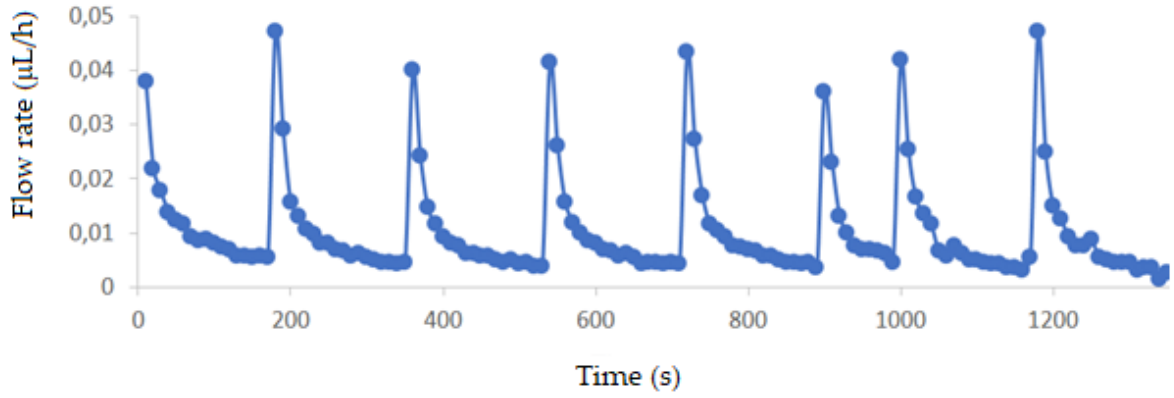

Figure 7.4 - Front track method 10 µL/h insulin pump flow behaviour

Table 7.2 – Uncertainty contributions for flow rate of 3 µL/h

Uncertainty components	Estimation	$u(x_i)$	c_i	$(c_i \cdot x_i)^2$/d.o.f
Displacement /mm	2.39	$1.50 \cdot 10^{-2}$	$3.48 \cdot 10^{-4}$	$1.48 \cdot 10^{-23}$
Radius /mm	0.575	$4.52 \cdot 10^{-3}$	$2.90 \cdot 10^{-3}$	$5.91 \cdot 10^{-22}$
Time /s	2987.23	$2.97 \cdot 10^{-3}$	$-2.79 \cdot 10^{-7}$	$9.46 \cdot 10^{-39}$
Repeatability /(µL/s)	$4.78 \cdot 10^{-5}$	$4.78 \cdot 10^{-5}$	1.00	$2.60 \cdot 10^{-20}$
Lens focus /(µL/s)	$1.3 \cdot 10^{-7}$	$1.3 \cdot 10^{-7}$	1.00	$5.71 \cdot 10^{-26}$
Stability /(µL/s)	$6.76 \cdot 10^{-6}$	$6.76 \cdot 10^{-6}$	1.00	$6.58 \cdot 10^{-24}$

Expansion coefficient /ºC^{-1}	0.0001	$2.89 \cdot 10^{-8}$	$5.97 \cdot 10^{-4}$	$1.77 \cdot 10^{-48}$
Temperature /ºC	19.28	0.005	$-8.34 \cdot 10^{-9}$	$6.05 \cdot 10^{-44}$
Flow rate* /(μL/h)	3.00			
$u_{comb}\,Q$ /(μL/h)	0.18			
$U_{exp}\,Q$ /(μL/h)	0.36			

Note: *Flow rate calculated according to Eq. 5.1.

The measurements performed with the 0.5 mm diameter capillary without coating had an initial wait time of 10 minutes, and an acquisition time of 10 s for flow rates between 1 and 10 μL/h and of 30 s for the flow rate of 0.25 μL/h. The total duration of the test performed with a flow rate of 0.25 μL/h was of one hour. For the flow rates of 1 and 3 μL/h the tests ran for 30 minutes, and for 6 μL/h the test lasted 25 minutes. For the highest flow rate, 10 μL/h, the total duration was of 10 minutes. The results of these measurements are presented in Table 7.3. The results show that within the range of the measured flow rates, the uncertainties do vary significantly. The highest uncertainty contribution for all measurements was once again the repeatability, having an even bigger contribution in this capillary compared to the 1.15 mm diameter capillary ($4.17 \cdot 10^{-16}$ for the 10 μL/h flow rate and $1.19 \cdot 10^{-17}$ for the 6 μL/h flow rate). The 0.25 μL/h results were inconclusive. Additionally, the flow rate measurement of 6 μL/h showed not only the lowest uncertainty value, but also the lowest error.

Table 7.3 - Front track method results with 0.5 mm internal diameter capillary without coating

Nominal flow rate / (μL/h)	Measured flow rate /(μL/h)	Relative Error / %	Relative Uncertainty / %
1	0.42	-58	16
3	2.05	-32	14
6	6.04	0.67	7.4
10	10.15	1.5	21

The measurements performed with the 0.5 mm diameter capillary with coating had initial waiting times of 10 and 30 minutes, and acquisition times of 10 and 30 s. For the tests performed with initial waiting time of 10 minutes and acquisition time of 10 s, the total duration of the test for each flow rate imposed was the same as the one of the 0.5 mm diameter capillary without the coating. For the tests performed with initial waiting time of 30 minutes and acquisition time of 30 s, the total duration was of two hours for a flow rate of

0.25 μL/h, one hour and a half for a flow rate of 1 μL/h, one hour for a flow rate of 3 μL/h, 25 minutes for a flow rate of 6 μL/h and, finally, 10 minutes for the highest flow rate, 10 μL/h.

The results of the measurements performed with an acquisition time of 10 s and a waiting time of 10 min are presented in Table 7.4. The results show that within the range of the measured flow rates, the uncertainties vary less than they did for the 0.5 mm diameter capillary without the coating. The highest uncertainty contribution for all measurements was once more the repeatability, having a bigger contribution in this capillary compared to the 1.15 mm diameter capillary for the flow rate of 10 µL/h ($urep^2 = 9.86 \cdot 10^{-18}$) but a lower contribution for the flow rate of 6 µL/h ($urep^2 = 3.18 \cdot 10^{-19}$). Compared to the 0.5 mm diameter capillary without coating, the repeatability uncertainty component is lower for the capillary with coating. Additionally, the flow rate measurement of 6 µL/h showed the lowest uncertainty value again.

Table 7.4 - Front track method with 0.5 mm internal diameter capillary with coating, 10 s acquisition time, 10 min wait time

Nominal flow rate / (µL/h)	Measured flow rate /(µL/h)	Relative Error / %	Relative Uncertainty / %
0.25	0.30	20	7.7
1	0.85	-15	11
3	3.00	0.00	13
6	5.64	-6.0	9.5
10	10.02	0.20	11

The results of the measurements performed with an acquisition time of 30 s and a waiting time of 30 min are presented in Table 7.5. The results show similar uncertainties, but higher errors. For the flow rates between 1 and 6 µL/h the uncertainty values improved slightly compared to the values obtained with 10 s acquisition time and 10 minutes waiting time. A contributing factor for this improvement is the test time, which was twice or more long for the flow rates of 1 and 3 µL/h.

The repeatability uncertainty contribution was lower for the flow rate of 6 µL/h ($urep^2 = 1.54 \cdot 10^{-19}$) and higher for the flow rate of 10 µL/h ($urep^2 = 1.70 \cdot 10^{-17}$) compared to the values of the tests that ran with 10 s acquisition time and 10 min wait time. For the 10 µL/h flow rate the uncertainty value didn't improve, which can be explained by the fact that, for a 0.5 mm diameter capillary, the field of view of the camera only allows for 10 minutes of test time. For the 0.25 µL/h flow rate the uncertainty also did not improve, even though the test time was doubled.

Table 7.5 - Front track method results with 0.5 mm internal diameter capillary with coating, 30 s acquisition time, 30 min wait time

Nominal flow rate / (μL/h)	Measured flow rate /(μL/h)	Relative Error / %	Relative Uncertainty / %
0.25	0.29	16	9.9
1	1.11	11	9.6
3	2.81	-6.3	11
6	5.45	-9.2	8.3
10	9.21	-7.9	13

7.1.2. Drop method

As shown in Figure 7.5, the insulin pump (1) was connected to a polypropylene capillary tube (2), which ended inside the evaporation trap (3); a LED lamp (4) was turned on and pointed towards the evaporation trap; a translucid paper (5) was placed in between the evaporation trap and the lamp, in order to diffuse de light; the thermometer (6) measured the temperature of the water contained in a beaker placed near the evaporation trap, since it is not possible to measure the temperature of the droplet hanging at the tip of the tube inside the evaporation trap; the camera (7) was positioned so that at the tip of the tube was centred within the field of view of the camera.

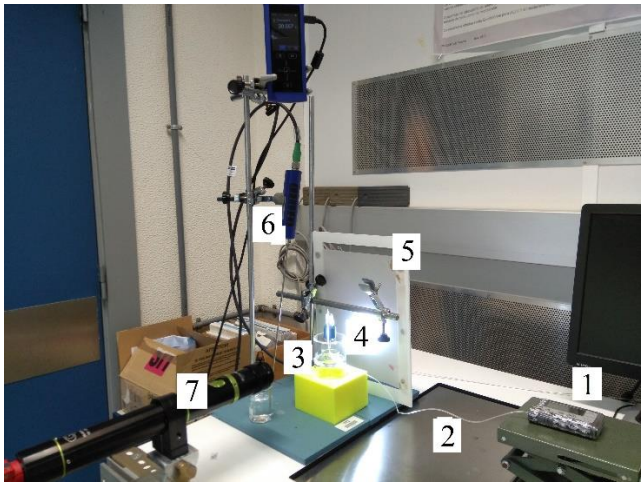

Figure 7.5 - Drop method experimental setup for insulin pump calibration

All tests were done with an acquisition time of 10 s, and a total duration of two hours for the flow rate of 0.25 μL/h and of one hour for flow rates between 1 and 10 μL/h.

The projected area of the drop was obtained by the python image processing software, and knowing the polypropylene capillary tube diameter, 1.49658 mm, measured by interferometry, the scale and volume values were calculated.

Additionally, after each flow test was finished, an evaporation test was performed with the insulin pump switched off, at the same working conditions, in order to determine the evaporation correction to be applied to the flow rate.

The results of the measurements are presented in Table 7.6. Even though the errors are low, the uncertainties are higher when compared to the uncertainty values obtained with the front track method. The results show that within the range of the measured flow rates, the uncertainties vary significantly. The highest uncertainty contribution for all measurements was the repeatability, once again. The flow variability of the insulin pump is observed once more in Figure 7.6, where the insulin pump continues to show a pulse-like behaviour in the flow delivery. In Table 7.7, the uncertainty components of the measurement of the flow rate of 10 µL/h are presented. The uncertainty calculation was determined according to the GUM methodology [22] considering Equation 6.1.

Table 7.6 - Drop method results

Nominal flow rate / (µL/h)	Measured flow rate /(µL/h)	Relative Error / %	Relative Uncertainty / %
0.25	0.25	-16	1321
1	1.01	1.00	274
3	3.01	0.33	96
6	6.00	0.00	66
10	10.03	0.30	30

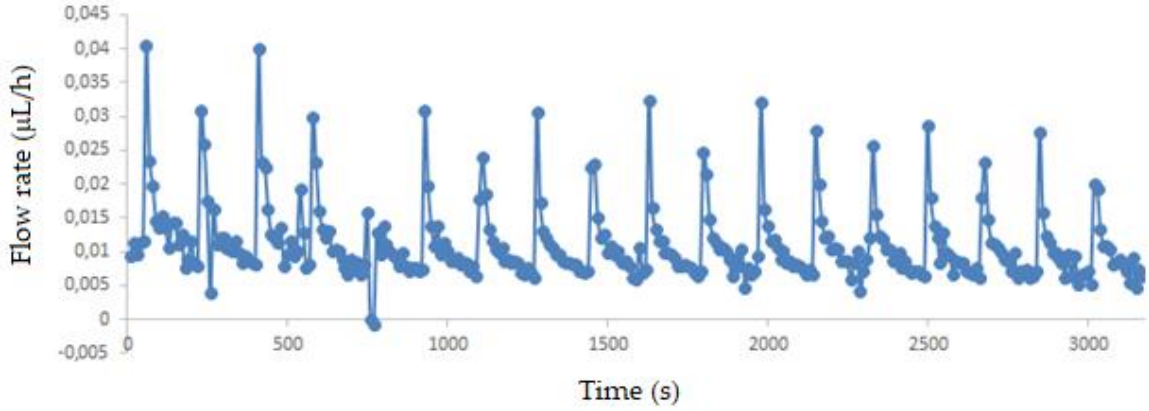

Figure 7.6 - Drop method 10 µL/h insulin pump flow behaviour

Table 7.7 - Uncertainty contributions for a flow rate of 10 µL/h

Uncertainty components	Estimation	$u(x_i)$	c_i	$(c_i \cdot x_i)^2$/d.o.f
Volume /mm³	7.985	$5.39 \cdot 10^{-4}$	$1.65 \cdot 10^{-7}$	$5.43 \cdot 10^{-19}$
Time /s	3270.42	$2.97 \cdot 10^{-3}$	$4.92 \cdot 10^{-18}$	$4.84 \cdot 10^{-37}$
Repeatability /µL/s)	$5.93 \cdot 10^{-5}$	$5.93 \cdot 10^{-5}$	1.00	$4.41 \cdot 10^{-19}$
Evaporation /(µL/s)	$4.92 \cdot 10^{-5}$	$7.42 \cdot 10^{-6}$	1.00	$6.06 \cdot 10^{-26}$
Flow rate* /(µL/h)	10.03			
u_{comb} /(µL/h)	1.50			
U_{exp} /(µL/h)	3.95			

Note: *Flow rate calculated according to Eq. 6.1.

7.1.3. Gravimetric method

As shown in Figure 7.7, the insulin pump (1) was connected to a polypropylene capillary tube (2), which ended inside the evaporation trap (3) where its tip was submerged in the water contained in the calibrating vessel (4); this container is placed on the Mettler Toledo AX26 balance (5) along with the evaporation trap.

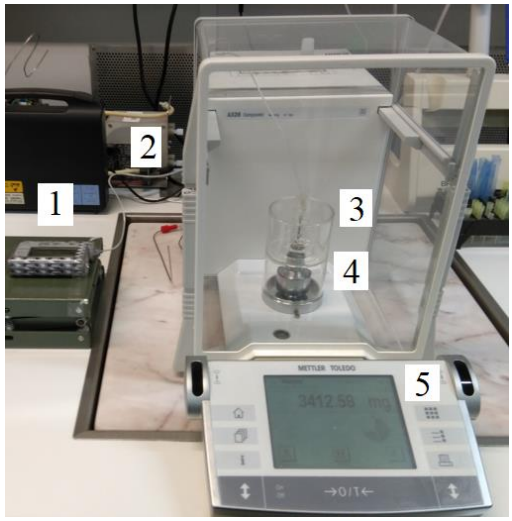

Figure 7.7 - Gravimetric method experimental setup for insulin pump calibration

The 10 μL/h flow rate was measured with an acquisition time of 30 s, and total duration of two hours, using a customised application developed in LabVIEW.

The result of the measurement is presented in Table 7.8. The obtained uncertainty value is the lower than the ones obtained by the optical methods, however the error is higher. The flow variability of the insulin pump is observed once more in Figure 7.8. In Table 7.9, the uncertainty components of the measurement of the flow rate of 10 µL/h are presented. The uncertainty calculation was determined according to the GUM [22] considering Equation 2.22. The highest uncertainty contribution was the repeatability, once again.

Table 7.8 - Gravimetric method results

Nominal flow rate / (µL/h)	Measured flow rate /(µL/h)	Relative Error / %	Relative Uncertainty / %
10	11.49	15	5.7

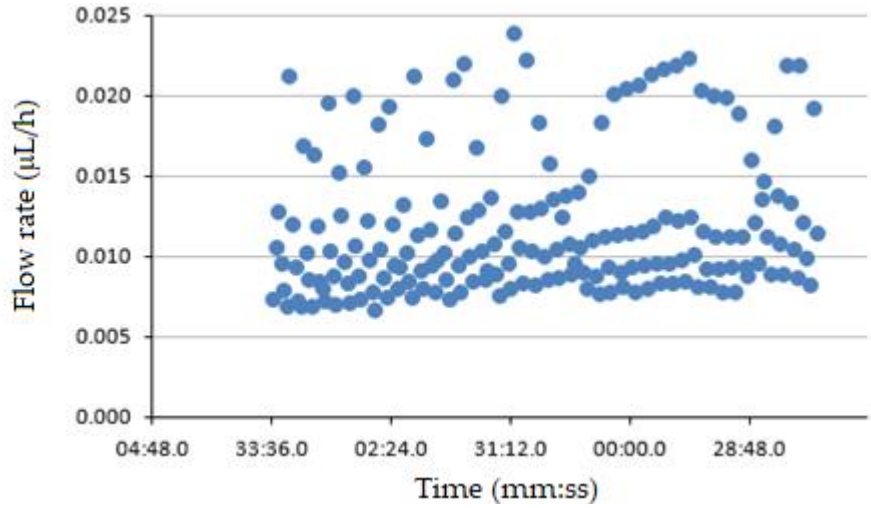

Figure 7.8 – Gravimetric method 10 µL/h insulin pump flow behaviour

Table 7.9 – Gravimetric method uncertainty contributions for the flow rate of 10 µL/h

Uncertainty components	Estimation	$u(x_i)$	c_i	$(c_i \cdot x_i)^2$/d.o.f
Final mass /g	3.09	$3.42 \cdot 10^{-5}$	$1.27 \cdot 10^{-4}$	$7.08 \cdot 10^{-39}$
Water density /(g/mL)	0.998049	$5.98 \cdot 10^{-4}$	$-3.10 \cdot 10^{-6}$	$2.36 \cdot 10^{-37}$
Air density /(g/mL)	0.001185	$2.89 \cdot 10^{-6}$	$2.71 \cdot 10^{-6}$	$7.50 \cdot 10^{-50}$
Balance weight density /(g/mL)	8.00	$2.50 \cdot 10^{-3}$	$5.72 \cdot 10^{-11}$	$8.34 \cdot 10^{-54}$
Temperature /ºC	20.7	$4.47 \cdot 10^{-2}$	$-7.41 \cdot 10^{-10}$	$2.42 \cdot 10^{-44}$
Expansion coefficient /(ºC)	$2.40 \cdot 10^{-4}$	$6.93 \cdot 10^{-6}$	$-2.26 \cdot 10^{-6}$	$1.20 \cdot 10^{-48}$
Initial mass /g	3.07	$3.42 \cdot 10^{-5}$	$-1.27 \cdot 10^{-4}$	$7.08 \cdot 10^{-39}$
Evaporation /(mL/s)	$1.04 \cdot 10^{-7}$	$1.47 \cdot 10^{-8}$	1.00	$9.26 \cdot 10^{-37}$

Initial time /s	1820	$7.00 \cdot 10^{-4}$	$3.91 \cdot 10^{-10}$	$1.12 \cdot 10^{-52}$
Final time /s	9720	$7.00 \cdot 10^{-4}$	$-3.91 \cdot 10^{-10}$	$1.12 \cdot 10^{-52}$
Buoyancy /g	0.0003	$3.94 \cdot 10^{-6}$	$1.27 \cdot 10^{-4}$	$1.25 \cdot 10^{-42}$
Repeatability /(mL/s)	$1.204 \cdot 10^{-6}$	$8.90 \cdot 10^{-8}$	1.00	$3.45 \cdot 10^{-31}$
Flow rate* /(μL/h)	11.49			
u_{comb} /(μL/h)	0.33			
U_{exp} /(μL/h)	0.66			

Note: *Flow rate calculated according to Eq. 3.22.

7.1.4. Conclusions

The results from all the used calibration methods revealed a large flow rate variability caused by the pulse-like behaviour of the pushing mechanism of the insulin pump piston and this significantly affected the error and uncertainty of the measurements, in order to decrease this uncertainty component an analyse of the data of a dose cycle time and delivered doses as a function of time could be done if the measuring time is large enough.

Between both the optical methods, the front track method showed lower uncertainty values for all the tested flow rates, mainly because of need to improve the volume method determination uncertainty in the drop method.

In the front track method, the results obtained with the 0.5 mm internal diameter capillary with coating showed the lowest uncertainty values among all the capillaries, however, it also showed higher errors when compared to the 1.15 mm capillary. The low uncertainties may be linked to the coating, as it can allow for a reduced friction between the calibration fluid (in this case water) and the surface of the capillary. Additionally, for the 0.5 mm diameter capillaries, the measurements of 6 μL/h flow rates showed lower uncertainty values than the 10 μL/h flow rates. This may be due to fact that, for this capillary size, the maximum test time for a 10 μL/h flow rate is 10 minutes, while a 6 μL/h flow rate test can run for half an hour.

The gravimetric method showed the lowest uncertainty value for the flow rate of 10 μL/h, but a larger error. Also, the total test duration in the gravimetric method was two hours compared to only 10 minutes in the front tracking method, due to its limitations with the camera's field of view. Due to the gravimetric method limitation range, it is not possible to go down 10 μL/h with reasonable uncertainties. In this work, with the front track method it is possible to measure below 10 μL/h with uncertainties of 10 %. These uncertainty values could be improved if the test duration is increased.

From the results obtained it can be assumed that the front tracking method, when compared to the gravimetric method, proved to be a reliable calibration method for low flow rates at which the tested insulin pump operates.

7.2. Nexus 3000 syringe pump

The high precision push-pull syringe pump system from the manufacturer Chemyx, model Nexus 3000, with a step resolution of 0.012 μm, was calibrated at flow rates of 1 μL/h, 1.2 μL/h, 3 μL/h, 4.2 μL/h, 6 μL/h, 10 μL/h, 30 μL/h, 60 μL/h, 90 μL/h, 100 μL/h, 500 μL/h and 1000 μL/h by the front tracking method and at flow rates of 1 μL/h, 10 μL/h, 100 μL/h, 500 μL/h and 1000 μL/h by the drop method and the gravimetric method.

7.2.1. Front tracking method

As shown in Figure 7.9, on the Nexus 3000 flow generator (1) was installed a 1 mL A-class glass syringe (2), which was connected to a stainless steel capillary tube (3), which itself was connected to a glass capillary tube (4); a LED lamp (5) was turned on and pointed towards the capillary; a translucid paper (6) was placed in between the capillary tube and the LED lamp in order to diffuse de light; the camera (7) was positioned so that at the right edge of its field of view the meniscus of the liquid appeared. The clamp (8) was used to keep the capillary tube in a straight horizontal fixed position. Since it is not possible to measure the temperature of the fluid inside the glass capillary tube, a beaker (9) containing water was placed near the capillary tube, so that the thermometer (10) could measure, as accurately as possible, the temperature of the calibration fluid.

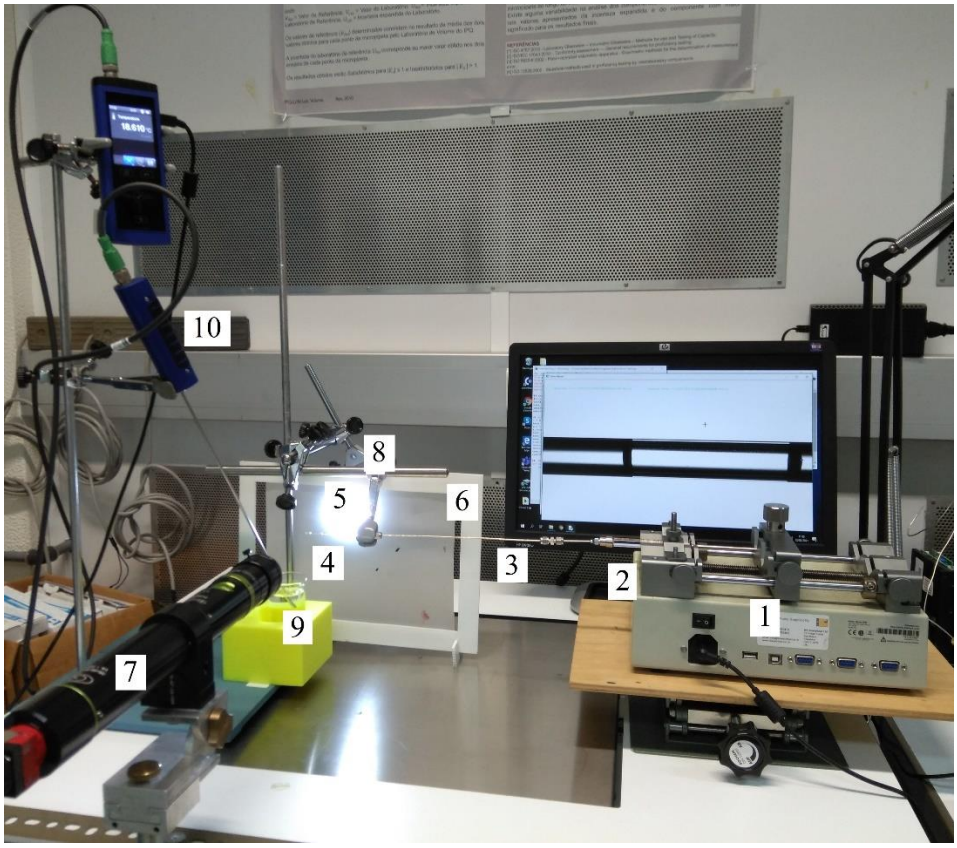

Figure 7.9 - Front tracking method experimental setup for Nexus 3000 calibration

7.2.1.1. Flow meter comparison

The Sensirion thermal flow meter, show in Figure 7.10, was used during the Nexus 3000 syringe pump calibration, via the front track method, at flow rates of 1.2 μL/h, 3 μL/h, 4.2 μL/h, 6 μL/h, 30 μL/h, 60 μL/h and 90 μL/h, in order to verify if the measured flow rates were concordant.

Figure 7.10 - Sensirion flow meter

Using an identical setup to the one shown in Figure 7.9, the flow meter was placed between two stainless steel capillary tubes, one connected to the syringe and the other to the glass capillary tube, with the attachment show in Figure 7.11.

Figure 7.11 - Flow meter attachment to stainless steel capillary tube

Measurements were performed using three different glass capillary tubes. The first capillary had an internal diameter of 1.15 mm (Setup NS.1) while the other two had internal diameters of 0.5 mm, one with an internal coating (Setup NS.2) and the other without (Setup NS.3).

The measurements performed with the 1.15 mm diameter capillary (setup NS.1) had an acquisition time of 10 s for flow rates between 1.2 and 60 μL/h and of 5 s for the flow rate of 90 μL/h. The total duration of the tests performed with the flow rates of 1.2 μL/h, 3 μL/h, 4.2 μL/h and 6 μL/h was of one hour. For the flow rates of 30 μL/h, 60 μL/h and 90 μL/h the tests lasted as long as the field of view of the camera allowed for the minimum magnification of 0.43x, which was 30, 15 and 10 minutes, respectively.

The measurements performed with both the 0.5 mm diameter capillaries (setup NS.2 and setup NS.3) had an acquisition time of 5 s for flow rates between 1.2 μL/h and 6 μL/h and of 1 s for the flow rates between of 30 μL/h and 90 μL/h. For the flow rates of 1.2 μL/h, 3 μL/h, 4.2 μL/h and 6 μL/h the total duration of each test was as long as the field of view of the camera allowed for the magnification of 1.5x, which was 35, 30, 20 and 15 minutes, respectively. For the flow rates of 30 μL/h, 60 μL/h and 90 μL/h the tests lasted as long as the

field of view of the camera allowed for the magnification of 0.75x, which was 3, 1.5 and 1 minutes, respectively.

Tables 7.10 and 7.11 show the comparison of the uncertainty values obtained when using the older equation ($y = 0.001 \cdot \Delta t^{-0.525}$) and the newer one for the 1.15 mm capillary ($y = 0.0003 \cdot \Delta t^{-0.474}$) and the 0.5 mm capillary ($y = 0.0006 \cdot \Delta t^{-0.835}$), respectively.

Table 7.10 – Stability uncertainty contribution comparison on 1.15 mm capillary

Nominal flow rate /(μL/h)	Uncertainty equation	Measured flow rate /(μL/h)	Relative Error / %	Relative Uncertainty / %
1	Old	1.04	4.0	8.2
	New	1.04	4.0	5.5
10	Old	9.92	-0.80	3.6
	New	9.92	-0.80	3.5
100	Old	99.11	-0.89	3.4
	New	99.11	-0.89	3.4
500	Old	496.08	-0.78	3.4
	New	496.08	-0.78	3.4
1000	Old	999.84	-0.02	3.5
	New	999.84	-0.02	3.5

Table 7.11 – Stability uncertainty contribution comparison on 0.5 mm capillary with internal coating

Nominal flow rate /(μL/h)	Uncertainty equation	Measured flow rate /(μL/h)	Relative Error / %	Relative Uncertainty / %
1	Old	1.00	0.00	22
	New	1.00	0.00	7.8
10	Old	10.25	2.5	7.8
	New	10.25	2.5	6.7
100	Old	105.48	5.48	4.9
	New	105.48	5.48	4.8
500	Old	495.56	-0.91	4.8
	New	495.56	-0.91	4.8
1000	Old	1024.68	2.5	4.2
	New	1024.68	2.5	4.2

The results show that for the 1.15 mm capillary the expanded uncertainty values remain the same for the flow rates of 100 μL/h and above, but are reduced for the lower flow rates, more noticeably for 1 μL/h. For the 0.5 mm capillary the same changes are observed, with the uncertainty value decreasing significantly for the 1 μL/h flow rate.

The results of the tests, of the comparison between the measured flow rate by the front tracking method and by the Sensirion thermal flow meter, performed with the glass capillary tubes with internal diameters of 1.15 mm (setup NS.1) and 0.5 mm, with an internal coating (setup NS.2) and without (setup NS.3) are presented in Table 7.12, where the relative error is calculated considering the measured flow rate by the flow meter as the nominal value.

Table 7.12 - Comparison between the Sensirion flow meter and the Front tracking method measured flow rates

Nominal flow rate /(μL/h)	Setup	Flow meter measured flow rate /(μL/h)	Front tracking measured flow rate /(μL/h)	Relative Error / %	Relative Uncertainty / %
90	NS.1	90.47	90.22	-0.28	3.4
	NS.2	88.54	85.03	-4.0	4.5
	NS.3	94.15	92.54	-1.7	4.4
60	NS.1	62.84	60.31	-4.0	3.4
	NS.2	62.94	62.97	0.05	4.4
	NS.3	60.65	60.62	-0.05	4.8
30	NS.1	30.65	29.98	-2.2	3.3
	NS.2	30.85	30.32	-1.7	4.5
	NS.3	30.80	30.90	0.32	4.2
6	NS.1	6.18	6.04	-2.3	3.6
	NS.2	5.99	5.85	-2.3	4.5
	NS.3	6.06	6.08	0.33	4.4
4.2	NS.1	4.40	4.21	-4.3	3.9
	NS.2	4.02	4.05	0.75	7.2
	NS.3	4.33	4.28	-1.2	4.4
3	NS.1	3.05	2.89	5.2	4.1
	NS.2	3.12	2.97	-4.2	5.9
	NS.3	3.56	2.84	-20	4.6
1.2	NS.1	1.20	1.20	0.00	6.5
	NS.2	0.78	1.09	40	7.0
	NS.3	1.21	0.82	-32	12

The results show that for all the measured flow rates, the uncertainty values are the lowest for the measurements performed with the 1.15 mm diameter capillary (setup NS.1). When analysing the uncertainty components of the measurements performed with the 1.15 mm and 0.5 mm capillaries for the flow rate of 6 μL/h, presented in Tables 7.13 and 7.14 respectively, it is possible to understand why this happens. Since the total duration of the measurement using the 0.5 mm capillary is much lower than the one using the 1.15 mm capillary, the uncertainty related to the total duration, and any other time dependent uncertainty component, such as the stability, is higher for the 0.5 mm.

Table 7.13 - Uncertainty contributions of setup NS.1 for flow rate of 6 μL/h

Uncertainty components	Estimation	$u(x_i)$	c_i	$(c_i \cdot x_i)^2$/d.o.f
Displacement /mm	5.49	$1.50 \cdot 10^{-2}$	$3.06 \cdot 10^{-4}$	$8.93 \cdot 10^{-24}$
Radius /mm	0.575	$4.52 \cdot 10^{-3}$	$5.84 \cdot 10^{-3}$	$9.68 \cdot 10^{-21}$
Time /s	3398	$2.97 \cdot 10^{-3}$	$-4.94 \cdot 10^{-7}$	$9.25 \cdot 10^{-38}$
Repeatability /(μL/s)	$1.12 \cdot 10^{-5}$	$1.12 \cdot 10^{-5}$	1.00	$7.78 \cdot 10^{-23}$
Lens focus /(μL/s)	$1.30 \cdot 10^{-7}$	$1.30 \cdot 10^{-7}$	1.00	$5.71 \cdot 10^{-30}$
Stability /(μL/s)	$6.36 \cdot 10^{-6}$	$6.36 \cdot 10^{-6}$	1.00	$5.71 \cdot 10^{-30}$
Expansion coefficient /ºC^{-1}	0.00001	$2.89 \cdot 10^{-8}$	$1.57 \cdot 10^{-3}$	$8.34 \cdot 10^{-47}$
Temperature /ºC	19.07	0.005	$-1.68 \cdot 10^{-8}$	$9.90 \cdot 10^{-43}$
Flow rate* /(μL/h)	6.04			
u_{comb} Q /(μL/h)	0.11			
U_{exp} Q /(μL/h)	0.22			

Note: *Flow rate calculated according to Eq. 5.1.

Table 7.14 - Uncertainty contributions of setup NS.2 for flow rate of 6 μL/h

Uncertainty components	Estimation	$u(x_i)$	c_i	$(c_i \cdot x_i)^2$/d.o.f
Displacement /mm	4.35	$1.50 \cdot 10^{-2}$	$3.73 \cdot 10^{-4}$	$1.97 \cdot 10^{-23}$
Radius /mm	0.25	$2.51 \cdot 10^{-3}$	$1.89 \cdot 10^{-1}$	$1.01 \cdot 10^{-15}$
Time /s	526	$2.97 \cdot 10^{-3}$	$-3.09 \cdot 10^{-6}$	$1.41 \cdot 10^{-34}$
Repeatability /(μL/s)	$1.39 \cdot 10^{-5}$	$1.39 \cdot 10^{-5}$	1.00	$3.55 \cdot 10^{-22}$
Lens focus /(μL/s)	$1.30 \cdot 10^{-7}$	$1.30 \cdot 10^{-7}$	1.00	$5.71 \cdot 10^{-30}$
Stability /(μL/s)	$3.21 \cdot 10^{-6}$	$3.21 \cdot 10^{-6}$	1.00	$3.33 \cdot 10^{-25}$
Expansion coefficient /ºC^{-1}	0.00001	$2.89 \cdot 10^{-8}$	$1.15 \cdot 10^{-3}$	$2.43 \cdot 10^{-47}$
Temperature /ºC	19.29	0.005	$-1.62 \cdot 10^{-8}$	$8.69 \cdot 10^{-43}$
Flow rate* /(μL/h)	5.85			
u_{comb} Q /(μL/h)	0.13			
U_{exp} Q /(μL/h)	0.26			

Note: *Flow rate calculated according to Eq. 5.1.

The obtained uncertainty values of the measurements performed with the 0.5 mm capillaries are very similar between the flow rates of 6 μL and 90 μL/h. The uncertainty of the measurements performed using the capillary with the internal coating (setup NS.2) is higher for the flow rates of 3 μL and 4.2 μL/h and significantly lower for the flow rate of 1.2 μL/h, compared to the values obtained using the capillary without the internal coating (setup NS.3). These uncertainty differences are mainly due to the fact that, for the same flow rate, the total duration of some tests was cut shorter because the software was not recognizing the meniscus correctly, thus making the meniscus tracker either remain in the same position or jump back to its initial one. This issue happened in almost all the tests performed with the 0.5 mm capillaries, being that the results previously presented in Table 8.12 are the ones which had the least interruptions. One way to reduce this problem is to the lens magnification for the test, however, with a higher magnification the field of view of the camera is reduced, and so is the total duration, which is already very short. If one was to consider the lowest total duration for each flow rate and adjust the time of the other measurements of the same flow rate to be the same, it would be possible to observe with higher accuracy the difference each capillary has on the measurement results.

In Table 7.15 the results of the measurements presented previously were adjusted in such a way that, for each flow rate, the total duration of each measurement was made to be equal to the lowest total duration, for the same flow rate. In other words, if for a certain flow rate, the total duration of the measurement was 10 minutes using setup NS.1, 5 minutes using setup NS.2 and 7 minutes using setup NS.3, only the first 5 minutes of the measurements performed with setups NS.1 and NS.3 would be considered. The results show that, considering an equal measurement duration, the obtained uncertainty values using the 0.5 mm capillaries are always lower than the values obtained with the 1.15 mm capillary. Therefore, if one could increase the duration of the measurements performed with the 0.5 mm capillaries, by means of, for example, a moving camera that follows the meniscus, it would be possible to reduce the obtained uncertainty values. The measurements performed with the capillary without the internal coating usually present lower uncertainty values compared to the capillary with the coating.

Table 7.15 – Comparison of setups NS.1, NS.2 and NS.3 considering same total durations of measurements

Nominal flow rate /(μL/h)	Setup	Initial total duration / s	Initial relative Uncertainty / %	Adjusted total duration / s	Relative Uncertainty / %
90	NS.1	576	3.4	22	6.3
	NS.2	62	4.5		6.1
	NS.3	22	4.4		4.4
60	NS.1	762	3.4	52	6.4
	NS.2	75	4.4		4.5
	NS.3	52	4.8		4.8
30	NS.1	1744	3.3	154	4.5
	NS.2	178	4.5		4.5
	NS.3	154	4.2		4.2
6	NS.1	3398	3.6	526	6.3
	NS.2	526	4.5		4.5
	NS.3	942	4.4		4.6
4.2	NS.1	3428	3.9	662	6.5
	NS.2	662	7.2		7.2
	NS.3	1263	4.4		4.7
3	NS.1	3549	4.1	897	7.2
	NS.2	897	5.9		5.9
	NS.3	1734	4.6		4.9
1.2	NS.1	3398	6.5	642	19
	NS.2	1980	7.0		11
	NS.3	642	12		12

7.2.1.2. Additional measurements

Using the setup shown in Figure 7.9, without the flow meter, measurements were performed with the glass capillary tube with an internal diameter of 1.15 mm (Setup N.1). All the performed measurements had an initial wait time of 15 minutes. The set acquisition time and total duration of the measurements are presented in Table 7.16. For the flow rates of 100 μL/h, 500 μL/h and 1000 μL/h the total duration of each test was as long as the field of view of the camera allowed for the magnification of 0.5x.

Table 7.16 - Acquisition times and total duration of front tracking measurements using setup N.1

Nominal flow rate / (μL/h)	Acquisition time / s	Duration
1	30	2 h
10	10	1 h 30 min
100	1	10 min
500	1	2 min
1000	1	1 min

The results of the measurements are presented in Table 7.17. The results show very similar uncertainty values for the flow rates between 10 μL/h and 1000 μL/h, even though uncertainties usually increase as the flow rate decreases. This is levelled out by the fact that lowering the flow rate increases the amount of time that the measurement can last. Therefore, if one could increase the duration of the measurements, in particular for the flow rates between 100 μL/h and 1000 μL/h, it would be possible to decrease the obtained uncertainty values.

Table 7.17 – Front tracking method results of Nexus 3000 calibration (setup N.1)

Nominal flow rate / (μL/h)	Measured flow rate /(μL/h)	Relative Error / %	Relative Uncertainty / %
1	1.04	4.0	5.5
10	9.92	-0.80	3.5
100	99.11	-0.89	3.4
500	496.08	-0.78	3.4
1000	999.84	-0.02	3.5

7.2.2. Drop method

As shown in Figure 7.12, on the Nexus 3000 flow generator (1) was installed a 1 mL A-class glass syringe (2), which was connected to a stainless steel capillary tube (3), which ended inside the evaporation trap (6); a translucid paper (4) was placed in between the evaporation trap and the LED lamp (5), in order to diffuse de light; the evaporation trap (6) was placed on its holder (7); the camera (8) was positioned so that the tip of the tube was centred within the field of view of the camera. A clamp (9) was used to keep the capillary tube in a fixed position; Since it is not possible to measure the temperature of the fluid inside the capillary tube, or of the droplet itself, a beaker containing water (10) was placed inside the evaporation trap, so that the temperature of the contained fluid was as close as the temperature of the droplet. To avoid small variations in the position of the edge of the tube inside the evaporation trap during the measurements, a guider (11) was used.

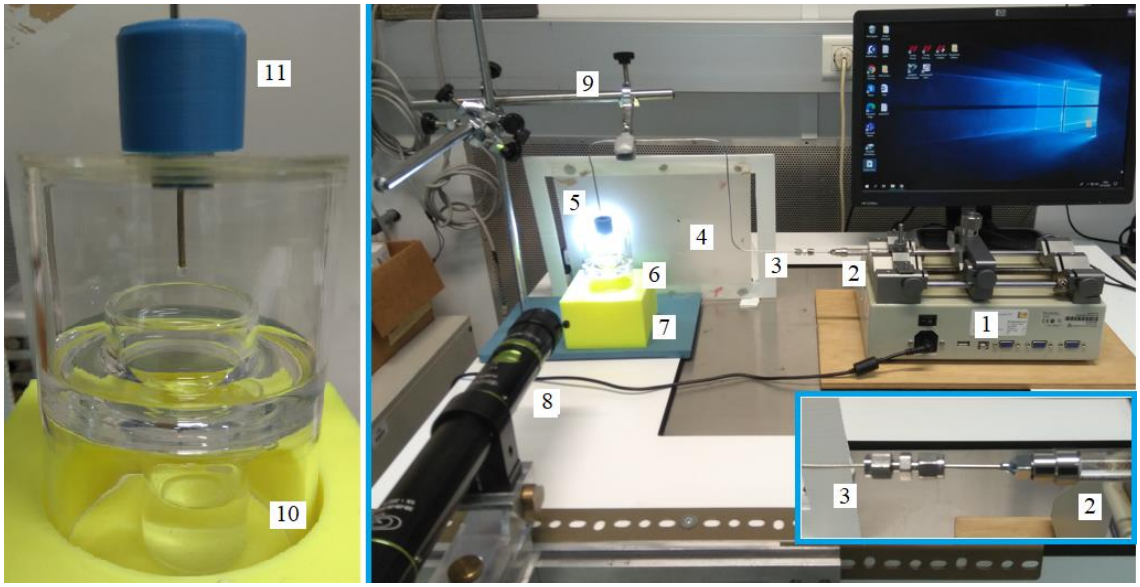

Figure 7.12 - Drop method experimental setup for Nexus 3000 calibration

All the performed measurements had an initial wait time of 15 minutes. The set acquisition time were the same as the ones that are presented in Table 6.1, as well as the total duration for the flow rates of 1 μL/h and 10 μL/h. For the flow rates of 100 μL/h, 500 μL/h and 1000 μL/h the total duration of each test was as long as the time it took for the drop to fully form and fall.

The results of the measurements are presented in Table 7.18. The obtained uncertainty values are higher than the ones obtained by the front tracking method for the flow rates of 100 µl/h and under. For the flow rates of 500 μL/h and 1000 µl/h the uncertainty values are similar to the ones obtained by the front tacking method. The error of the 1 µl/h measurement is noticeably higher in this method due to the evaporation. In Table 7.19, the uncertainty components of the measurement of the flow rate of 10 µL/h are presented. The uncertainty calculation was determined according to the GUM methodology [22] considering Equation 6.1.

Table 7.18 - Drop method results

Nominal flow rate / (µL/h)	Measured flow rate /(µL/h)	Relative Error / %	Relative Uncertainty / %
1	0.87	-13	95
10	9.65	-3.5	30
100	102.13	2.1	6.7
500	496.10	-0.78	3.1
1000	990.92	-0.92	3.8

Table 7.19 – Drop method uncertainty contributions for the flow rate of 10 µL/h

Uncertainty components	Estimation	$u(x_i)$	c_i	$(c_i \cdot x_i)^2$/d.o.f
Volume /mm³	5.35	$5.39 \cdot 10^{-4}$	$1.47 \cdot 10^{-8}$	$4.30 \cdot 10^{-21}$
Time /s	36752	$2.97 \cdot 10^{-3}$	$1.38 \cdot 10^{-22}$	$3.82 \cdot 10^{-46}$
Repeatability /µL/s)	$1.40 \cdot 10^{-5}$	$1.40 \cdot 10^{-5}$	$1.95 \cdot 10^{-10}$	$3.15 \cdot 10^{-23}$
Evaporation /(µL/s)	$2.53 \cdot 10^{-3}$	$3.82 \cdot 10^{-4}$	$1.46 \cdot 10^{-7}$	$4.26 \cdot 10^{-19}$
Flow rate* /(µL/h)	9.65			
u_{comb} /(µL/h)	1.4			
U_{exp} /(µL/h)	2.89			

Note: *Flow rate calculated according to Eq. 6.1.

7.2.3. Gravimetric method

As shown in Figure 7.13, on the Nexus 3000 flow generator (1) was installed a 1 mL A-class glass syringe (2), connected to a stainless steel capillary tube (3), which ended inside the evaporation trap (4) where its tip was submerged in the water contained in the calibrating vessel (5); this container is placed on the Mettler Toledo AX26 balance (7) along with the evaporation trap and guider (6) used to avoid direct contact between tube and the evaporation trap during the measurements.

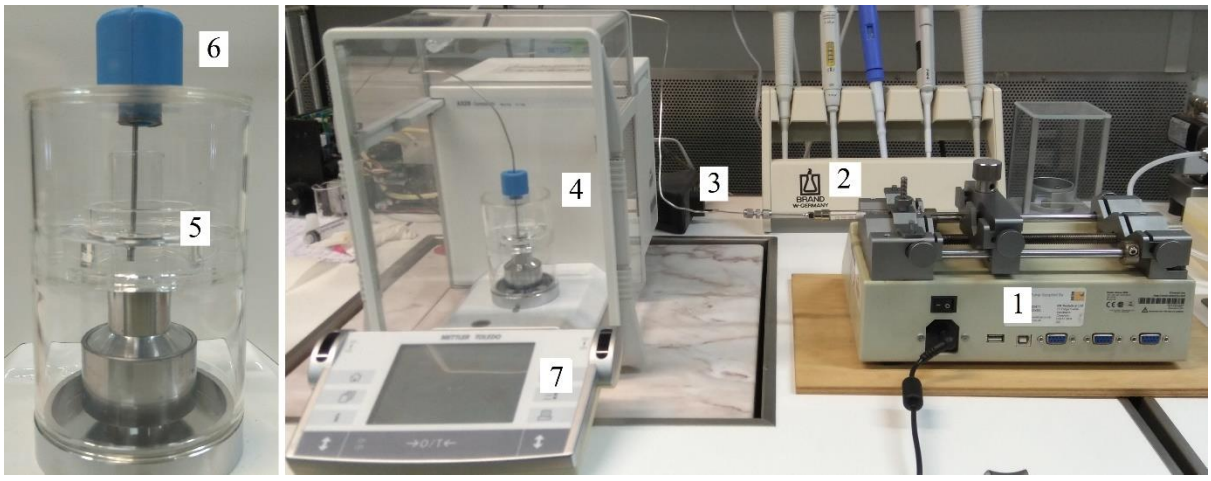

Figure 7.13 - Gravimetric method experimental setup for Nexus 3000 calibration

The Nexus 3000 syringe pump was calibrated at flow rates of 1 µL/h, 10 µL/h, 100 µL/h, 500 µL/h, and 1000 µL/h by the gravimetric method using a customised application developed in LabVIEW. All measurements had an initial wait time of 15 minutes and a set

acquisition time of 30 s. The total duration of the measurements of the flow rates between 10 and 500 μL/h was of two hours. For the flow rate of 1000 μL/h the test ran for one hour, while for the flow rate of 1 μL/h the total duration was of fourteen hours.

The results of the measurements are presented in Table 7.20. The obtained error and uncertainty values are higher than the ones obtained by the front tracking method for the flow rates of 10 μl/h and under. The errors are higher in this method due to the evaporation of the calibration fluid, which is especially noticeable for the 1 μL/h flow rate measurement, as the water contained in the calibrating vessel is being evaporated at a faster rate than the one at which the syringe pump delivers the water. In Table 7.21, the uncertainty components of the measurement of the flow rate of 10 μL/h are presented. The uncertainty calculation was determined according to the GUM [22] considering equation 3.22. The highest uncertainty contribution was the repeatability.

Table 7.20 – Gravimetric method results of Nexus 3000 calibration

Nominal flow rate / (μL/h)	Measured flow rate /(μL/h)	Relative Error / %	Relative Uncertainty / %
1	-1.90	-290	8.9
10	8.97	-10	4.2
100	95.57	-4.4	2.7
500	494.09	-1.2	0.88
1000	986.75	-1.3	0.60

Table 7.21 – Gravimetric method Uncertainty contributions for the flow rate of 10 μL/h

Uncertainty components	Estimation	$u(x_i)$	c_i	$(c_i \cdot x_i)^2$/d.o.f
Final mass /g	3.11	$3.42 \cdot 10^{-5}$	$9.31 \cdot 10^{-5}$	$2.05 \cdot 10^{-39}$
Water density /(g/mL)	0.998052	$5.98 \cdot 10^{-4}$	$2.40 \cdot 10^{-6}$	$8.42 \cdot 10^{-38}$
Air density /(g/mL)	0.001198	$2.89 \cdot 10^{-6}$	$2.10 \cdot 10^{-6}$	$2.69 \cdot 10^{-50}$
Balance weight density /(g/mL)	8.00	$2.50 \cdot 10^{-3}$	$5.72 \cdot 10^{-11}$	$3.12 \cdot 10^{-54}$
Temperature /ºC	20.72	$7.29 \cdot 10^{-2}$	$2.39 \cdot 10^{-11}$	$1.84 \cdot 10^{-49}$
Expansion coefficient /(ºC)	$1.00 \cdot 10^{-5}$	$2.89 \cdot 10^{-7}$	$-1.71 \cdot 10^{-6}$	$1.19 \cdot 10^{-54}$
Initial mass /g	3.08	$3.42 \cdot 10^{-5}$	$-9.31 \cdot 10^{-5}$	$2.05 \cdot 10^{-39}$
Evaporation /(mL/s)	$1.04 \cdot 10^{-7}$	$1.47 \cdot 10^{-8}$	1.00	$9.26 \cdot 10^{-37}$
Initial time /s	0.25	$7.00 \cdot 10^{-4}$	$2.22 \cdot 10^{-10}$	$1.16 \cdot 10^{-53}$
Final time /s	10777	$7.00 \cdot 10^{-4}$	$-2.22 \cdot 10^{-10}$	$1.16 \cdot 10^{-53}$

Buoyancy /g	0.0004	$4.47 \cdot 10^{-6}$	$9.31 \cdot 10^{-5}$	$6.00 \cdot 10^{-43}$
Repeatability /(mL/s)	$7.997 \cdot 10^{-7}$	$5.02 \cdot 10^{-8}$	1.00	$2.51 \cdot 10^{-32}$
Flow rate* /(L/h)	8.97			
u_{comb} /(μL/h)	0.19			
U_{exp} /(μL/h)	0.38			

Note: *Flow rate calculated according to Eq. 3.22.

7.2.4. Conclusions

Using the new stability uncertainty equations it was possible to reduce significantly the uncertainty values of the flow rates of 10 μL/h and under.

Between both optical methods, the front track method showed lower uncertainty values for all the tested flow rates. In the front track method, the results obtained with the 1.15 mm internal diameter capillary showed the lowest uncertainty values among all the capillaries, however, this is due to the total duration of each measurement being higher for this capillary when compared to the 0.5 mm capillaries. If it were possible to increase the test duration, by means of a moving camera system, the uncertainty values would be lower for the 0.5 mm capillary with coating.

The gravimetric method showed the lowest uncertainty value for the flow rates of 100 μL/h and above. However, the total test duration in the gravimetric method was two hours compared to only 10 minutes in the front tracking method, due to its limitations with the camera's field of view. Again, if it were possible to increase the test duration with the front tracking method the uncertainty value would be lower than the gravimetric result. For the flow rates of 10 μL/h and below the front tracking method presents the lowest uncertainty values. The drop method results are similar to the front track method results for the flow rates of 500 μL/h and 1000 μL/h, however these are higher than the gravimetric method. For the remaining flow rates the uncertainty results are higher than the front tracking and gravimetric method results.

7.3. BBraun infusion pump

The BBraun infusion pump system was calibrated at flow rates of 10 μL/h, 100 μL/h and 1000 μL/h by the front tracking method, by the drop method and by the gravimetric method.

7.3.1. Front tracking method

As shown in Figure 7.14, inside the BBraun infusion pump (1) was installed the Omnifix 10 mL polypropylene syringe (2), which was connected to a teflon capillary tube (3), which itself was connected to a capillary tube (6); a translucid paper (4) was placed in between the capillary tube and the LED lamp (5), which was turned on and pointed towards the capillary, in order to diffuse de light; the thermometer measured the temperature of the calibration fluid contained in a beaker (7) placed near the capillary tube, since it is not possible to measure the temperature inside the tube; the camera (8) was positioned so that at the right edge of its field of view the meniscus of the liquid appeared. A clamp (9) was used to keep the capillary tube in a straight horizontal fixed position.

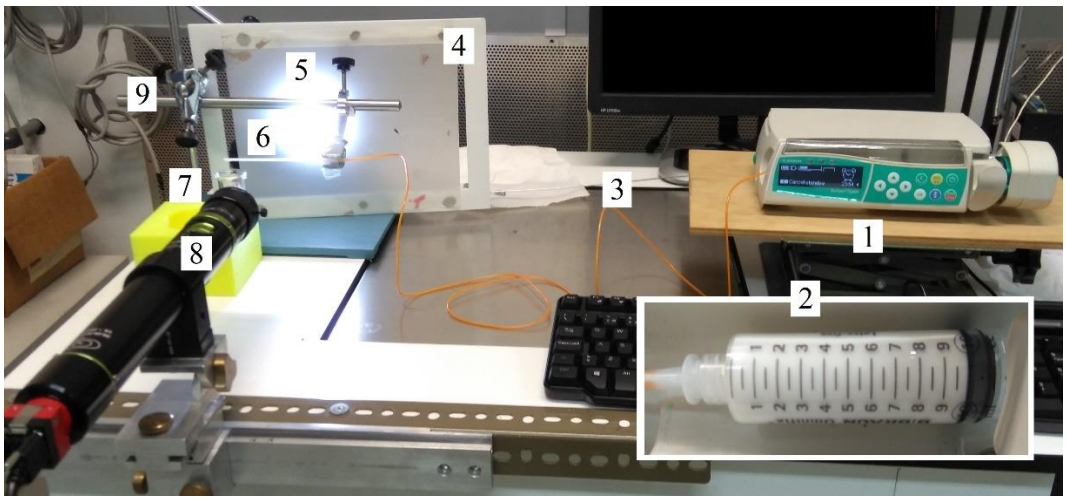

Figure 7.14 - Front track method experimental setup for the BBraun infusion pump calibration

In Figure 7.15, one can observe the beaker in which the calibration fluid is contained during the measurement, in order to measure the temperature before and after the test.

Figure 7.15 - Beaker containing the calibration fluid

Measurements were performed using two different capillary tubes and water as the calibration fluid. The first capillary tube was a glass capillary with an internal diameter of 1.15 mm (setup B.1) and the second one was a polypropylene capillary with an internal diameter of 1.61 mm (setup B.2). The measurements were performed with set acquisition times of 10 s and 1 s for flow rates of 100 μL/h and 1000 μL/h, respectively. The total duration of each test was as long as the field of view of the camera allowed for the minimum magnification of 0.43x. The comparison of the results of the measurements performed with setups B.1 and B.2 are presented in Table 7.22.

Table 7.22 - Comparison between setup B.1 and B.2

Nominal flow rate / (μL/h)	Setup	Measured flow rate /(μL/h)	Relative Error / %	Relative Uncertainty / %
100	B.1	92.32	-7.7	13
	B.2	100.98	0.98	7.7
1000	B.1	1008.84	0.88	9.3
	B.2	991.03	-0.90	5.4

The results show that setup B.2 presents lower uncertainties, almost half, than setup B.1, for both the tested flow rates. Initially this was not expected as glass is affected less by variations of the ambient conditions, such as temperature, than polypropylene. However, when analysing the uncertainty components of the measurements in Tables 7.23 and 7.24 it is possible to understand why there is such a difference. Firstly, the uncertainty related to the radius of the capillary is higher for the 1.15 mm tube. Additionally, the total duration of the measurement using the 1.15 mm capillary is much lower than the one using the 1.61 mm capillary, around half of the time for the same field of view. Therefore, the uncertainty related to the total duration is higher for the 1.15 mm. The highest uncertainty contribution for both measurements was the repeatability, being higher for the 1.15 mm capillary.

Table 7.23 - Uncertainty contributions of setup B.1 for flow rate of 1000 µL/h

Uncertainty components	Estimation	$u(x_i)$	c_i	$(c_i \cdot x_i)^2$/d.o.f
Displacement /mm	11.09	$1.50 \cdot 10^{-2}$	$2.53 \cdot 10^{-2}$	$4.17 \cdot 10^{-16}$
Radius /mm	0.575	$4.52 \cdot 10^{-3}$	$9.75 \cdot 10^{-1}$	$7.54 \cdot 10^{-12}$
Time /s	41.10	$2.97 \cdot 10^{-3}$	$-6.82 \cdot 10^{-3}$	$3.37 \cdot 10^{-21}$
Repeatability /(μL/s)	$1.19 \cdot 10^{-2}$	$1.19 \cdot 10^{-2}$	1.00	$4.99 \cdot 10^{-10}$
Lens focus /(μL/s)	$1.30 \cdot 10^{-7}$	$1.30 \cdot 10^{-7}$	1.00	$5.71 \cdot 10^{-30}$
Stability /(μL/s)	$5.15 \cdot 10^{-4}$	$5.15 \cdot 10^{-4}$	1.00	$2.23 \cdot 10^{-16}$
Expansion coefficient /ºC^{-1}	0.00001	$2.89 \cdot 10^{-8}$	$-4.36 \cdot 10^{-1}$	$5.03 \cdot 10^{-37}$
Temperature /ºC	21.56	0.005	$-2.80 \cdot 10^{-6}$	$7.10 \cdot 10^{-34}$
Flow rate* /(μL/h)	1008.84			
u_{comb} Q /(μL/h)	45.69			
U_{exp} Q /(μL/h)	93.67			

Note: *Flow rate calculated according to Eq. 5.1.

Table 7.24 - Uncertainty contributions of setup B.2 for flow rate of 1000 µL/h

Uncertainty components	Estimation	$u(x_i)$	c_i	$(c_i \cdot x_i)^2$/d.o.f
Displacement /mm	10.57	$1.50 \cdot 10^{-2}$	$2.60 \cdot 10^{-2}$	$4.70 \cdot 10^{-16}$
Radius /mm	0.805	$2.94 \cdot 10^{-3}$	$6.84 \cdot 10^{-1}$	$3.27 \cdot 10^{-13}$
Time /s	78.19	$2.97 \cdot 10^{-3}$	$-3.52 \cdot 10^{-3}$	$2.39 \cdot 10^{-22}$
Repeatability /(μL/s)	$6.99 \cdot 10^{-3}$	$6.99 \cdot 10^{-3}$	1.00	$3.10 \cdot 10^{-11}$
Lens focus /(μL/s)	$1.30 \cdot 10^{-7}$	$1.30 \cdot 10^{-7}$	1.00	$5.71 \cdot 10^{-30}$
Stability /(μL/s)	$3.58 \cdot 10^{-4}$	$3.58 \cdot 10^{-4}$	1.00	$5.17 \cdot 10^{-17}$
Expansion coefficient /ºC^{-1}	0.00024	$6.93 \cdot 10^{-7}$	$-2.31 \cdot 10^{-1}$	$1.31 \cdot 10^{-32}$
Temperature /ºC	20.84	0.005	$-2.75 \cdot 10^{-6}$	$7.18 \cdot 10^{-34}$
Flow rate* /(μL/h)	991.03			
u_{comb} Q /(μL/h)	0.0073			
U_{exp} Q /(μL/h)	26.25			

Note: *Flow rate calculated according to Eq. 5.1.

Due to the reasons mentioned above, the following measurements were done using the 1.61 mm capillary tube (setup B.2).

Measurements were performed, using setup B.2, different acquisition times, and water as the calibration fluid for flow rates of 100 μL/h and 1000 μL/h, as well as propofol as the calibration fluid for the flow rate of 10 μL/h. For the flow rate of 1000 μL/h, tests were performed with acquisition times of 1 s, 5 s and 10 s. For the flow rate of 100 μL/h, tests were performed with acquisition times of 10 s and 30 s. For the flow rate of 10 μL/h, which is the lowest flow rate the BBraun can generate, tests were performed with acquisition times of 30 s and 300 s. The results of the measurements are presented in Table 7.25. In general, the uncertainty results decrease as the acquisition times increase. For the flow rate of 1000 μL/h, the uncertainty results do not differ greatly between the acquisition times of 1 s and 5 s. However, there is a more noticeable difference in the uncertainty result for the acquisition time of 10 s. Higher acquisition times were not tested for this flow rate since there would not be enough measured points to have a readable result. For the flow rate of 100 μL/h, the uncertainty results are much lower for the acquisition time of 30 s than of 10 s. The reason for this is that, for this particular flow rate, the repeatability is two orders of magnitude smaller, as the peaks of the variability of the BBraun infusion pump happen around every thirty seconds, as shown in Figure 7.16. Thus, by taking measurements every 30 s, these peaks disappear, as can be observed in Figure 7.17.

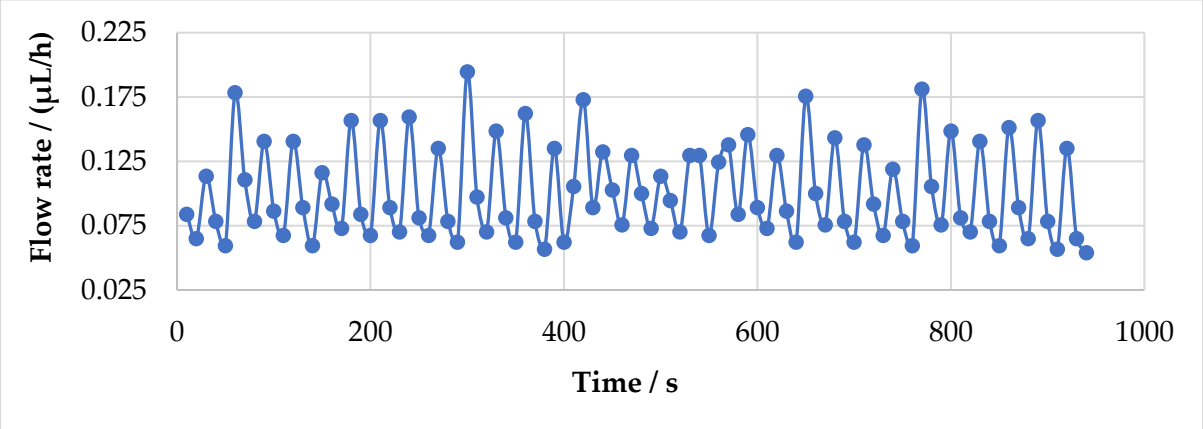

Figure 7.16 - Front track method 100 µL/h BBraun infusion pump flow behaviour with 10 s acquisition

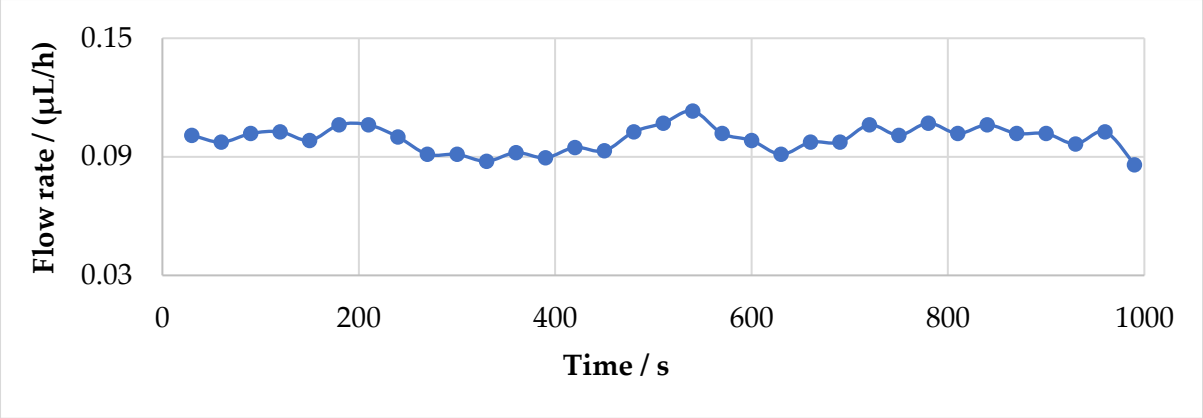

Figure 7.17 - Front track method 100 µL/h BBraun infusion pump flow behaviour with 30 s acquisition

For the flow rate of 10 μL/h, the difference between the uncertainty results obtained for an acquisition time of 30 s and of 300 s is quite significant, as the uncertainty for the 300 s time is about half of the obtained value for the 30 s time. This is due to same reason seen above for the flow rate of 100 μL/h. For the 10 μL/h flow rate, the repeatability of the measurement taken with an acquisition time of 300 s is of a lower order of magnitude than the one obtained with 30 s. The peaks of the variability of the BBraun pump, for this particular flow rate, happen around every three hundred seconds, as shown in Figure 7.18. Thus, similarly as what was done before, by taking measurements every 300 s, these peaks are attenuated, as can be observed in Figure 7.19.

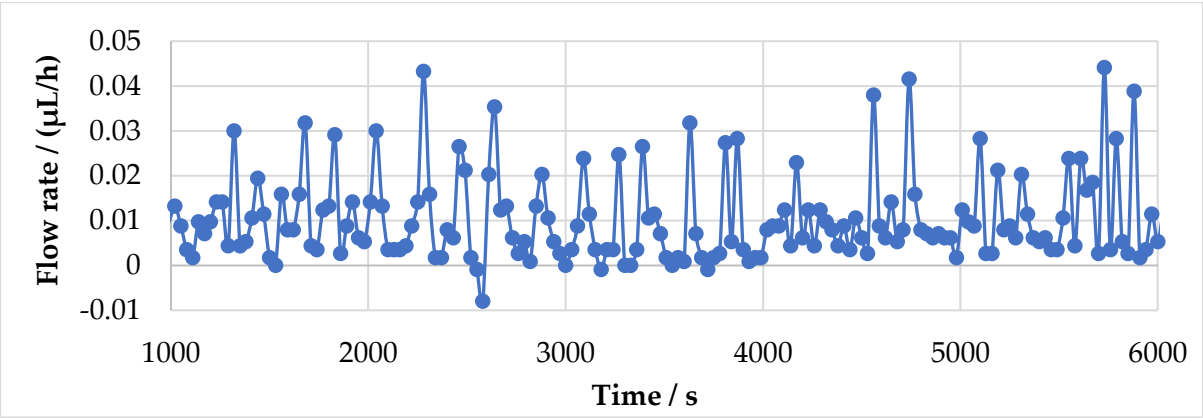

Figure 7.18 - Front track method 10 µL/h BBraun infusion pump flow behaviour with 30 s acquisition

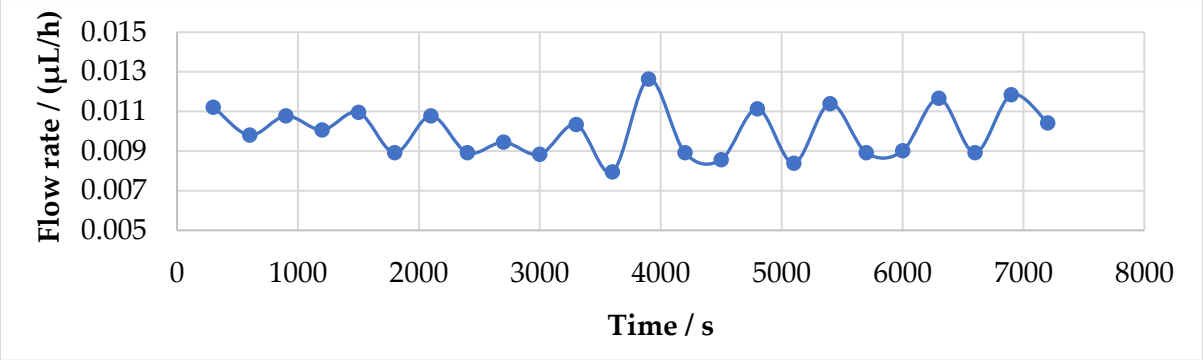

Figure 7.19 - Front track method 10 µL/h BBraun infusion pump flow behaviour with 300 s acquisition

Table 7.25 - Comparison between acquisition times for different flow rates

Nominal flow rate / (µL/h)	Acquisition time / s	Measured flow rate /(µL/h)	Relative Error / %	Relative Uncertainty / %
10	30	10.26	2.6	17
	300	9.95	-0.50	8.9
100	10	100.98	0.98	7.7
	30	99.18	-0.82	2.9
1000	1	991.03	-0.90	5.4
	5	997.78	-0.22	5.2
	10	1008.29	0.83	3.4

For the reasons explained above, moving forward, all the measurements performed with flow rates of 10 μL/h, 100 μL/h and 1000 μL/h, were taken with acquisition times of 300 s, 30 s and 10 s, respectively.

Finally, measurements were performed, using setup B.2 and different calibration fluids, which are described in chapter 4.2, for flow rates of 10 μL/h, 100 μL/h and 1000 μL/h. The results of the measurements are presented in Table 7.26.

Table 7.26 – Front tracking BBraun infusion pump calibration with different fluids

Nominal flow rate / (µL/h)	Calibration fluid	Measured flow rate /(µL/h)	Relative Error / %	Relative Uncertainty / %
10	Water	9.95	-0.50	8.9
	Propofol	9.99	-0.10	6.6
	Dobutamine	10.06	0.60	5.3
	Dopamine	9.94	-0.60	4.9
	Gelaspan	9.92	-0.80	5.1
	Solution A	10.26	2.6	5.0
	Solution B	9.99	-0.10	5.4
	Solution F	10.17	1.7	5.0
	Solution G	10.26	2.6	4.4
	Solution H	10.01	0.10	4.5
100	Water	99.18	-0.82	2.9
	Propofol	99.87	-0.13	3.4
	Dobutamine	101.66	1.7	3.0
	Dopamine	106.89	6.9	2.8
	Gelaspan	99.40	-0.60	2.7
	Solution A	102.42	2.4	3.4
	Solution B	101.68	1.7	3.0
	Solution C	99.89	-0.11	3.2
	Solution D	100.95	0.95	3.3
	Solution E	101.68	1.7	2.5
	Solution F	100.95	0.94	3.0
	Solution G	99.39	-0.61	3.0
	Solution H	100.95	0.95	2.6
1000	Water	1008.29	0.83	3.4
	Propofol	1047.69	4.8	3.1
	Dobutamine	979.73	-2.0	3.3
	Dopamine	1002.94	0.29	4.3
	Gelaspan	1003.45	0.35	2.6
	Solution A	998.65	-0.14	3.5
	Solution B	1020.60	2.1	2.8
	Solution C	998.65	-0.14	3.6
	Solution D	997.09	-0.29	3.1
	Solution E	990.99	-0.90	2.5
	Solution F	990.67	-0.93	3.5
	Solution G	1003.47	0.35	2.8
	Solution H	1009.09	0.91	2.7

7.3.2. Drop method

As shown in Figure 7.20, on the BBraun flow generator (1) was installed a 10 mL polypropene syringe (2), which was connected to a teflon tube (3), which itself was connected to a stainless-steel capillary (11) that ended inside the evaporation trap (6); a translucid paper (4) was placed in between the evaporation trap and the LED lamp (5), in order to diffuse de light; the evaporation trap (6) was placed on its holder (7); the camera (8) was positioned so that the tip of the tube was centred within the field of view of the camera. A clamp (9) was used to keep the tube in a fixed position; Since it is not possible to measure the temperature of the fluid inside the capillary tube, or of the droplet itself, a beaker or a similar container containing the calibration fluid (12) was placed inside the evaporation trap, so that the temperature of the contained fluid was as close as the temperature of the droplet. To avoid small variations in the position of the edge of the tube inside the evaporation trap during the measurements, a guider (10) was used.

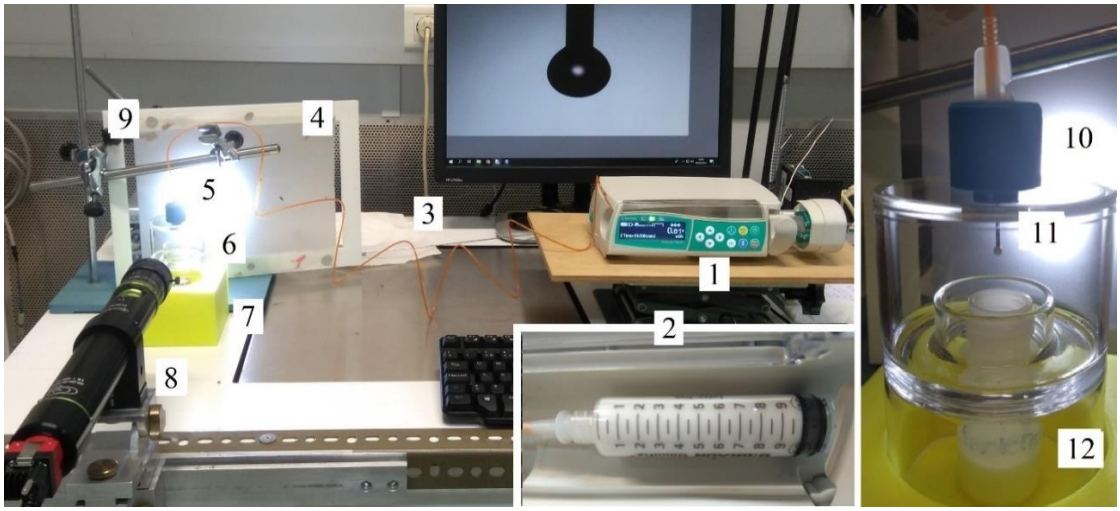

Figure 7.20 - Drop method experimental setup for the BBraun infusion pump calibration

Measurements were performed, using different calibration fluids, which are described in chapter 4.2, for flow rates of 10 μL/h, 100 μL/h and 1000 μL/h. Tests were done with acquisition times of 300 s, 30 s and 10 s for the flow rates of 10 μL/h, 100 μL/h and 1000 μL/h, respectively. The total duration of each test was as long as the drop took to fully form and fall.

The projected area of the drop was obtained by the python image processing software, and knowing the stainless-steel capillary tube diameter, 0.91188 mm, the scale and volume values were calculated.

The results of the measurements are presented in Table 7.27. The results show that the uncertainty values obtained for the 1000 μl/h flow rate tests are similar to the ones obtained by the front tracking method, as they were in the Nexus 3000 syringe pump calibration. For

the flow rate of 100 µl/h and under, the uncertainty values are significantly higher that the front tracking method results.

Table 7.27 – Drop method BBraun infusion pump calibration with different fluids

Nominal flow rate / (µL/h)	Calibration fluid	Measured flow rate /(µL/h)	Relative Error / %	Relative Uncertainty / %
10	Dopamine	9.89	-1.1	26
	Gelaspan	10.36	3.6	24
	Solution A	9.57	-4.3	25
	Solution B	10.18	1.8	28
	Solution C	10.26	2.6	22
	Solution D	10.35	3.5	22
	Solution G	11.42	14	22
	Solution H	10.10	1.0	26
100	Water	99.15	-0.85	8.7
	Dopamine	99.59	-0.41	9.3
	Gelaspan	99.55	-0.45	8.1
	Solution A	101.97	2.0	7.5
	Solution B	101.06	1.1	8.4
	Solution C	100.84	0.84	8.2
	Solution D	101.74	1.7	7.2
	Solution G	104.32	4.3	8.0
	Solution H	104.04	4.0	7.8
1000	Water	1040.20	4.0	3.7
	Dopamine	1028.87	2.9	6.7
	Gelaspan	1025.74	2.6	5.4
	Solution A	999.18	-0.08	2.7
	Solution B	990.80	-0.92	3.6
	Solution C	1037.30	3.7	7.6
	Solution D	1048.78	4.9	2.7
	Solution G	1047.26	4.7	3.1
	Solution H	1078.59	7.9	7.5

7.3.3. Gravimetric method

As shown in Figure 7.21, on the BBruan infusion pump (1) was installed a 10 mL polypropylene syringe (2), connected to a teflon tube (3), which itself was connected to a needle (5) that ended inside the evaporation trap (4) where its tip was submerged in the calibration fluid contained in the calibrating vessel (6); this container is placed on the Mettler

Toledo AX26 balance (7) along with the evaporation trap and guider (8) used to avoid direct contact between needle and the evaporation trap during the measurements.

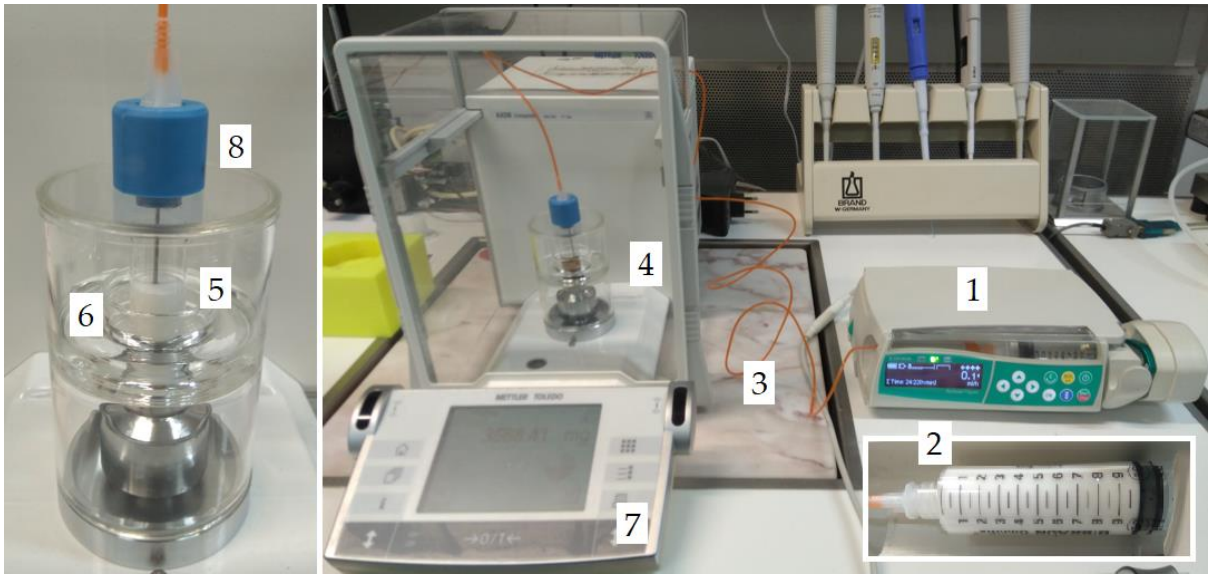

Figure 7.21 - Gravimetric method experimental setup for the BBraun infusion pump calibration

The connection between the Teflon tube and the needle is shown in Figure 7.22.

Figure 7.22 - Connection between the Teflon tube and the needle

The BBraun infusion pump was calibrated at flow rates of 10 μL/h, 100 μL/h and 1000 μL/h by the gravimetric method using a customised application developed in LabVIEW. All measurements had an initial stabilization set according to the nominal flow rate, as indicated in Table 6.4. The set acquisition time was of 30 s for all measurements and the total test duration was two hours. The results of the measurements performed using the different calibration fluids, which are described in chapter 4.2., are presented in Table 7.28. The obtained uncertainty values are higher than the ones obtained by the front tracking method for the fluids tested at flow rates of 10 µl/h and lower for the flow rates above. The uncertainty calculation was determined according to the GUM [22] considering equation 3.22. The highest uncertainty contribution was the repeatability.

Table 7.28 – Gravimetric method BBraun infusion pump calibration with different fluids

Nominal flow rate / (μL/h)	Calibration fluid	Measured flow rate /(μL/h)	Relative Error / %	Relative Uncertainty / %
10	Water	9.08	-9.2	12
	Propofol	9.56	-4.4	11
	Gelaspan	10.26	2.6	11
	Dopamine	10.62	6.2	18
	Solution C	9.94	-0.60	12
100	Water	99.87	-0.13	2.3
	Propofol	94.01	-6.0	0.79
	Dobutamine	100.11	0.11	1.1
	Gelaspan	100.32	0.32	0.87
	Solution A	96.56	-3.4	1.2
	Solution B	98.52	-1.5	1.0
	Solution C	99.70	-0.30	1.1
	Solution D	98.24	-1.8	1.0
1000	Water	995.96	-0.40	1.1
	Propofol	1000.84	0.08	0.43
	Dobutamine	1001.76	0.18	1.1
	Dopamine	1003.07	0.31	0.44
	Gelaspan	993.6	-0.64	0.39
	Solution A	995.07	-0.49	0.24
	Solution B	987.62	-1.2	0.35
	Solution C	997.54	-0.25	0.40
	Solution D	988.80	-1.1	0.54

These results show that the relative mean flow deviation from the nominal value, i.e., the relative error, and the respective relative expanded uncertainty, of the drug samples are of the same magnitude of the ones of water. Thus, the sum of the modulus of these values (|relative error| + relative expanded uncertainty) of each sample is of the same magnitude as the one obtained for water. For the flow rates between 100 μL/h and 1000 μL/h, the results of the relative error and expanded uncertainty sum of the samples comply with the maximum permissible error of 2 %, described in the standard IEC 60601-2-24:2012 [37]. From these results, one can concluded that water can be used as an appropriate reference fluid to calibrate these kind of infusion systems in the microflow rate range.

Additionally, the overall results of all the methods reveal that the mechanical properties of the tested drugs do not have a significant effect on the flow rate accuracy and uncertainty of the tested infusion system that operates in the microflow range.

7.3.4. Conclusions

Between both the optical methods, the front tracking method showed lower uncertainty values for all the tested flow rates.

In the front track method, the results obtained with the 1.61 mm internal diameter capillary showed the lowest uncertainty values compared to the 1.15 mm capillary. As seen in in the Nexus 3000 pump calibration, this can be due to the total duration of each measurement being higher for the 1.61 capillary. If it were possible to increase the test duration, by means of a moving camera system, the uncertainty values would be lower for the 1.15 mm capillary.

The gravimetric method showed the lowest uncertainty value for the flow rates of 100 μL/h and above. Again, the total test duration in the gravimetric method was two hours compared to only 1 minute for the flow rate of 1000 μL/h and 10 minutes for the flow rate of 100 μL/h in the front tracking method, due to its limitations with the camera's field of view. For the flow rates of 10 μL/h and below the front tracking method presents the lowest uncertainty values of all the tested methods. The drop method results are higher than the ones obtained by the other calibration methods.

8.

CONCLUSIONS AND FUTURE WORK

The work carried out throughout this dissertation aimed to validate methodologies for calibrating microflow rate measuring instruments by the optical methods developed at IPQ. Measurements were performed at several flow rates, with different fluids, with different flow generators, using two optical methods, in order to perform the validation of those measurement methods implemented at the LVC down to 100 μL/h by comparing their measurement results to the results obtained by the primary method, which is the gravimetric method. The uncertainty values obtained with the drop method on all the tested flow generators was higher than the results obtained by gravimetry. Also, for flow rates above 100 μL/h the test can only run up to a maximum of 10 minutes, before the weight of the drop causes it to fall. Thus, even if the uncertainty values were concordant with the gravimetric results, the number of measurements taken during a test would be small. The same happens in the front tracking method, where the camera's field of view limits the duration of the tests of flow rates of 100 μL/h and 1000 μL/h down to 10 minutes and one minute, respectively. Therefore, the uncertainty values of these flow rates is lower than the gravimetric results. To overcome this, in the front tacking method, the development of a system that allows the movement of the camera as the measurements goes on, so that it can track the meniscus for the duration that it is being displaced along the capillary tube is recommended. For flow rates of 10 μL/h and under, the front tracking method showed significantly lower uncertainty values than the gravimetric method.

Thus, the front tracking method was validated, and can be used to calibrate instruments in the microflow rate range below 10 μL/h, although the obtained uncertainty values (> 3 %) are superior to the MeDDII project target value of 2% for a range of 5 nL/min (0.3 μL/h) up to 600 mL/min (3.6×10^7 μL/h).

Additionally, the BBraun infusion pump calibration results revealed that the tested pump complies with the maximum permissible error established by standard IEC 60601-2-24 [37] for all the tested fluids, either Newtonian or non-Newtonian, for flow rates between 100 and 1000 μL/h. It was observed that the physical properties of the non-Newtonian fluids

do not influence the correct functioning of the infusion pump. It was also observed that the sum of the modulus of the relative flow error and the expanded uncertainty obtained for water (the liquid used as reference in the gravimetric method) is of the same magnitude of the ones obtained for the non-Newtonian fluids for flow rates between 100 μL/h and 1000 μL/h. Therefore, water seems to be a reliable reference liquid to calibrate infusion pumps that work with viscoelastic fluids.

REFERENCES

[1] EURAMET, "Publishable Summary for 18HLT08 MeDDII Metrology for drug delivery,", 2020.

[2] EURAMET, "Metrology for Drug Delivery," [Online]. Available: http://www.drugmetrology.com. [Accessed 2nd February 2021].

[3] U. R. Kim, R. A. Peterfreund e M. A. Lovich, Drug infusion systems: Technologies, performance, and pitfalls, vol. 124, Lippincott Williams and Wilkins, pp. 1493-1505, 2017.

[4] F. Ogheard, E. Batista, H. Bissig, H.T. Petter, P. Lucas, A.K. Niemann, "Metrological assessment of micro flow-meters and drug delivery devices in the scope of the "MeDD" EMRP project," 2015.

[5] Elsa Batista, Isabel Godinho, R. F. Martins, Ricardo Mendes, João Robarts, "Development of an experimental setup for microflow measurement using interferometry," 2020.

[6] E. Batista, A. Furtado, J. Pereira, M. Ferreira, H. Bissig, E. Graham, A. Niemann, A. Timmerman, J. Alves e Sousa, F. Ogheard, A.W. Boudaoud, "New EMPIR project – Metrology for Drug Delivery," 2020.

[7] N.V. Raghavendra, "Engineering Metrology and Measurements," 2013.

[8] E. Batista, "2. Metrologia, Apresentação PowerPoint," 2019.

[9] Henson A. "DCMAS-Workshop", 2014.

[10] "Sistema Português da Qualidade." [Online]. Available: http://www1.ipq.pt/PT/SPQ/Pages/SPQ.aspx [Accessed: 10- Feb-2021]

[11] E. Batista, "1. Estruturas da Qualidade, Apresentação PowerPoint," 2019.

[12] "Decreto-Lei nº 71/2012," Diário da República, 1.ª série - Nº 58, 2012.

[13] "IPQ." [Online]. Available: http://www1.ipq.pt/PT/IPQ/Pages/IPQ.aspx. [Accessed: 10-Feb-2021].

[14] "Metrologia" [Online]. Available: http://www1.ipq.pt/PT/Metrologia/Pages/Entrada0.aspx [Accessed: 11- Feb-2021]

[15] IPQ, NML "Volume and Flow Laboratory" leaflet, 2020.

[16] E. Batista, "5. Calibração de instrumentos volumétricos I, Apresentação PowerPoint," 2019.

[17] E. Batista, "5. Calibração de instrumentos volumétricos II, Apresentação PowerPoint," 2019.

[18] IPQ, NML "Laboratory of Properties of liquids" leaflet, 2020.

[19] EURAMET, "Metrology for Drug Delivery," [Online]. Available: http://www.drugmetrology.com. [Accessed: 18 – Feb- 2021].

[20] "Laboratorio de propriedades dos liquidos" [Online]. Available: http://www1.ipq.pt/pt/metrologia/spropliquid/Pages/PropLiq.aspx [Accessed: 12-Feb-2021]

[21] J. C. Silva, Manual de elaboração de relatórios e tratamento de resultados experimentais, Versão 4.2, FCT-UNL, Fevereiro 2005.

[22] JCGM, Evaluation of measurement data – Guide to expression of uncertainty in measurement (GUM), 1st ed., 2008.

[23] IPQ, Vocabulário Internacional de Metrologia, 1a edição Luso - Brasileira ed., Caparica, 2012.

[24] P. Guedes, Metrologia Industrial, 1ª edição, Lisboa, Outubro 2011.

[25] António Cruz, "Incerteza de Medição" Introdução ao conceito – IPQ, Dezembro 2005.

[26] IPQ, "Guia para a expressão de incerteza de medição nos laboratórios de calibração", 2ª ed., Caparica, Dezembro 2005.

[27] E. Batista, J. A. Sousa and R. F. Martins, "Calibration of Insulin Pumps," J Diabetes Treat, vol. 4, p. 1075, 2019.

[28] Kerstin Thurow, Thomas Kruger and Norbert Stoll, "An Optical Approach for the Determination of Droplet Volumes in Nanodispensing", 2009.

[29] Mezger, T., "Applied Rheology," Anton Paar, 2015.

[30] H. A. Barnes, "Viscosity Institute of Non-Newtonian Fluid Mechanics," University of Wales, 2002.

[31] H. A. Barnes, "A Handbook of Elementary Rheology", Institute of Non-Newtonian Fluid Mechanics, University of Wales, 2000.

[32] WHITEPAPER, "A basic Introduction to Rheology", Marven Instrument Limited, 2016.

[33] H. A. Barnes, "Viscosity", Institute of Non-Newtonian Fluid Mechanics, University of Wales, 2002.

[34] G. Schramm, "A practical approach to rheology and rheometry", Thermo Electron (Karlsruhe) gmbh, 2004.

[35] IPQ, NP EN ISO 3696:2000 – "Água para fins laboratoriais," 2000.

[36] Bissig, H., Petter, H.T., Lucas, P., Batista, E. et al., "Primary standards for measuring flow rates from 100 nl/min to 1 ml/min – gravimetric principle", Biomedical Engineering, 60 (4): 301-316, 2015.

[37] IEC 60601-2-24:2012 Medical electrical equipment - Part 2-24: Particular requirements for the basic safety and essential performance of infusion pumps and controllers

[38] "Propofol." [Online]. Available: https://www.drugs.com/propofol.html [Accessed: 20- Jul-2021]

[39] "Clinical Pharmacokinetics and Pharmacodynamics of Propofol." [Online]. Available: https://www.ncbi.nlm.nih.gov/pmc/articles/PMC6267518/ [Accessed: 20- Jul-2021]

[40] "Phenylethylamine". ChemicalLand21.com. Retrieved 21 September 2015.

[41] "Catecholamine". Britannica. Retrieved 21 September 2015.

[42] "Gelaspan Solução Para Perfusão." [Online. Available: https://www.bbraun.pt/pt/products/b/gelaspan-4.html [Accessed: 20- Jul-2021]

[43] "Gelaspan solution for infusion." [Online]. Available: https://www.hpra.ie/homepage/medicines/medicines-information/findmedicine/results/item?pano=PA0736/034/001&t=Gelaspan%20Solution%20for%20Infusion [Accessed: 20- Jul-2021]

[44] OIML R 124: "Refractometers for the measurement of the sugar content of grape must", 1997.

[45] M. Alvares, "Implementação de um sistema de medição de microcaudais com recurso a métodos óticos" (Master Thesis in Mechanical Engineering, FCT/UNL), 2020.

[46] E. Batista, "Calibration methodologies of microflow measuring instruments" (Doctorate Thesis in Mechanical Engineering, FCT/UNL), 2021.

[47] Wang, B., Demuran A., Gyuricsko E., Hu, H., "An experimental study of pulse micro-flows", 2011.

[48] Wolf, A. V., "Aqueous Solutions and Body Fluids", Hoeber, 1966.

APPENDIXES

APPENDIX A - Drop method uncertainty components determination

A.1 Uncertainty associated with the scale determination

The measured volume increases of the same two consecutive photographs tested with different selected scales are presented in Table A. The obtained standard deviation was equal to 0.0003572 mm^3 and the uncertainty was equal to 0.0001129 mm^3.

Table A.1 - Measurements used to determine the uncertainty associated with the scale determination

Pixels	Scale / (mm/px)	Volume increase / mm^3
252 px	0.00361857142857142	0.00970876484903016
250 px	0.00364752000000000	0.00994364425914007
248 px	0.00367693548387096	0.01018616161008000
251 px	0.00363298804780876	0.00982526879192980
249 px	0.00366216867469879	0.01006392898244000
244 px	0.00373721311475409	0.01069537769331990
246 px	0.00370682926829268	0.01043662991155970
247 px	0.00369182186234817	0.01031038173297020
245 px	0.00372195918367346	0.01056494770370970
243 px	0.00375259259259259	0.01082796352009030

A.2 Uncertainty associated with the lens focus

The measured volumes of the same drop with the camera placed in different positions, as well as the time of each measurement and the corrected volume are presented in Table B. The evaporation contribution was determined by subtracting the volume of the

first drop to the last one and dividing the difference by the time between their measurements. To obtain the corrected volumes, the evaporation rate was multiplied by the time between the first and the current measurement and was then added to the measured volume. The obtained standard deviation was equal to 0.003972 mm^3 and the uncertainty was equal to 0.001026 mm^3.

Table A.2 - Measurements used to determine the uncertainty associated with the lens focus

Camera Position	Measured volume / mm^3	Time of measurement / hh:mm:ss	Corrected volume / mm^3
1	3.09465091868018	10:14:56	3.09465091868018
2	3.08524544912107	10:16:02	3.09407346163281
3	3.07345250195193	10:16:52	3.08896840273015
4	3.06790477216601	10:17:38	3.08957353014938
5	3.06037659897502	10:18:32	3.08926827628618
6	3.05718438693161	10:19:10	3.09115885932529
7	3.05045631681598	10:19:48	3.08951358429218
8	3.04396437968705	10:20:36	3.08944201989907
9	3.03399753514466	10:21:20	3.08536051703117
10	3.02449046604498	10:23:04	3.08976425552576
11	2.99556185706581	10:25:44	3.08223688899930
12	3.00241127431221	10:26:28	3.09497164792020
13	2.98528166864214	10:27:02	3.08238980627133
14	2.98862464150437	10:27:56	3.09295569846135
15	2.98523706664068	10:28:34	3.09465091868018

A.3 Uncertainty associated with the contour determination

The measured volume increases of the same two consecutive photographs tested with different lighting conditions are presented in Table C. The obtained standard deviation was equal to 0.002013 mm^3 and the uncertainty was equal to 0.0003106 mm^3.

Table 8.3 - Measurements used to determine the uncertainty associated with contour determination

Brightness	Measured volume of 1st photograph / mm^3	Measured volume of 2nd photograph / mm^3	Volume increase / mm^3
-100	2.69651226961050	2.71469544263809	0.01818317302759
-95	2.69882357677903	2.71193121538612	0.01310763860709
-90	3.16439964049247	3.18039790585832	0.01599826536585
-85	3.16809464828486	3.18324523393939	0.01515058565453
-80	3.17103632630843	3.18624201432390	0.01520568801547

-75	3.17477794011690	3.19110272931733	0.01632478920043
-70	3.17309277887957	3.18968309638992	0.01659031751035
-65	3.17667667416996	3.19249880372345	0.01582212955349
-60	3.17692297588581	3.19113075474847	0.01420777886266
-55	3.17164719552234	3.18809472100994	0.01644752548760
-50	3.16725362805722	3.18443016443440	0.01717653637718
-45	3.59293790911249	3.61071109334805	0.01777318423556
-40	3.59346439519450	3.61277315739553	0.01930876220103
-35	3.59408595890354	3.61247831778367	0.01839235888013
-30	3.59713830614002	3.61249340457978	0.01535509843976
-25	3.59144918729684	3.60850443432358	0.01705524702674
-20	3.58709217318270	3.60385006457746	0.01675789139476
-20	3.58709217318270	3.60385006457746	0.01675789139476
-15	3.58868234206257	3.60594326438971	0.01726092232714
-10	3.58073032078100	3.59898021907470	0.01824989829370
-5	3.58124241054382	3.59803489428482	0.01679248374100
0	3.57802231274312	3.59508423694360	0.01706192420048
5	3.58120180770892	3.59855055009917	0.01734874239025
10	3.57891472820020	3.59562827244055	0.01671354424035
15	3.57483793032160	3.59382350666160	0.01898557634000
20	3.56211335191762	3.57978789179344	0.01767453987582
25	3.56095918778712	3.57805484625286	0.01709565846574
30	3.57492947948449	3.59119748847378	0.01626800898929
35	3.56325709561130	3.58301176426614	0.01975466865484
40	3.56682981147246	3.58445158542278	0.01762177395032
45	3.56174473301562	3.57235726127621	0.01061252826059
50	3.14209910559971	3.16167566900433	0.01957656340462
55	3.13979599673668	3.15668310304096	0.01688710630428
60	3.13940768863630	3.15839637902638	0.01898869039008
65	3.13975154697068	3.15623336531948	0.01648181834880
70	3.14050757575418	3.15674257038376	0.01623499462958
75	3.13893856349132	3.15540794548497	0.01646938199365
80	3.13833040999277	3.15415485667753	0.01582444668476
85	3.14033035414330	3.15656876242234	0.01623840827904
90	3.14512404518323	3.15548225626631	0.01035821108308
95	3.14447889224730	3.16062618903814	0.01614729679084
100	3.14463577812989	3.15695645603736	0.01232067790747

APPENDIX B - Drop method image capture and processing softwares

The image capture and processing programs, developed specifically for the Drop method when using the Alvium 1800U-1240 camera, require the installation of the following packages (or newer versions):

- *Python* v3.9 (https://www.python.org/downloads/)
- OpenCV v4.2
- NumPy v1.18
- TkInter

To install the OpenCv and pymba packages, open the command line and type the following commands:

- *pip install opencv-python*
- *pip install pymba*

B.1 Drop method image capture program instructions

1. Open the program through IDLE software. Right-click on the program file and select "Edit with IDLE" → "Edit with IDLE 3.9 (64-bit)";

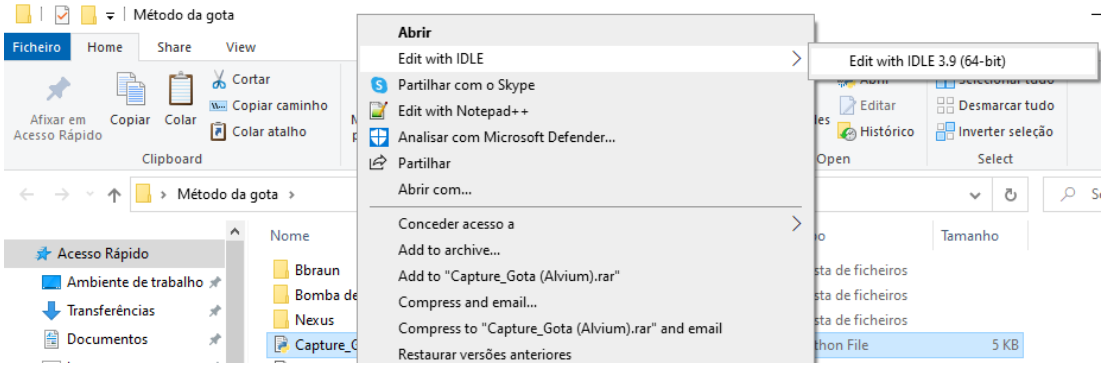

Figure B.1 – Image capture software start

2. Change the necessary data in the script (acquisition time – that is, time, in seconds, between two consecutive photographs – with the designation "user_time_interval" and the total number of photographs to be taken – designated "total_images". The duration of the test is equal to the number of photographs to be captured times the acquisition time. Thus, in the example given in Figure B.2, the total test time is 3600 s);

```
## user inputs
user_time_interval = 10
total_images = 360
```

Figure B..1 – Image capture user inputs

3. Run the program (click "Run" → "Run Module");

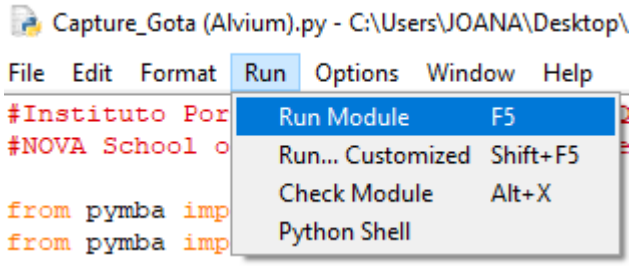

Figure B.2 - Image capture software run start

4. To setup the camera's internal parameters, write "1" and click the key "Enter". These parameters can be changed in the source code (as indicated in point 2);
5. To select the work directory (directory where the photographs of the essay will be stored), write "2" and press "Enter";
6. To start image mode, ie to view the captured image, write "3" and press "Enter". Press "q" to exit;

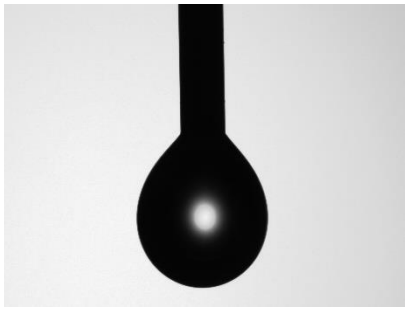

Figure B.3 - Image mode

7. To capture an image of the tube without any suspended drop, write “4” and press “Enter”. Press “q” to capture and save photo in the working directory. This image is saved by the program under the name “Background”, and is used for image segmentation during image processing;

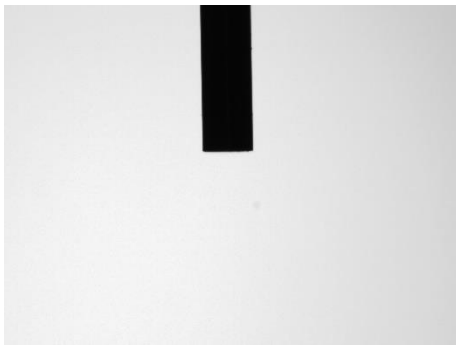

Figure B.4 - Image capture of the tube without a hanging drop

8. To start capturing the image, write “5” and press “Enter”;
9. If it is necessary to interrupt the test, click on the command window and press “Ctrl + C”, and the test is interrupted and the results are saved in a .txt file;
10. At the end of the test, write “0” and press “Enter”. If the results have not been saved previously, they will be saved in this step, then the program is terminated. The photographs taken during the rehearsal are automatically saved by the program in the work directory with the designation “Drop (number)”;
11. The generated file in txt format contains a column with the time intervals between measurements in s.

B.2 Drop method image processing program instructions

1. Open the program through IDLE software. Right-click on the program file and select “Edit with IDLE” → “Edit with IDLE 3.9 (64-bit)”;

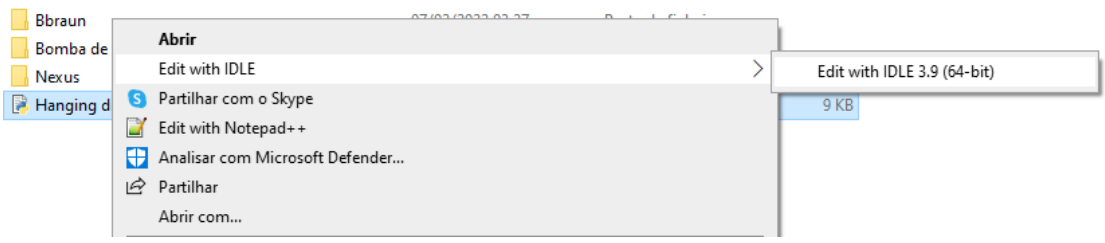

Figure B.5 - Image processing software start

2. Change the necessary data (tube diameter or threshold) in the script;

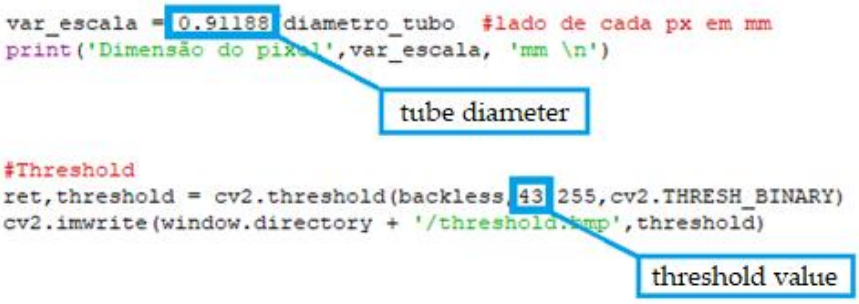

Figure B.6 - Image processing user inputs

3. Run the program (click "Run" → "Run Module");

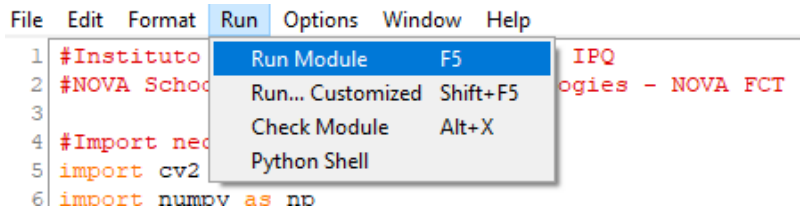

Figure B.7 - Image processing program run start

4. Click on "1. Choose directory" to select the work directory (directory where the photographs of the essay are located) and create the "Contours" folder, where the contours of the drop will be stored for later analysis;

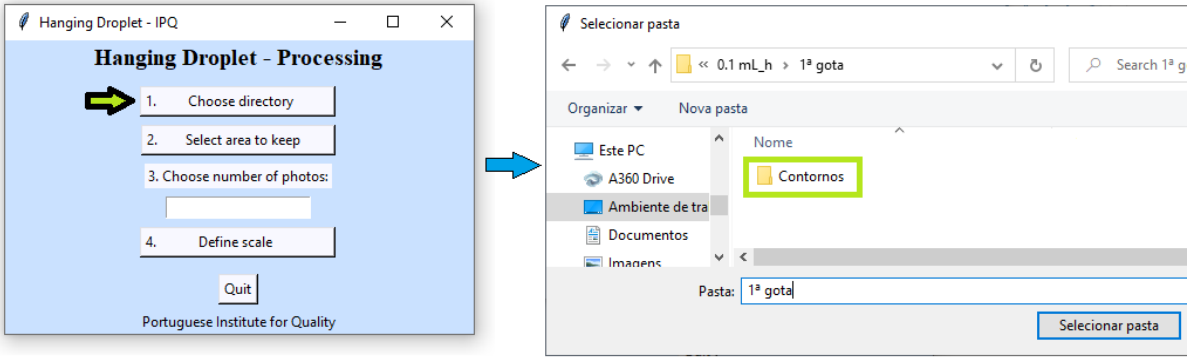

Figure B.8 - Image processing work directory

5. Click on "2. Select area to keep" to select the rectangle of the area (of the drop) to be analyzed and click "s" key to record. To select the area, click with the left mouse button on the starting point (it is suggested to start at a corner of the tube) and, with the mouse still pressed, drag down → right → left. The selected area should be just below the pipe (but not including any part of the pipe, as seen in Figure A.10 where there is a small gap between the pipe end and the selected area). If the selected area

is not the one you want, click on the "Esc" key, click on "2. Select area to keep" and repeat the process;

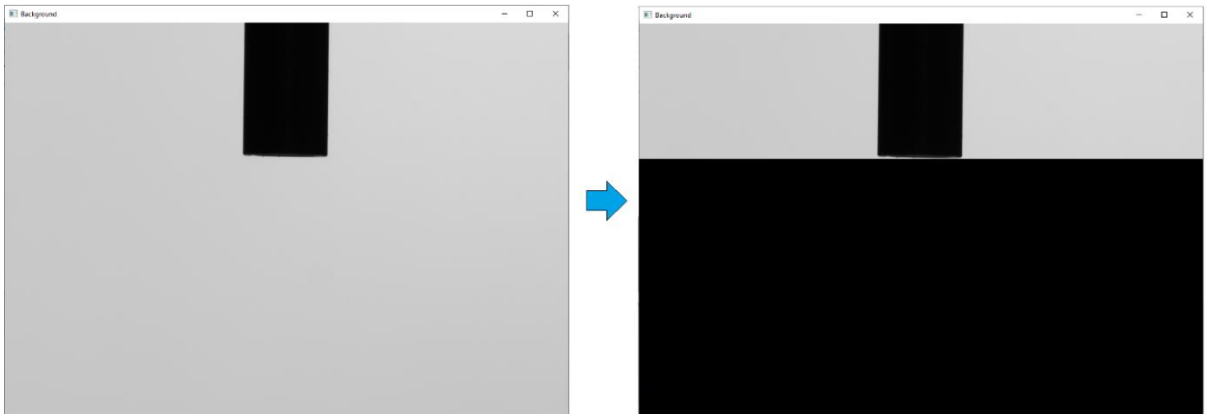

Figure B.9 - Area of interest selection

6. In "3. Choose number of photos:" write the number of photos to be analyzed;
7. Click on "4. Define scale" and select rectangle, which includes the tube diameter, to calculate the scale and press "Enter";

Figure B.10 - Tube diameter selection – scale definition

8. After calculating volumes, click "Quit".
9. The generated file in txt format. Contains the scale value and a column with the calculated volumes.

APPENDIX C – Solutions composition

Tables C.1 and C.2 show the composition of each solution from A to F, and of solutions G and H, respectively, where the nominal density value of each liquid at 20 °C, $\rho_{20°C}$, in g·cm^{-3}, is obtained using Annex D.

Table C.1 – Composition of solutions A-F

Liquids	$X_{m_{NaCl}}$ / (cg·g)	$X_{m_{Glucose}}$ / (cg·g)	$\rho_{20°C}$ / (g·cm^{-3})[1)]	m_{NaCl} / g	$m_{NaCl\ pure}$ / g	$m_{Glucose}$ / g	$m_{Glucose\ monohydrate}$ / g	$m_{solution}$ / g	Volume / mL
A	0.9	0	1.0046	4.52	**4.54**	0	0	**502.30**	500
B	0	10	1.0375	0	0	51.9	**56.6**	**518.75**	500
C	0	20	1.0797	0	0	107.97	**117.8**	**539.85**	500
D	0.45	5	1.0095	1.13	**1.13**	12.71875	**13.88**	**504.75**	500
D'	0.45	0	1.0015	1.13	1.13	0	0	250.38	250
D'	0	5	1.0175	0	**0**	12.71875	13.88	254.38	250
E	0.45	10	1.0195	1.13	**1.13**	25.9375	**28.30**	**509.75**	500
E'	0.45	0	1.0015	1.12669	1.13	0		250.38	250
E'	0	10	1.0375	0	0	25.9375	28.29781	259.38	250
F	0.9	10	1.02105	2.26	**2.27**	25.9375	**28.30**	**510.53**	500
F'	0.9	0	1.0046	2.26035	2.27	0	0	251.15	250
F'	0	10	1.0375	0	0	25.9375	28.30	259.38	250

Table C.2 - Composition of solutions G and H

Liquids	$X_{m_{Glycerol}}$ / (cg·g)	$\rho_{20°C}$ / (g·cm^{-3})[1)]	$m_{Glycerol}$ / g	$m_{Glycerol\ pure}$ / g	$m_{solution}$ / g	Total volume / mL
G	52.0392	1.1309	294.26	**295.73**	**565.45**	500
H	58.8319	1.1498	338.22	**339.92**	**574.90**	500

Tables C.3 and C.4 show the nominal dynamic viscosity, η, in mPa·s, of each solution from A to F, and of solutions G and H, respectively, at 20 °C, which was obtained using Annex D.

Table C.3 – Dynamic viscosity of solutions A-F

Liquids	$X_{m_{NaCl}}$ / (cg·g)	$X_{m_{Glucose}}$ / (cg·g)	$\eta_{20℃}$ / (mPa·s)[1)]
A	0.9	0	1.018
B	0	10	1.330
C	0	20	1.904
D	0.45	5	1 - 1.2
D'	0.45	0	1.010
D'	0	5	1.145
E	0.45	10	1 - 1.3
E'	0.45	0	1.010
E'	0	10	1.330
F	0.9	10	1 - 1.3
F'	0.9	0	1.018
F'	0	10	1.330

Table C.4 – Dynamic viscosity of solutions G and H

Liquids	$X_{m_{Glycerol}}$ / (cg·g)	$\eta_{20℃}$ / (mPa·s)[1)]
G	52.0392	6.682
H	58.8319	10.000

ANNEXES

ANNEX D - Concentrative properties of sodium chloride, glucose and glycerol aqueous solutions

Figure D.1 shows some concentrative properties of sodium chloride aqueous solutions [48], most importantly, the nominal values of density, ρ, in g·cm^{-3}, dynamic viscosity, η, in mPa·s, and mass fraction, in percent, that were used to calculate the corresponding density and dynamic viscosity of solutions with mass fractions of 0.45% and 0.9% of sodium chloride. The calculations were done via interpolation, according to Equation D.1, were x and y are the mass fraction and the density or dynamic viscosity, respectively.

Solute	Mass %	m/mol kg^{-1}	c/mol L^{-1}	ρ/g cm^{-3}	n	Δ/°C	η/mPa s
	8.0	0.820	0.816	1.0816	1.3504		1.538
	9.0	0.933	0.927	1.0922	1.3525		1.638
	10.0	1.048	1.041	1.1029	1.3547		1.754
	11.0	1.166	1.156	1.1136	1.3568		1.884
	12.0	1.287	1.273	1.1244	1.3589		2.028
	13.0	1.410	1.392	1.1353	1.3610		2.186
	14.0	1.536	1.514	1.1463	1.3631		2.361
	15.0	1.665	1.638	1.1574	1.3652		2.551
Sodium chloride NaCl	0.5	0.086	0.086	1.0018	1.3339	0.30	1.011
	1.0	0.173	0.172	1.0053	1.3347	0.59	1.020
	2.0	0.349	0.346	1.0125	1.3365	1.19	1.036
	3.0	0.529	0.523	1.0196	1.3383	1.79	1.052
	4.0	0.713	0.703	1.0268	1.3400	2.41	1.068

Figure D.1 – Concentrative properties of sodium chloride aqueous solutions

$$y = y_1 + \frac{(y_2 - y_1)}{(x_2 - x_1)}(x - x_1) \quad \text{(D.1)}$$

Figure D.2 shows concentrative properties of glucose aqueous solutions [48], from where the nominal values of density and dynamic viscosity of solutions with mass fractions of 5%, 10% and 20% of glucose were taken directly.

Solute	Mass %	m/mol kg^{-1}	c/mol L^{-1}	ρ/g cm^{-3}	n	Δ/°C	η/mPa s
D-Glucose	0.5	0.028	0.028	1.0001	1.3337	0.05	1.010
$C_6H_{12}O_6$	1.0	0.056	0.056	1.0020	1.3344	0.11	1.021
	2.0	0.113	0.112	1.0058	1.3358	0.21	1.052
	3.0	0.172	0.168	1.0097	1.3373	0.32	1.083
	4.0	0.231	0.225	1.0136	1.3387	0.43	1.113
	5.0	0.292	0.282	1.0175	1.3402	0.55	1.145
	6.0	0.354	0.340	1.0214	1.3417	0.67	1.179
	7.0	0.418	0.398	1.0254	1.3432	0.79	1.214
	8.0	0.483	0.457	1.0294	1.3447	0.91	1.250
	9.0	0.549	0.516	1.0334	1.3462	1.04	1.289
	10.0	0.617	0.576	1.0375	1.3477	1.17	1.330
	12.0	0.757	0.697	1.0457	1.3508	1.44	1.416
	14.0	0.904	0.819	1.0540	1.3539	1.73	1.512
	16.0	1.057	0.944	1.0624	1.3571	2.03	1.625
	18.0	1.218	1.070	1.0710	1.3603	2.35	1.757
	20.0	1.388	1.199	1.0797	1.3635	2.70	1.904

Figure D..2 - Concentrative properties of glucose aqueous solutions

Figure D.3 shows concentrative properties of glycerol aqueous solutions [48], such as the nominal values of density, dynamic viscosity and mass fraction that were used to calculate the corresponding density and dynamic viscosity of solutions with mass fractions of 52.04% and 58.8% of glycerol. The calculations were done via interpolation, according to Equation D.1.

Solute	Mass %	m/mol kg^{-1}	c/mol L^{-1}	ρ/g cm^{-3}	n	Δ/°C	η/mPa s
Glycerol	20.0	2.715	2.271	1.0459	1.3572	5.46	1.737
$CH_2OHCHOHCH_2OH$	24.0	3.429	2.752	1.0561	1.3624	7.01	1.988
	28.0	4.223	3.242	1.0664	1.3676	8.77	2.279
	32.0	5.110	3.742	1.0770	1.3730	10.74	2.637
	36.0	6.108	4.252	1.0876	1.3785	12.96	3.088
	40.0	7.239	4.771	1.0984	1.3841	15.50	3.653
	44.0	8.532	5.300	1.1092	1.3897		4.443
	48.0	10.024	5.838	1.1200	1.3954		5.413
	52.0	11.764	6.385	1.1308	1.4011		6.666
	56.0	13.820	6.944	1.1419	1.4069		8.349
	60.0	16.288	7.512	1.1530	1.4129		10.681
	64.0	19.305	8.092	1.1643	1.4189		13.657

Figure D.3 - Concentrative properties of glycerol aqueous solutions

NOVA SCHOOL OF SCIENCE & TECHNOLOGY

VALIDATION OF METODOLOGIES FOR THE CALIBRATION OF MICRO FLOW RATE MEASURING INSTRUMENTS BY OPTICAL METHODS

JOANA AVISON AFONSO

2022